EFFECT OF MICROSTRUCTURE ON INTERNAL AND EXTERNAL HYDROGEN EMBRITTLEMENT OF AN ULTRAHIGH STRENGTH STEEL

Dilipkumar D. Dedhia
B.S., Madras University, 1972
B.E., Indian Institute of Science, 1976

A dissertation submitted to the faculty
of the Oregon Graduate Center
in partial fulfillment of the
requirements for the degree
Doctor of Philosophy
in
Materials Science

February 1980

The dissertation "Effect of Microstructure on Internal and External Hydrogen Embrittlement of an Ultrahigh Strength Steel" has been examined and approved by the following Examination Committee for Dilipkumar D. Dedhia:

William E. Wood, Thesis Advisor
Associate Professor

J. Fred Holmes
Professor

Nicholas G. Eror
Associate Professor

Jack H. Devletian
Associate Professor

ACKNOWLEDGEMENTS

I am grateful to Dr. William E. Wood for his guidance and encouragement during the entire course of this work. I am also thankful to Drs. Nick Eror, Jack Devletian and Fred Holmes for reading the manuscript and offering many helpful suggestions.

I especially wish to thank S. Shankar, Cheruvu Sastry, R. Padmanabhan and Dr. Khalid Khan for their many helpful suggestions and comments during all the stages of this work and for reading all or part of the manuscript in advance, offering valuable comments. I also thank Nongluck Suriyayothin for her readiness to help in all aspects of this work during the last hectic stages.

I am especially indebted to V. S. Rao Gudimetla for introducing me to statistical methods, on which the major conclusions of this work are based.

The hydrogen analysis data reported in this work were obtained at the Boeing Aerospace Co. under the supervision of Dr. K. B. Das and I wish to acknowledge his personal attention and interest in this work as well as the valuable discussions I had with him. I also thank Chuck Bauer for the numerous discussions I had with him.

Finally, I wish to acknowledge the efforts of Janijo Weidner who so speedily typed the manuscript and Barbara Ryall who did the art work.

This work was partially supported by the U.S. Army Research Office under Grant No. DAAG29-78-G-0158.

TABLE OF CONTENTS

LIST OF FIGURES

LIST OF FIGURES (Cont'd)

LIST OF TABLES

ABSTRACT

Effect of Microstructure on Internal and External
Hydrogen Embrittlement of an Ultra High Strength Steel

Dilipkumar D. Dedhia, Ph.D.
Oregon Graduate Center, 1980
Supervising Professor: William E. Wood

Hydrogen assisted cracking in low alloy ultrahigh strength AISI 4340 steel heat treated to above 200 ksi yield strength was slightly dependent on microstructural features such as grain size, carbide type, amount of retained austenite and grain boundary composition. The susceptibility of the steel to hydrogen was similar for both internal as well as external hydrogen induced embrittlement. Increasing the prior austenite grain size slightly improved the threshold stress intensity but did not have any effect on region II crack growth rates. The change from epsilon carbide to cementite increased the region II crack growth rates. The presence of retained austenite slightly improved the threshold stress intensity for hydrogen assisted cracking. However, its thermal and mechanical instability actually increased the region II crack growth rates.

Acoustic emission analysis confirmed the discontinuous nature of hydrogen assisted cracking. These discontinuous steps were found to be dependent upon the prior austenitic grain size. From acoustic emission results and based on the fact that the region II crack growth rates were

independent of grain size, it was possible to propose a mechanistic model for hydrogen assisted cracking which combined the models proposed by Troiano and Petch and Stables.

1. INTRODUCTION

As material's applications are being extended to higher strengths or to more hostile environments, the possibility of unexpected service failure increases. In many instances, compatibility of the steel with service environments, particularly those containing or capable of producing hydrogen, is the controlling factor for many of these failures. Interest in these problems has increased dramatically as the environmentally induced failures have been found in a variety of new applications. These include fuel containment vessels and power stages for rocket engines, oil and gas well casings, pipings and valves for transport of liquids and gases, high strength alloys, particularly for aerospace applications, chemical and petroleum industry process equipment, nuclear fusion power systems and a host of others. High strength martensitic steels containing as little as a few parts per million of dissolved hydrogen or exposed to seemingly innocuous environment such as water, fail in a delayed manner when subjected to a tensile stress exceeding a critical value. This type of failure is an especially serious problem in the application of high strength steels because both the time required for failure and the minimum stress for failure decreases as the tensile strength is increased. Adding to the problem is the fact that this type of delayed failure is observed predominantly in a temperature range in the vicinity of room temperature.

It is evident therefore, that because of the widespread commercial use of high strength steels and lack of complete understanding of

the basic mechanisms and the influence of composition, processing, design, and environment contributing to service failures, further study in the area of hydrogen assisted cracking is of special practical importance.

It has been reported[1] that a significant improvement in the mechanical properties can be obtained in the case of AISI 4340 steel by austenitizing at higher than conventional temperatures. The microstructural features suggested to be responsible for the improvements are grain size[2], reduced grain boundary segregation[3], amount of grain and lath boundary retained austenite[4] and martensite morphology[4]. This study was undertaken to evaluate the effect of variations in the above microstructural features on the susceptibility of the steel to hydrogen assisted cracking for internal hydrogen embrittlement (IHE) and hydrogen environmental embrittlement (HEE). An attempt is made to interpret the acoustic emission generated during hydrogen assisted cracking by correlating acoustic emission counts, events, and amplitude distribution with crack length and stress intensity.

2. BACKGROUND

2.1 CHARACTERISTICS OF HYDROGEN ASSISTED CRACKING

Some important and well established characteristics of hydrogen assisted cracking are as follows:

1. All high strength tempered martensitic steels are susceptible to hydrogen assisted cracking.

2. Hydrogen assisted cracking is sensitive to strain rate, the susceptibility being enhanced at lower strain rates.

3. A definite threshold stress intensity exists[5] below which hydrogen assisted cracking will not occur.

4. Since failure is initiated most readily in regions of triaxial stress, the severity of embrittlement increases as the radius of the notch or crack tip decreases.[6-8]

5. Upper and lower temperature limits exist beyond which hydrogen assisted cracking does not occur.

6. Hydrogen assisted crack growth rate when plotted as a function of stress intensity exhibits three stages region I where crack growth rate increases sharply with stress intensity, region II where the crack growth rate is independent of stress intensity, and region III where the crack growth rate again increases sharply as the fracture toughness of the material is approached (Figure 1).

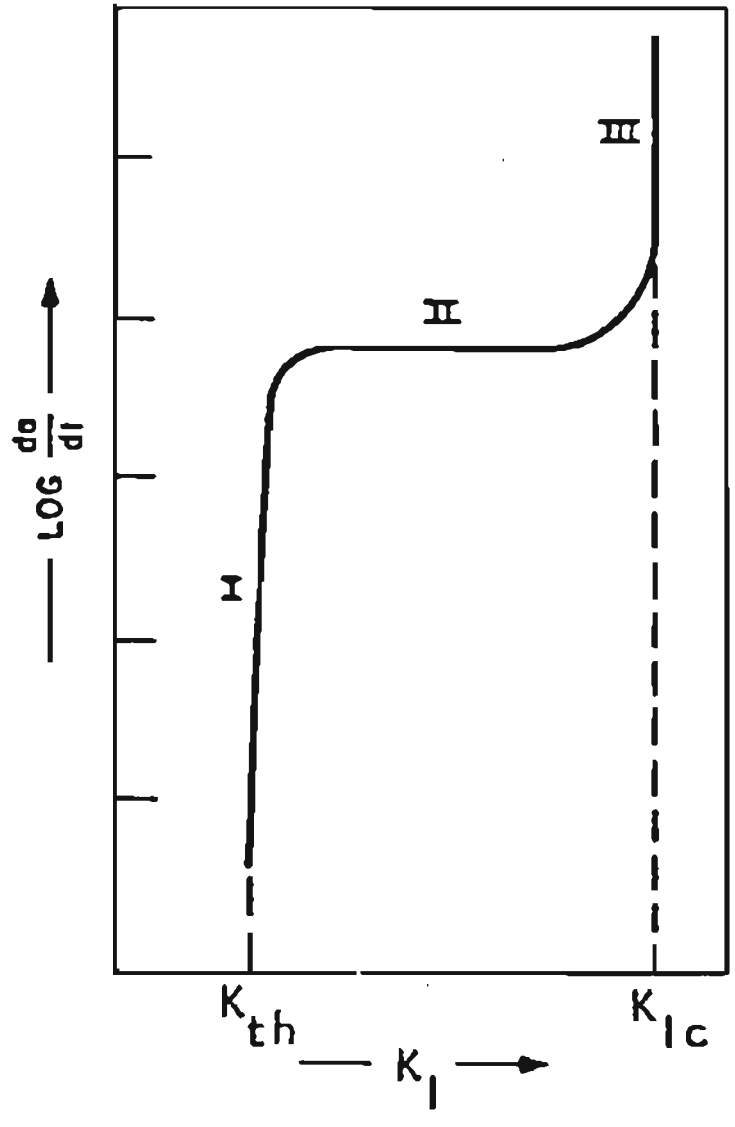

Figure 1. A schematic representation of the three stages of hydrogen assisted crack growth kinetics.

7. The effect of hydrogen on delayed cracking in high strength steels is the same whether the hydrogen is supplied as a molecular gas, through stress corrosion or by electrolytic charging.[9-14] A schematic diagram of the stress assisted hydrogen diffusion for internal and external hydrogen is shown in Figure 2.

2.2 THEORIES OF HYDROGEN ASSISTED CRACKING

Various attempts have been made to explain the possible mechanisms by which hydrogen causes delayed failure. There are three outstanding theories: (1) pressure theory of Zapffe and Sims, (2) adsorption theory of Petch and Stables and (3) lattice decohesion theory of Troiano and Oriani.

Zapffe and Sims[15] have proposed that the molecular hydrogen collects at defect sites in the steel and when the internal pressure of hydrogen exceeds the strength of the matrix, the hydrogen embrittlement cracking occurs.

A different version of pressure theory was proposed by Kazinczy[16]. According to this theory, the hydrogen embrittlement is caused by lowering the shear strength and cleavage strength. He explained this by assuming that molecular hydrogen at high pressure is trapped in a crack, which initiates fracturing. During crack extension, the hydrogen gas under pressure expands and the released energy adds to the Griffith energy required for crack extension.

More recently, Tetelman[17] has proposed that hydrogen precipitates at inclusions or carbides in molecular form, causing the initiation

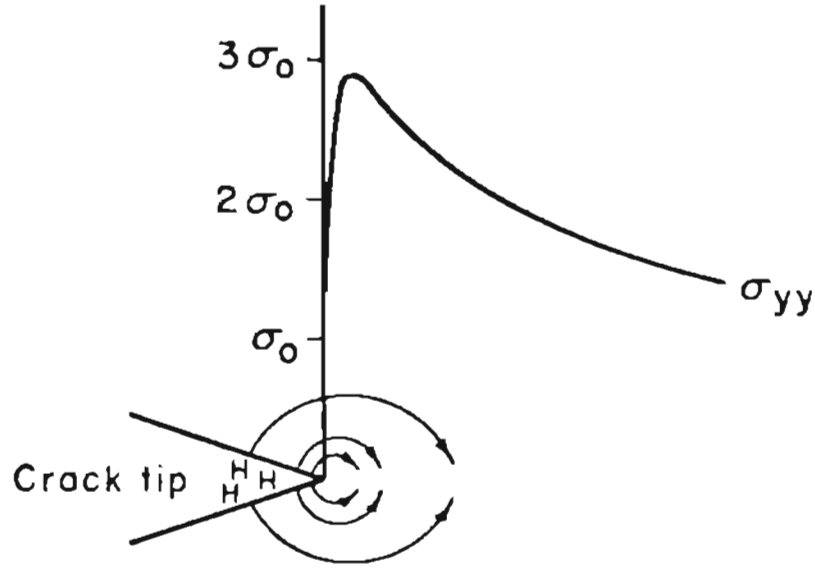

EXTERNAL HYDROGEN

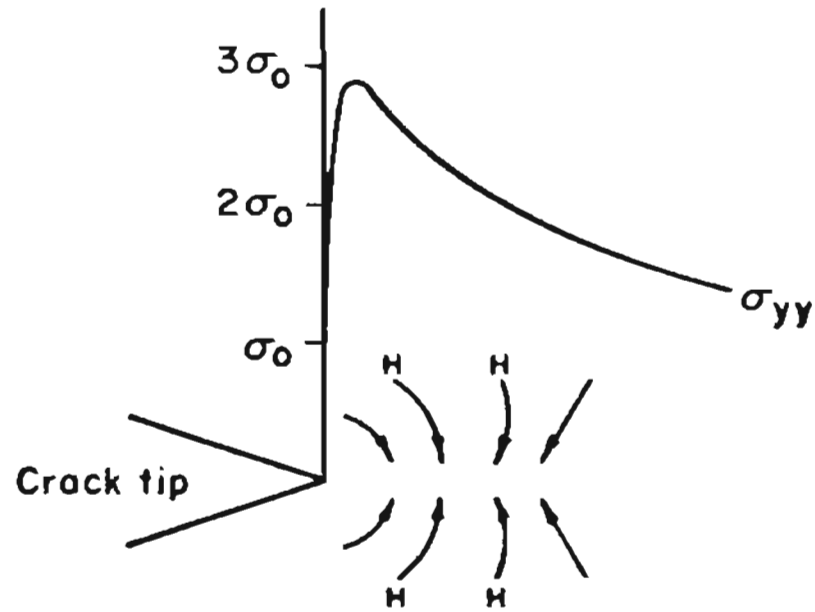

INTERNAL HYDROGEN

Figure 2. A schematic representation of the hydrogen diffusion path at the crack tip for internal and external hydrogen.

of voids or microcracks. According to this theory, the hydrogen pressure in these defects causes them to grow either by plastic deformation or cleavage, depending on the fracture toughness of the material.

Petch and Stables[18] proposed that the adsorbed hydrogen on the Griffith crack surface lowers the surface energy. This means that fracture will occur at a stress lower than that required in the absence of hydrogen. Petch[19] has reported that lowering the surface energy due to hydrogen adsorption is sufficient to account for a significantly reduced stress for crack propagation.

In the 1960 Campbell memorial lecture, Troiano[8] presented a decohesion model of hydrogen assisted cracking. According to his model, under the driving force of a stress gradient, hydrogen diffuses towards the region of maximum triaxiality in front of a notch or a sharp crack. There would be a critical concentration of hydrogen which by interaction with the 3-d electron shell of iron atoms can reduce the fracture strength of the lattice. The incubation time then would be the time required to achieve the critical concentration of hydrogen in the crack tip region. At that time, the crack jumps over the embrittled region and stops. For cracking to restart, hydrogen must diffuse to the new region of triaxiality and this discontinuous process repeats itself and results in a subcritical stable crack growth.

Oriani[20-23] modified Troiano's theory to show that the dissolved hydrogen reduces the maximum cohesive resistive force of the iron lattice. Based on this idea, he formulated a mechanistic model of hydrogen assisted

crack extension. According to his model, the crack grows when the local tensile elastic stress normal to the plane of crack equals the local maximum cohesive force per unit area as reduced by the large concentration of hydrogen drawn there by the effect of elastic stress on the chemical potential of hydrogen. The crack growth rate would then depend on how fast hydrogen can be transported to the crack tip region.

2.3 INFLUENCE OF MICROSTRUCTURE

Significant synergistic interactions between the final microstructure and such variables as solute concentration, grain size, substructure and thermal treatment are expected, since these are the very factors that control the microstructure. A number of investigators have studied the role of varying microstructure on the susceptibility of the steel to hydrogen assisted cracking with the following results.

In high strength steels, hydrogen assisted cracking often occurs along the prior austenite grain boundaries and therefore the grain size is an important factor in determining the susceptibility of the steel to hydrogen assisted cracking. According to a study by Proctor and Paxton[24], an increase in the grain size from 9 to 40 μm resulted in shorter failure times and apparently higher crack growth rates for AISI 4340 steel tested in 3.5 percent sodium chloride solution. This was in spite of the fact that the coarse grained material had a slightly lower yield strength. The threshold stress intensity for cracking was not affected for the range of grain sizes investigated. A study by Lessar and Gerberich[25] on AISI 4340 steel for internal hydrogen embrittlement revealed an increase

in threshold stress intensity with grain size for grain sizes above 40 μm. The increase in grain size also decreased the region II crack growth rates.

Small changes in the tempered carbide structure have a strong effect on the kinetics of hydrogen assisted cracking.AISI 4340 steel was found most susceptible to hydrogen assisted cracking after tempering at 260°C.[26] This was associated with the presence of grain boundary platelet carbides. Addition of silicon shifts the most susceptible condition to a tempering range of 375°-420°C, since it retards the change of carbide morphology from epsilon carbide to cementite.

The presence of thin films of retained austenite on lath and grain boundaries has been suggested[25] as a trap for hydrogen because of the lower diffusivity and higher solubility of hydrogen in austenite. In a recent study on environmental hydrogen embrittlement of AISI 4340 and 300M steels, Ritchie et al [27] showed that the presence of retained austenite decreased the region II crack growth rates by more than an order of magnitude. The effect of retained austenite may vary depending on its mechanical stability and the source of hydrogen.

The segregation of impurity elements like phosphorus and sulfur to the grain boundaries of steel reduces their cohesive strength and the effect in alloy steels is best demonstrated as temper embrittlement[28-29]. Many studies in the last few years have shown[3,30] by Auger electron spectroscopy that temper embrittled steels exhibit a large excess of such impurities on intergranular fracture surfaces. Since hydrogen also reduces the cohesive strength of the steel lattice, the presence of segregated impurities would have an additive effect on hydrogen assisted

cracking. In their study on HY130 and HY180 steels, McMahon and his coworkers[90] have demonstrated this additive effect of segregated impurities on hydrogen assisted cracking.

2.4 ACOUSTIC EMISSION

Acoustic emissions are the impulsively generated small amplitude elastic stress waves created by deformation or cracking in materials. The rapid release of kinetic energy from deformation mechanisms propagates elastic waves from the source and these are detected as small displacements on the surface of the material. The emissions indicate the onset and continuation of deformation and fracture and may be used to locate the source by triangulation techniques. A particular feature which makes acoustic emission analysis a most useful tool for the study of the behavior of materials is that the pattern of emission is determined by the time distribution of the impulsive deformations that occur within the material. Consequently, the study of defects could be carried out without prior knowledge of their existence or location.

The application of acoustic emission techniques involves affixing the sensors on the surface of the structure under investigation. The detected emissions are then amplified, selectively filtered and conditioned, and the parameters such as events, threshold counts, amplitude distribution and frequency spectrum are recorded.

The acoustic emission techniques have been used mostly on metals, even though its potential applications to a variety of materials including wood[31], ceramics[32], and composites[33] have been demonstrated.

Even though extensive work has been done in the past ten years on acoustic emission characterization of metals under different deformation and failure modes, a quantitative correlation of acoustic emission parameters to the extent of damage is still lacking.

3. EXPERIMENTAL PROCEDURE

3.1 MATERIAL PREPARATION

The steel used in this investigation was aircraft quality AISI 4340 alloy. The steel was received as 16 mm plate in a fully annealed condition. The analyzed composition of the steel is given in Table 1. Plane strain fracture toughness compact tension specimens (CTS) and double cantilever beam (DCB) specimens were machined from the plate in the LT orientation and their dimensions are shown in Figure 3 and 4. The CT specimens were used for crack growth rate and acoustic emission studies. The DCB specimens were used to obtain the threshold stress intensity data. 2.5 mm deep grooves were cut on either side of DCB specimens to prevent the crack from running out of the plane (Figure 4). A 0.2 mm crack starter slot was cut after heat treatment and for HEE testing, a fatigue crack was introduced in CT specimens.

3.2 HEAT TREATMENT

A controlled atmosphere tube furnace was utilized for all austenitization treatments. The temperature control on the furnace was accurate up to $\pm$ 5°C. The austenitization treatments consisted of one hour at 1200°C, 1100°C or 870°C followed by quench in an agitated oil bath. A variation of the 1200°C austenitization treatment consisted of a half hour hold at 870°C in a neutral salt bath prior to oil quenching. The tempering treatments were carried out in a salt bath furnace either at 180°C or 280°C. The various heat treatments used are listed in Table 2.

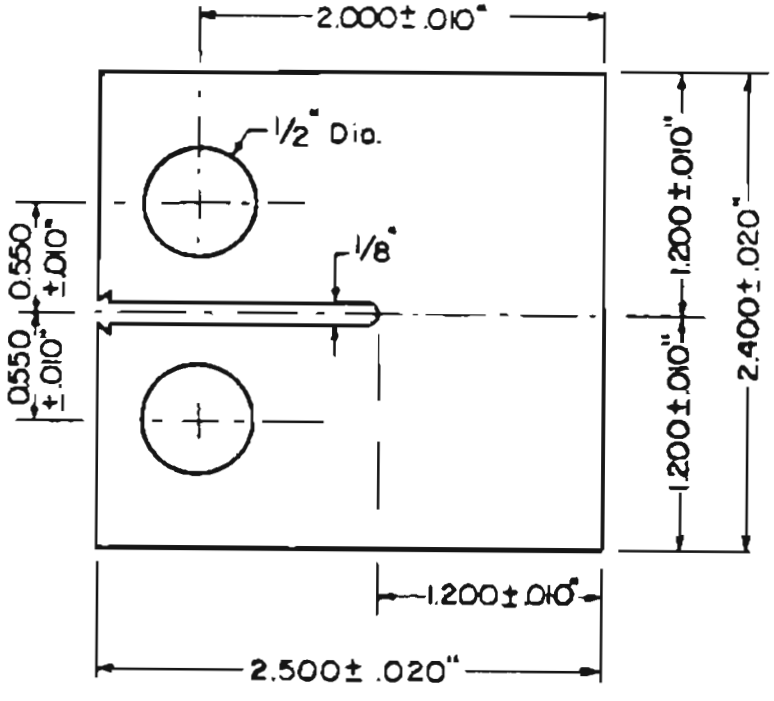

Figure 3. Geometry of the plane strain fracture toughness compact tension specimens used for crack growth rate testing.

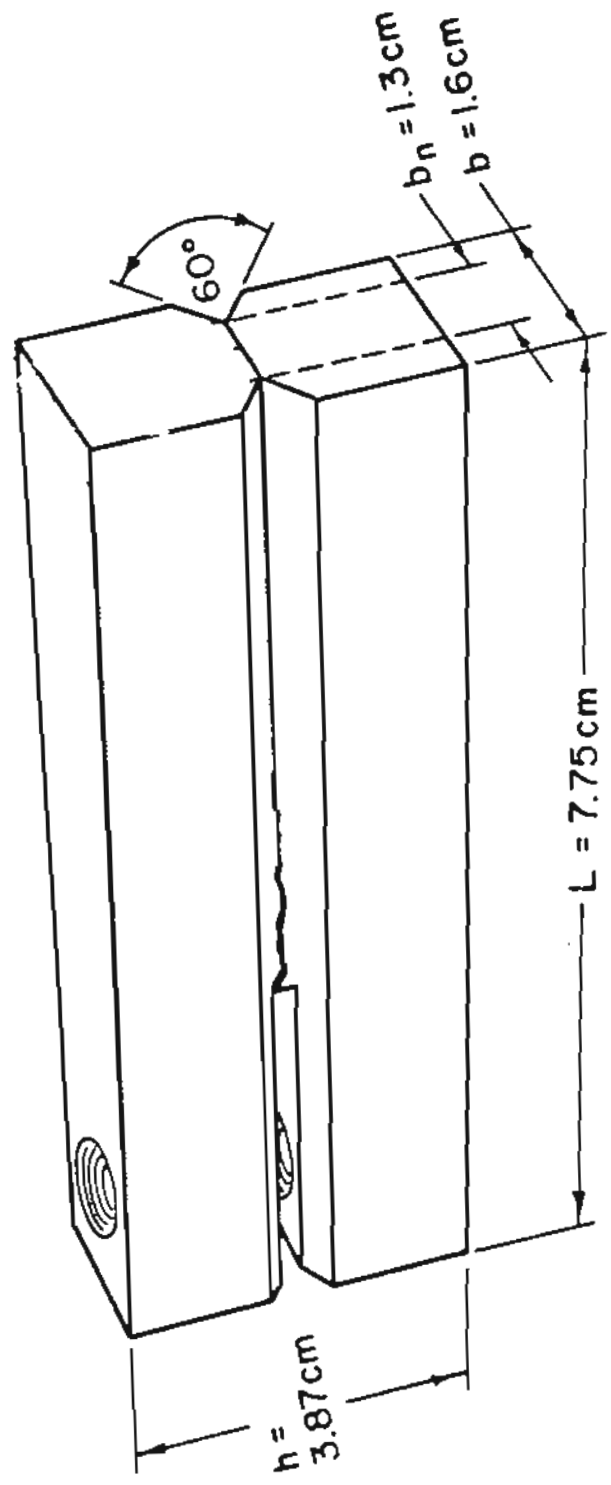

Figure 4. Double cantilever beam specimen used for obtaining threshold stress intensity for hydrogen assisted cracking.

The tensile and fracture toughness data for these heat treatments are listed in Table 3.

3.3 HYDROGEN CHARGING PROCEDURES

After heat treatment, the specimens were ground and cleaned in acetone to remove any grease or oil. To test for IHE, the specimens were cathodically charged in an electrolyte consisting of 4 percent sulfuric acid poisoned with phosphorous. Ten cc of 5 percent solution of phosphorous in carbon disulphide were added to 600 cc of the electrolyte. Each specimen was charged in a fresh bath for 24 hrs at a current density of 0.005 amperes per square cm. Immediately after charging, the specimens were wet ground on a 100 grit emery paper to clean the surface and then ultrasonically pickled in a 10 percent solution of hydrochloric acid. The specimens were then rinsed thoroughly and cadmium plated in a cyanide bath consisting of 28 gms/liter of CdO and 105 gms/liter of NaCN containing a commercial brightener. The pH was adjusted to 13 by the addition of NaOH. A current density of .02 amps/cm^2 was utilized for a 10 minute plating period. The purpose of cadmium plating was to contain the occulded hydrogen within the specimens. Prior to testing, the cadmium plated specimens were baked for 24 hours at room temperature to achieve a homogeneous distribution of hydrogen.

3.4 EXTERNAL HYDROGEN ENVIRONMENT

For HEE testing, a 3.5 percent aqueous solution of reagent grade sodium chloride was used. For crack growth analysis, the CT specimens

were immersed in the solution before loading. For threshold testing, the specimens were bolt loaded and then placed in the solution.

3.5 THRESHOLD TESTING

Threshold stress intensity data were obtained by bolt loaded DCB specimens. This type of specimens are ideally suited for obtaining the threshold stress intensity (K_{th}) below which hydrogen assisted cracking does not occur. For a fixed arm displacement, the stress intensity decreases as the crack grows, until a threshold stress intensity is reached. The stress intensity (K) is a function of arm deflection and crack length and is given by the relationship

$$K = \frac{VEh\ [3h(a + 0.6h)^2 + h^3]^{1/2}}{4\ [(a + 0.6h)^3 + h^2 a]}$$

where V = arm deflection

E = elastic modulus

h = half height of the specimens

a = crack length

The specimens were loaded by tightening the bolts while monitoring the arm deflection accurately with a Gaertner cathatometer until a preselected arm deflection is achieved. For IHE, the specimens were charged with hydrogen, Cd plated and baked prior to loading. For HEE, the specimens were loaded and then surrounded by the NaCl solution. The specimens were left under load for 100 hrs and then broken to measure the hydrogen

assisted crack extension. From the arm deflection and crack length data, the K_{th} was calculated using the above equation.

3.6 CRACK GROWTH TESTING

The ASTM specified CT specimens are ideally suited for studying crack growth rates as a function of applied stress intensity. For a fixed load, the stress intensity increases as the crack length increases. Crack growth rate data over a wide range of stress intensity can be obtained with a single specimen.

For IHE crack growth study, the hydrogen charged specimens were loaded to about 50 percent of K_{Ic} and the crack allowed to initiate. This established a sharp crack. The specimens were then unloaded and reloaded to obtain a predetermined initial stress intensity. The crack length was monitored with an Instron crack opening displacement (COD) gage. The clip gage displacement was recorded as a function of time. The crack length was obtained from the clip gage displacement through compliance calibration.

In the case of HEE, the fatigue precracked specimens were immersed in a 3.5 percent NaCl solution and then loaded to a predetermined stress intensity level. The crack growth rate data were obtained in the same way as described earlier.

3.7 ACOUSTIC EMISSION MONITORING

A schematic diagram of the acoustic emission monitoring system is given in Figure 5. An AET model AC 175L resonant frequency transducer was attached to the CT specimens undergoing either IHE or HEE crack growth test. The transducer was attached to the specimens with a viscous couplant. The transducer output was passed through a filter which has a bandpass range of 125-250 KHz. Most of the extraneous noise which is below 125 KHz was thus eliminated. The filtered signal was amplified with a 60 dB preamplifier. The preamplified signal was fed to two signal processors – model 201 signal processor and model 203 amplitude distribution analyzer. The model 201 signal processor can provide an additional gain of up to 40 dB and also produce cumulative threshold counts. The threshold counts are obtained by counting the number of times the signal exceeds a predetermined threshold level. The amplitude distribution analyzer counts the individual burst events and provides a cumulative events output. In addition, the amplitude distribution analyzer also sorts the events according to their amplitudes into 50 channels over a 60 dB dynamic range. The amplitude distribution output can be obtained at any time during a test on a log or linear scale as a frequency or cumulative frequency histogram.

In the crack growth rate studies during IHE or HEE, the transducer was attached to the CT specimens by a viscous couplant and the position of the transducer on the specimens is shown in Figure 5. A total gain of 70 dB was used and the threshold was set at 0.05 volt, which was slightly above the noise level. Cumulative counts, cumulative events and amplitude distributions were recorded as a function of crack length.

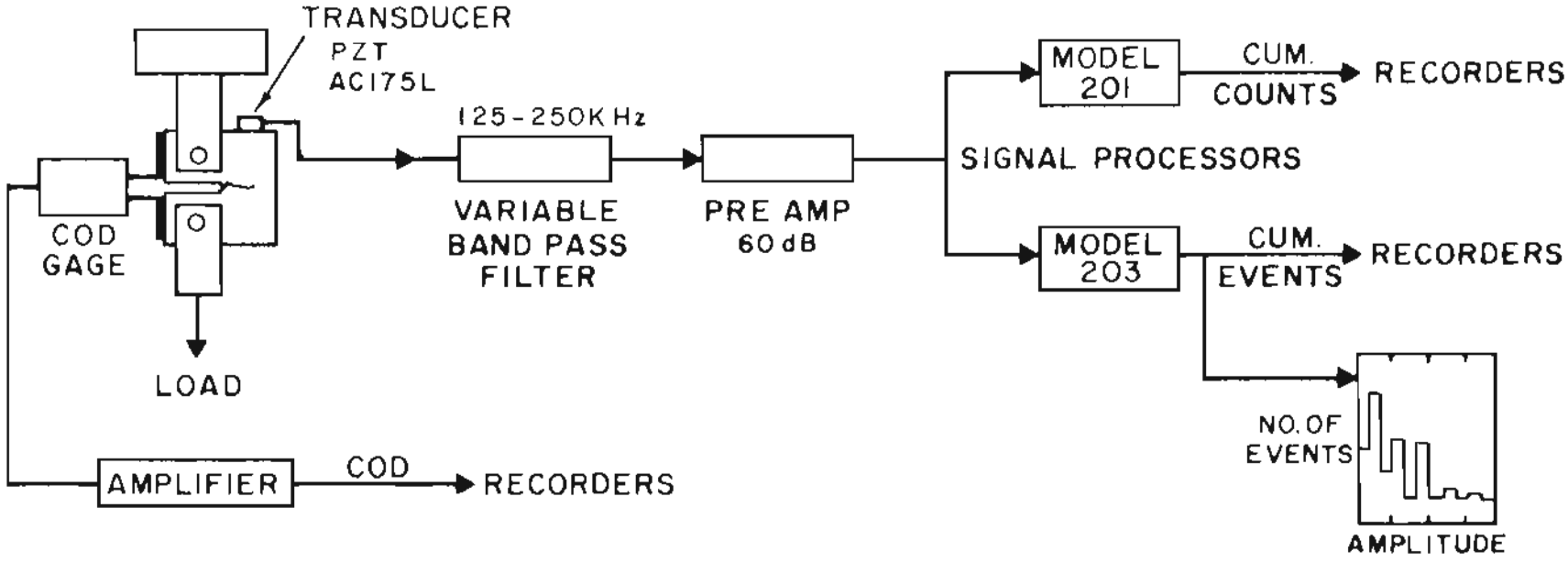

Figure 5. BLOCK DIAGRAM OF ACOUSTIC EMISSION TEST SYSTEM

3.8 FRACTOGRAPHY

The morphology of the fracture surfaces of CT specimens, from IHE as well as HEE, was studied as a function of stress intensity. A JSM 35 scanning electron microscope was used for this purpose. Because of the large depth of field of the SEM, this technique is excellent for characterizing the fracture surfaces. Fractographs were obtained at magnifications ranging from 50 to 1000X at 25 KeV secondary electron voltage.

3.9 HYDROGEN ANALYSIS

Immediately after fracture, coupons weighing about one gram were cut from the hydrogen charged CT specimens as well as the specimens exposed to the environment of 3.5 percent sodium chloride solution. These coupons were analyzed for its hydrogen content using the ultra sensitive hydrogen detector developed by the Boeing Co.[34] A schematic diagram of the hydrogen analyzer is given in Figure 6. During the time between fracture and analysis, the specimens were stored at liquid nitrogen temperature to prevent the hydrogen from diffusing out of the specimen. The hydrogen detector mentioned above can detect hydrogen concentrations of as low as a few parts per billion in a gas stream.[34].

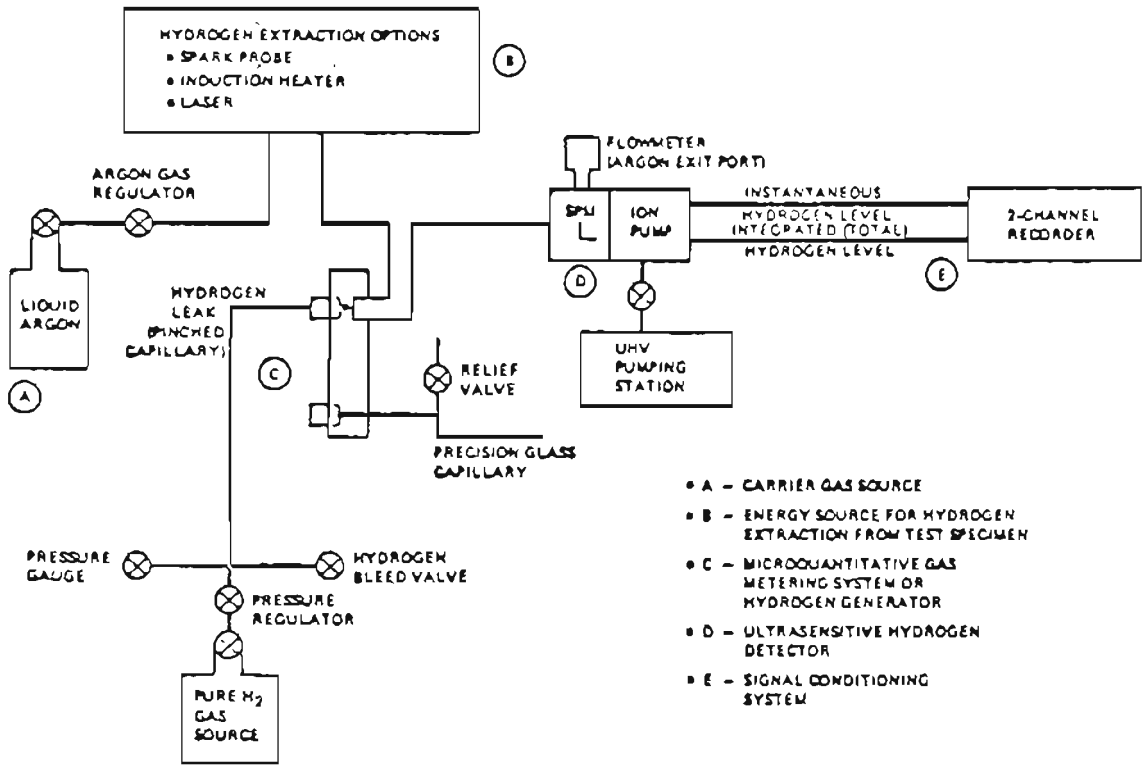

Figure 6. Schematic diagram of the hydrogen analysis instrumentation.

4. RESULTS

4.1 HEAT TREATMENT AND MICROSTRUCTURE

The heat treatments selected were such that to obtain a controlled variation in prior austenite grain size, carbide type and morphology, amount of retained austenite, amount of grain boundary segregation, and martensite substructure. An extensive microstructural analysis on AISI 4340 steel has been carried out by Wood and his coworkers[1,4,35-37] and Ritchie et al.[27] with the following results:

1. Austenitizing at temperatures between 870°C and 1200°C produces a range of grain sizes from 25 to 250 μm.

2. Austenitizing at 870°C followed by oil quenching results in an martensitic microstructure consisting of both plate and laths. A trace amount of retained austenite is also observed (Figure 7). Increasing the austenitizing temparature to 1200°C increases the amount of retained austenite (Figure 8) and the proportion of lath to plate martensite.

3. Austenitizing at 1200° and step quenching to 870°C prior to oil quenching results in a martensitic structure consisting of both plates and laths. An extensive network of 100-200Å thick films of retained austenite is also present, same as in the case of direct oil quench from 1200°C.

4. Tempering at 180° produces a tempered martensitic structure with a fine precipitate of epsilon carbide[27]. The retained austenite is not affected by 180°C tempering treatment.

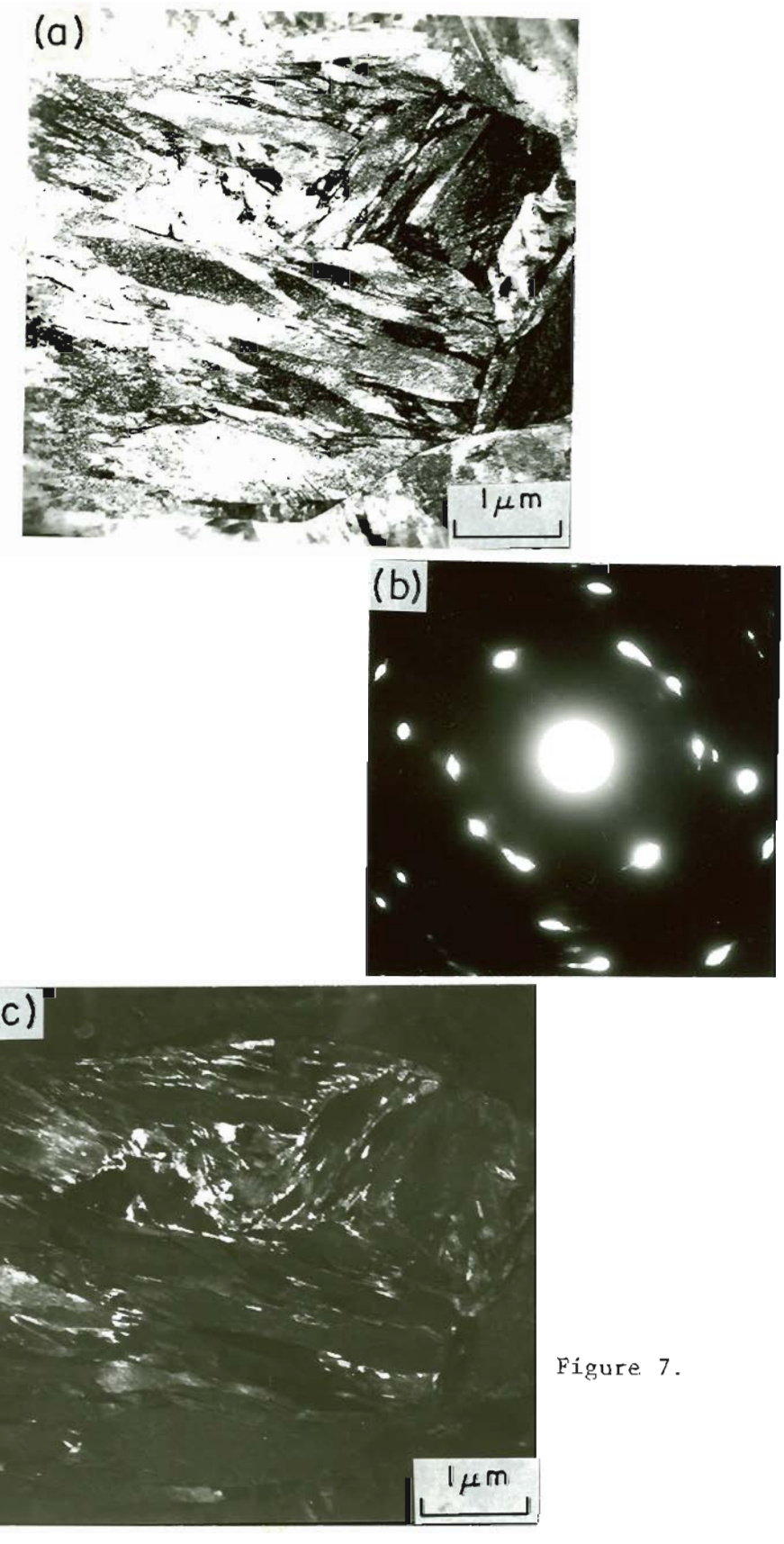

Figure 7.

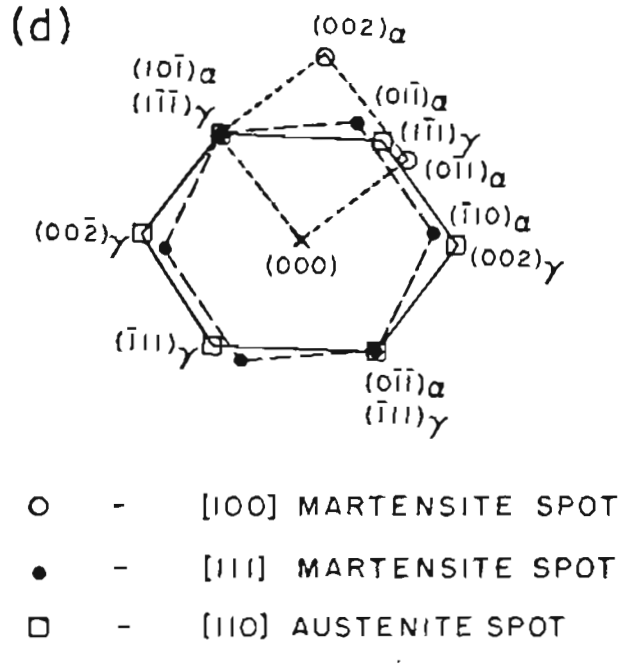

Figure 7. (cont.) Transmission electron micrographs of 4340 steel austenitised at 870°C.

(a) B.F. image showing prior austenite grain boundaries.

(b) S.A.D. pattern.

(c) D.F. image of (002) austenite reflection showing reverse contrast of retained austenite films.

(d) Schematic diagram of S.A.D. pattern.

(Courtesy: Cheruvu N. Sastry)

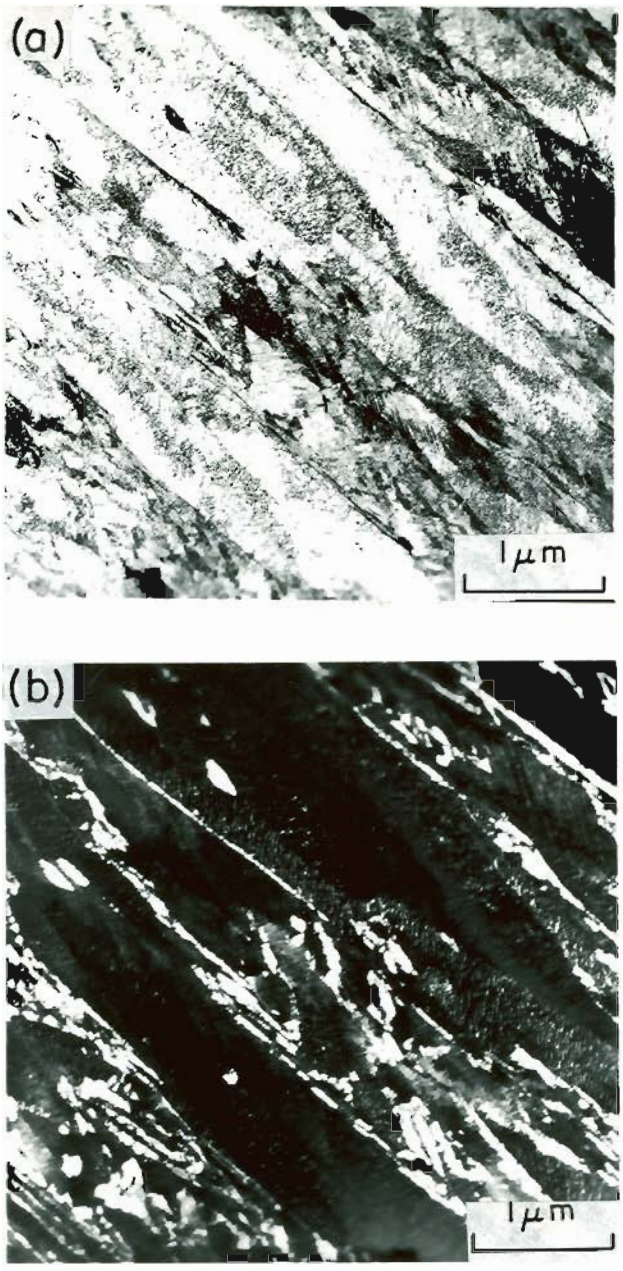

Figure 8. Transmission electron micrographs of 4340 steel austenitized at 1200°C.

(a) B.F. image showing prior austenite grain boundary.

(b) D.F. image of (111) austenite reflection showing retained austenite films at the lath and grain boundaries.

(Courtesy: Cheruvu N. Sastry)

5. Tempering at 280°C produces a tempered martensitic structure with coarse cementite[27] and the retained austenite decomposes to lower bainite or tempered martensite.

It has been shown that austenitizing at higher (1200°C) temperature followed by fast quenching prevents segregation of trace elements like antimony, phosphorus, sulfur, to prior austenitic grain boundaries[28,30]. Thus austenitizing at higher temperature would produce a larger grain size and less grain boundary segregation. Austenitizing at 1200°C and step quenching to 870°C followed by oil quenching would produce a larger grain size and extensive grain boundary segregation.

In the case of hydrogen assisted cracking, when the fracture mode is predominantly intergranular, substructural features like martensite morphology are not expected to play a primary role. The important microstructural features that would affect the susceptibility of the steel to hydrogen assisted cracking would then be grain size, the presence of retained austenite and carbides on the grain boundaries and the extent of grain boundary segregation. These are summarized in Table 4.

4.2 THRESHOLD STRESS INTENSITY AND MICROSTRUCTURE

The threshold stress intensity below which hydrogen assisted cracking did not occur was determined for each heat treatment for HEE and IHE (Table 5). The corresponding microstructural features for these heat treatments are listed in Table 4. The threshold stress intensity depends on yield strength and microstructure of the material, for a given hydrogen activity. In AISI 4340 steel, the variation in yield strength

above 200 ksi does not have any significant effect on threshold stress intensity and hence only the microstructural variations are expected to have an influence on the threshold stress intensity. The variation of threshold stress intensity as a function of microstructure was the same in both HEE and IHE.

Comparison of 870/180 and 1100/180 heat treatments revealed that the threshold stress intensity increased slightly. The only difference between the two microstructures was the difference in grain size. The increase in grain size from 25 μm to 125 μm increased the threshold stress intensity by about 1.5 ksi in. A similar trend was observed when 1100/280 and 870/280 heat treatments were compared, grain size being the only difference between these two heat treatments. A further increase in the grain size to 225 μm in the case of 1200/280 and to 250 μm in the case of 1200-870/280 heat treatments again similarly improved the threshold stress intensity.

The 870/180 and 870/280 heat treatments showed the same value of threshold stress intensity and apparently the change in carbide morphology from epsilon carbide to cementite did not affect the threshold stress intensity. Similarly, no change in threshold stress intensity was observed when 1100/180 and 1100/280 heat treatments were compared, thus eliminating the effect of carbide morphology on threshold stress intensity.

The difference in microstructures resulting from 1200/180 and 1200-870/180 heat treatment was that the step treatment resulted in grain

boundary segregation of impurities. The comparison of threshold stress intensity revealed that the impurity segregation slightly reduced the threshold stress intensity. Similarly, the impurity segregation in the case of 1200-870/280 slightly reduced the threshold stress intensity as compared to 1200/280 heat treatment. The 1200/180 heat treatment that resulted in grain and lath boundary retained austenite showed the highest threshold stress intensity among all the heat treatments, although the decomposition of retained austenite by 280°C tempering treatment reduced the threshold stress intensity. This is apparent when the threshold stress intensity values of 1200/180 and 1200/280 or 1200-870/180 and 1200-870/280 heat treatments were compared. The retained austenite was not affected by 180°C temper but was decomposed at 280°C to either lower bainite or tempered martensite.

The effect of microstructure on threshold stress intensity for hydrogen assisted cracking (IHE as well as HEE) can be summarized as follows: (i) increase in grain size and the amount of retained austenite increased the threshold stress intensity, (ii) grain boundary segregation and decomposition of retained austenite at the grain boundaries both decreased the threshold stress intensity and (iii) the carbide morphology did not have any effect on threshold stress intensity. The threshold stress intensity for any given heat treatment was generally lower in the case of IHE as compared to HEE.

4.3 CRACK GROWTH RATES AND MICROSTRUCTURE

The variation of crack growth rate as a function of instantaneous stress intensity (K) for all microstructures tested for IHE as well as HEE are shown in Figures 9-24. The curves show several clearly distinguishable regions of crack growth rates which are characteristically observed for hydrogen assisted cracking, namely region I, where the crack growth rate is strongly dependent on stress intensity,region II, where the rate is essentially independent of stress intensity, and region III, which is not always observed, where the crack growth rate increases rapidly as stress intensity approaches fracture toughness of the material. The constant crack growth rate in region II is thought to be the result of a limiting hydrogen mass transport or diffusion controlled mechanism[38]. The region III is suggested to be a result of a combined effect of hydrogen assisted cracking and mechanical failure by overload[38]. No suitable explanation of region I crack growth rate exists.

The region II crack growth rates are presented as a function of heat treatment (in Figures 25-26).For comparison, the region II crack growth rate was defined at a stress intensity at the mid point of K_{th} and K_{Ic}. This eliminated the effect of region I or II in distorting the region II crack growth rates. Even though the overall variations in stage II crack growth rates were small, some definite trends dependent upon the microstructure were evident. As was in the case of threshold stress intensity results, the variation in region II crack growth rates as a function of heat treatments was the same in the case of HEE as well as IHE.

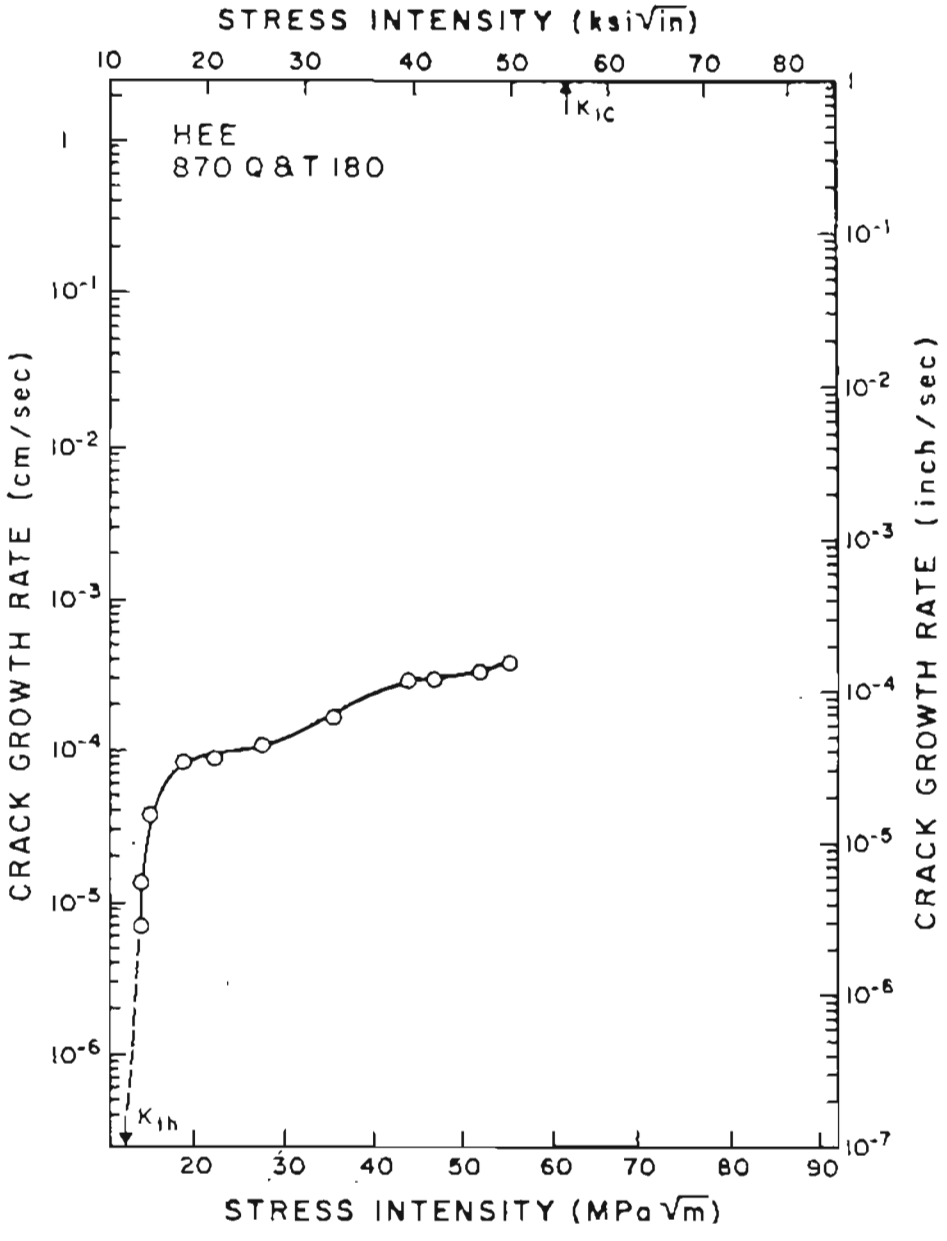

Figure 9. Crack growth rate as a function of stress intensity for 870/180 heat treatment in the environment of 3.5% NaCl solution (HEE).

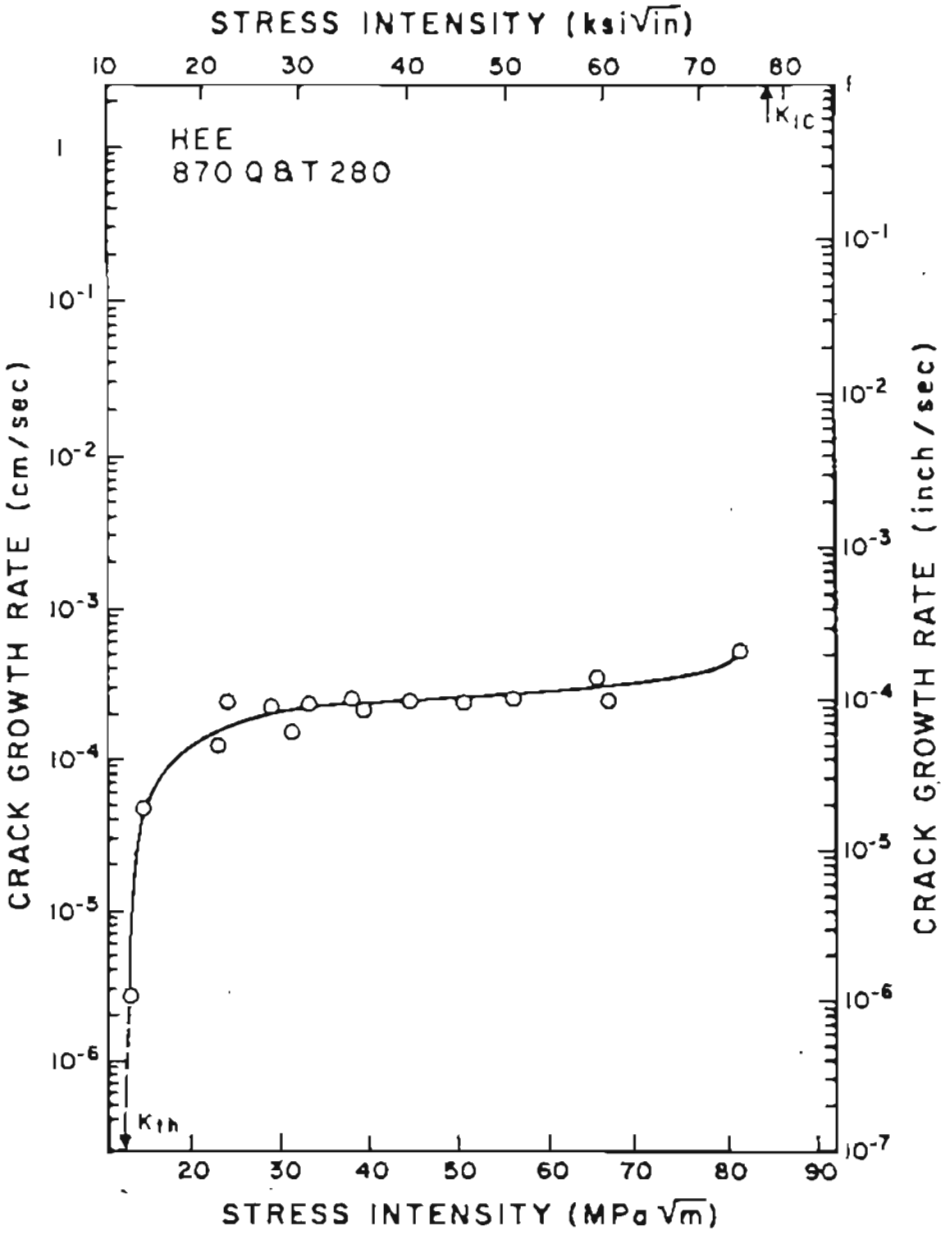

Figure 10. Crack growth rate as a function of stress intensity for 870/280 heat treatment in the environment of 3.5% NaCl solution (HEE)

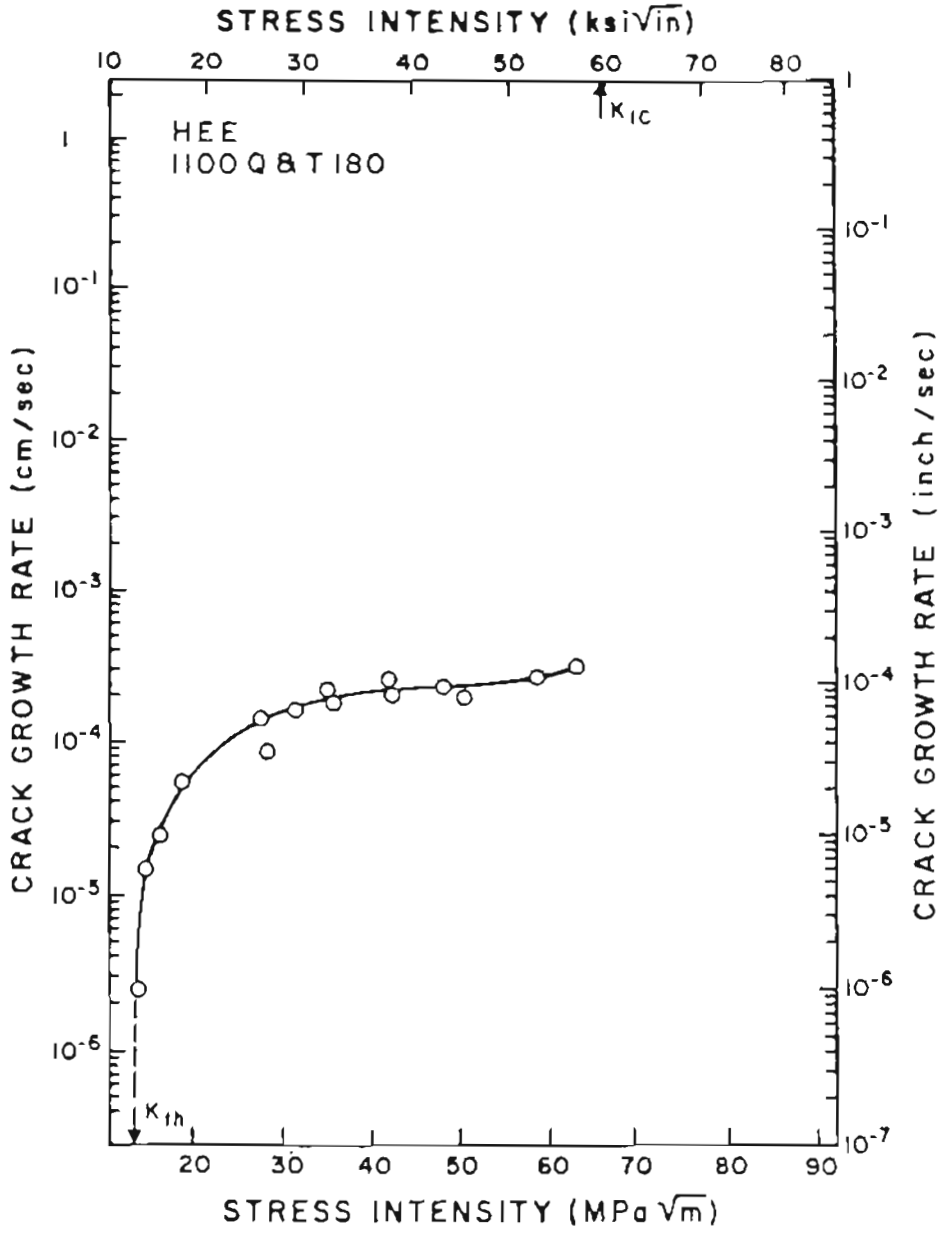

Figure 11. Crack growth rate as a function of stress intensity for 1100/180 heat treatment in the environment of 3.5% NaCl solution (HEE)

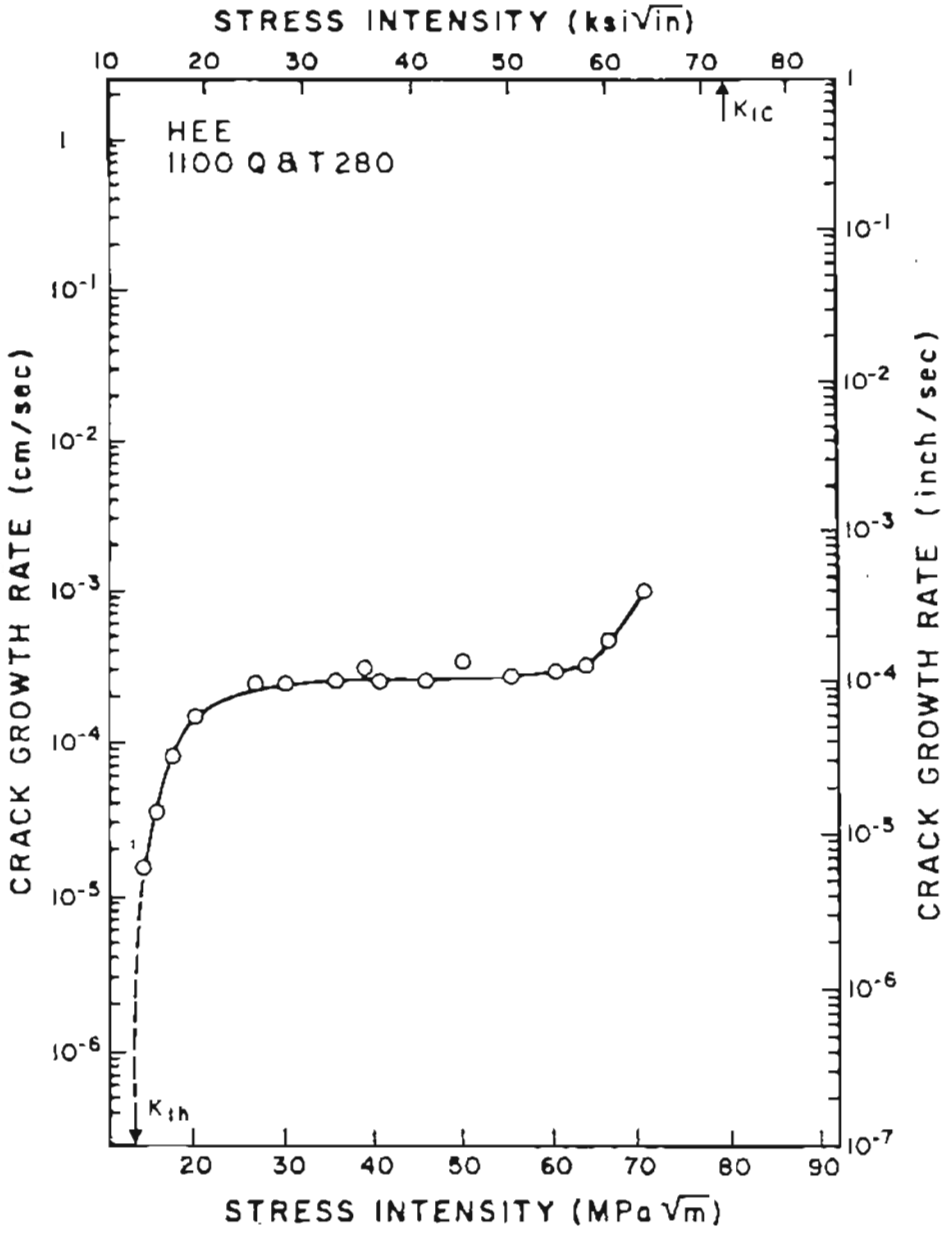

Figure 12. Crack growth rate as a function of stress intensity for 1100/280 heat treatment in the environment of 3.5% NaCl solution (HEE).

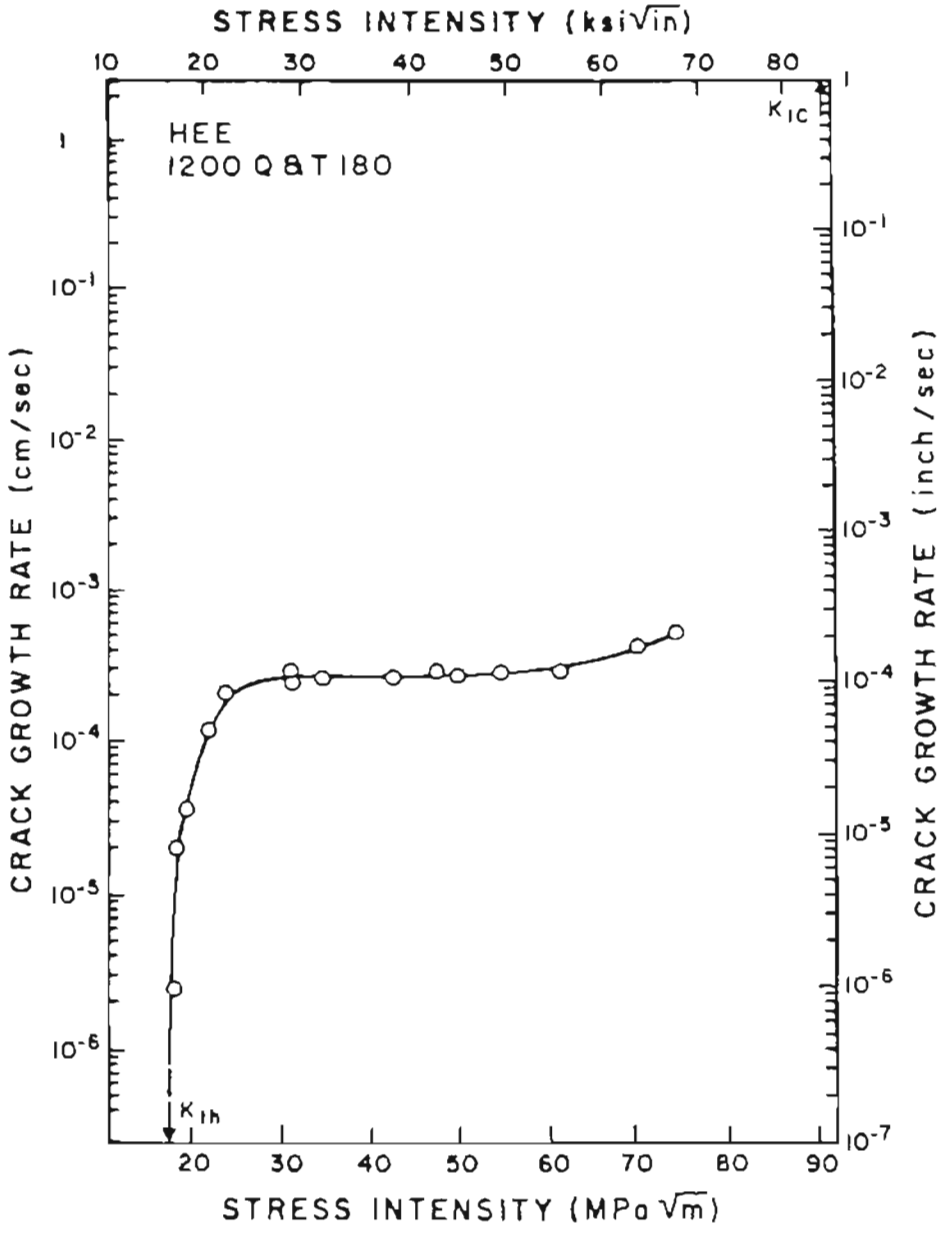

Figure 13. Crack growth rate as a function of stress intensity for 1200/180 heat treatment in the environment of 3.5% NaCl solution (HEE).

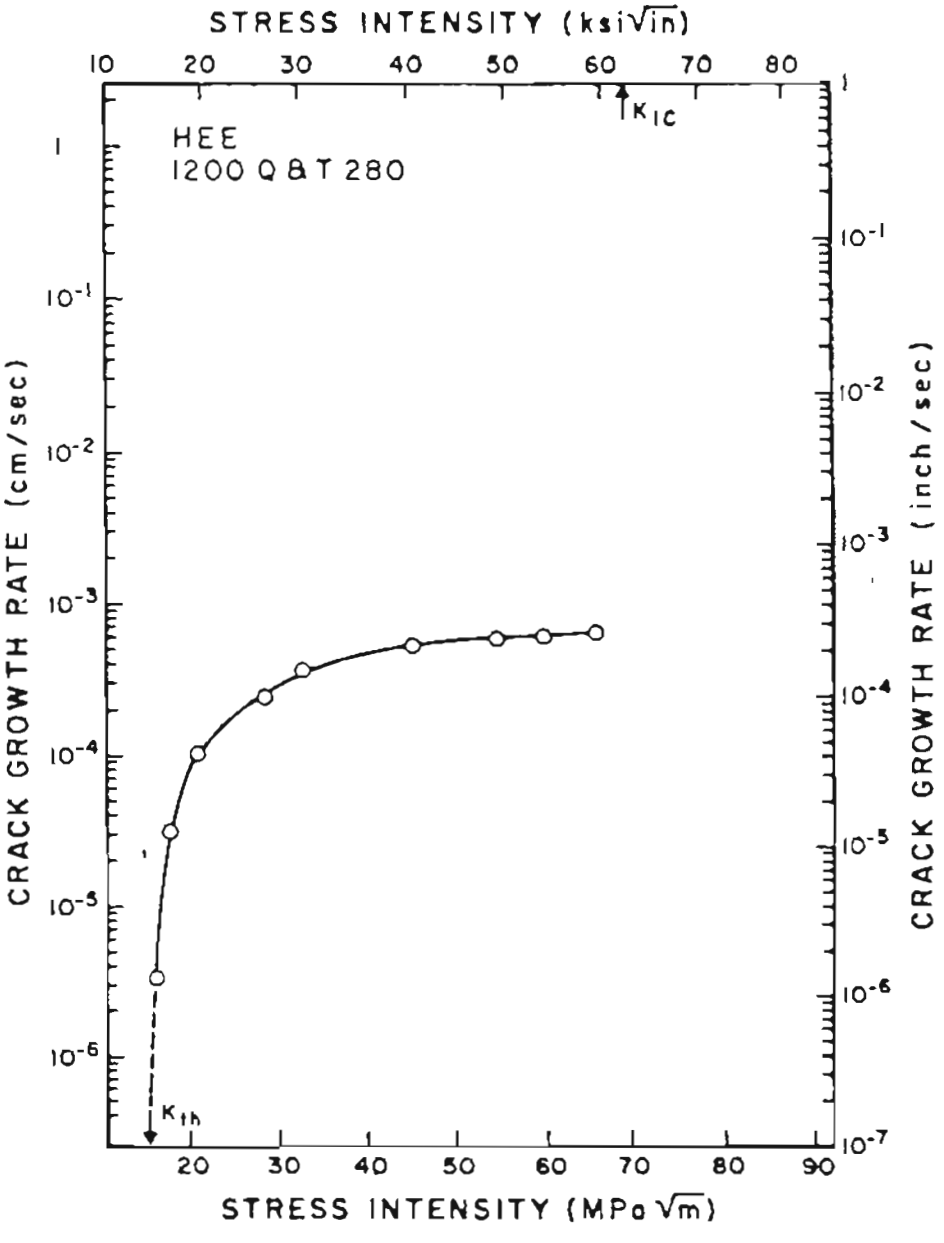

Figure 14. Crack growth rate as a function of stress intensity for 1200/280 heat treatment in the environment of 3.5% NaCl solution (HEE).

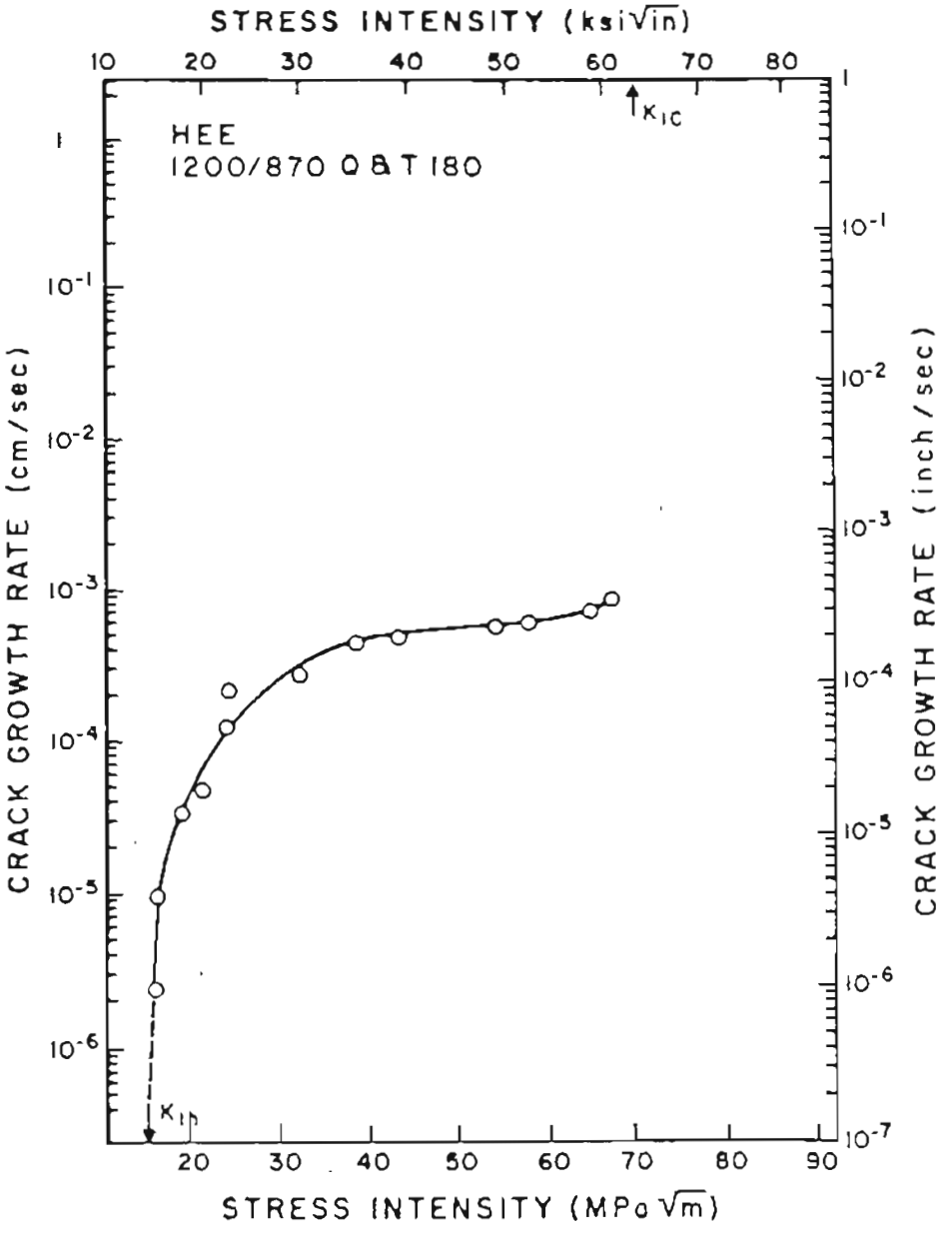

Figure 15. Crack growth rate as a function of stress intensity for 1200-870/180 heat treatment in the environment of 3.5% NaCl solution (HEE).

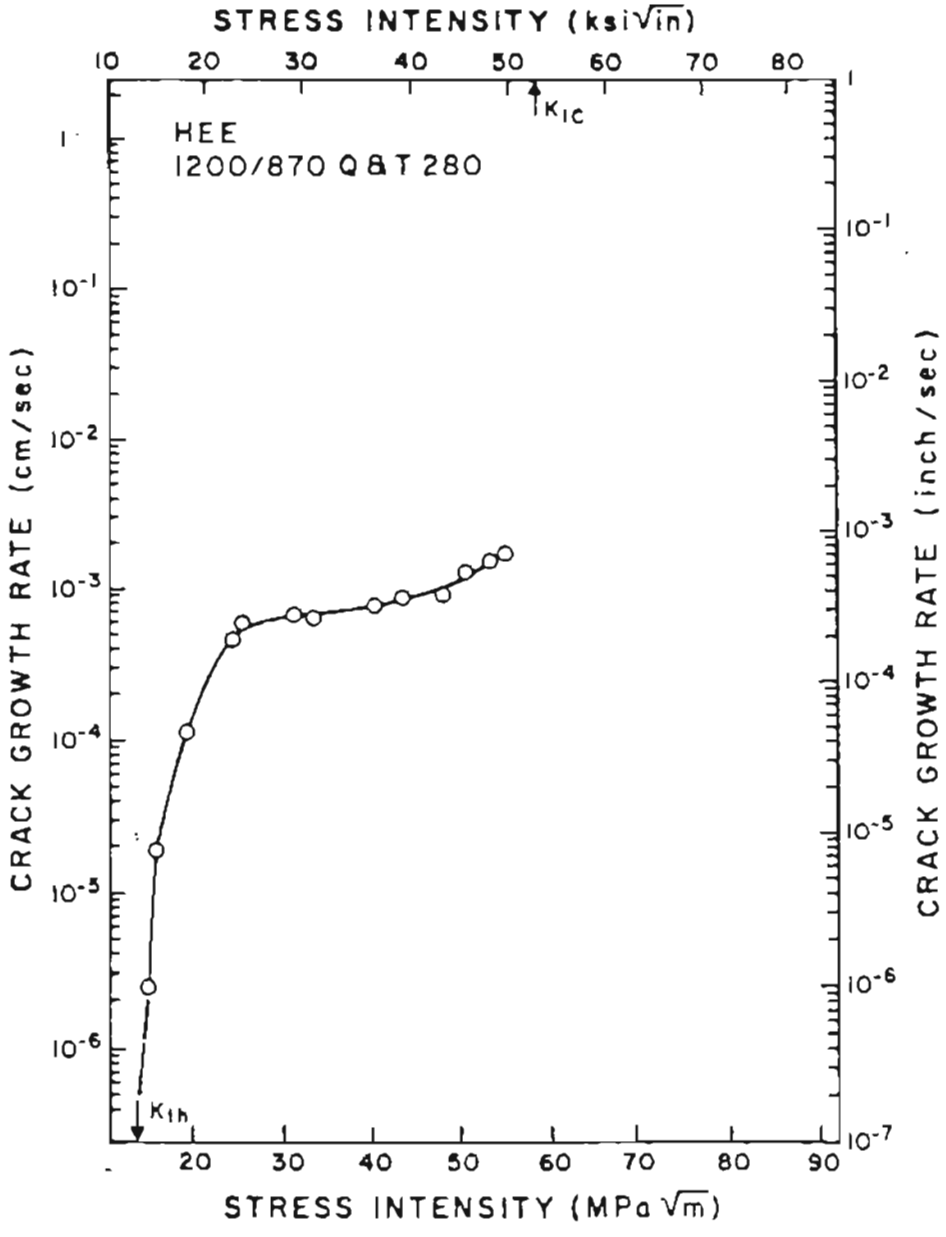

Figure 16. Crack growth rate as a function of stress intensity for 1200-870/280 heat treatment in the environment of 3.5% NaCl solution (HEE).

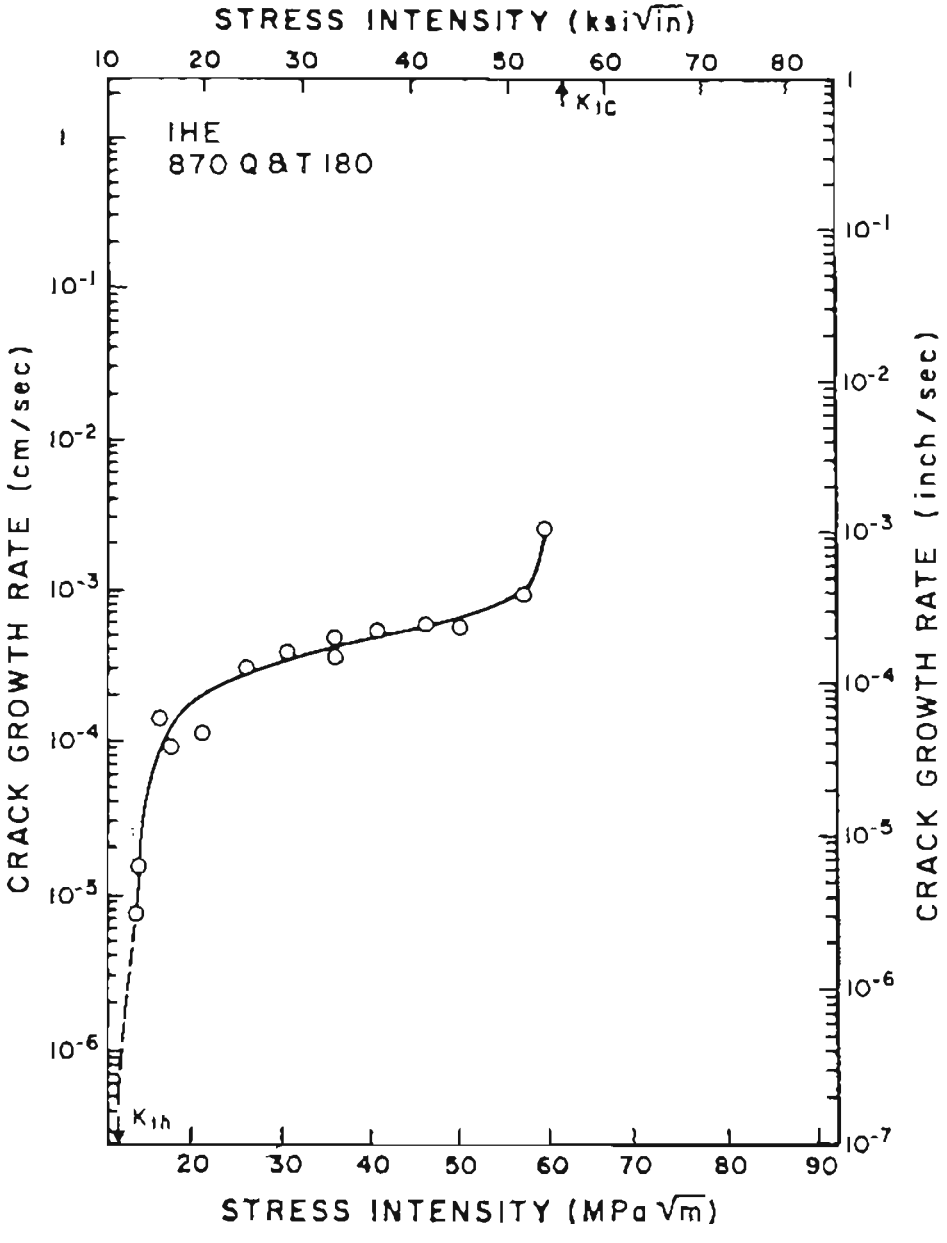

Figure 17. Crack growth rate as a function of stress intensity 870/180 heat treatment for hydrogen charged specimens (IHE).

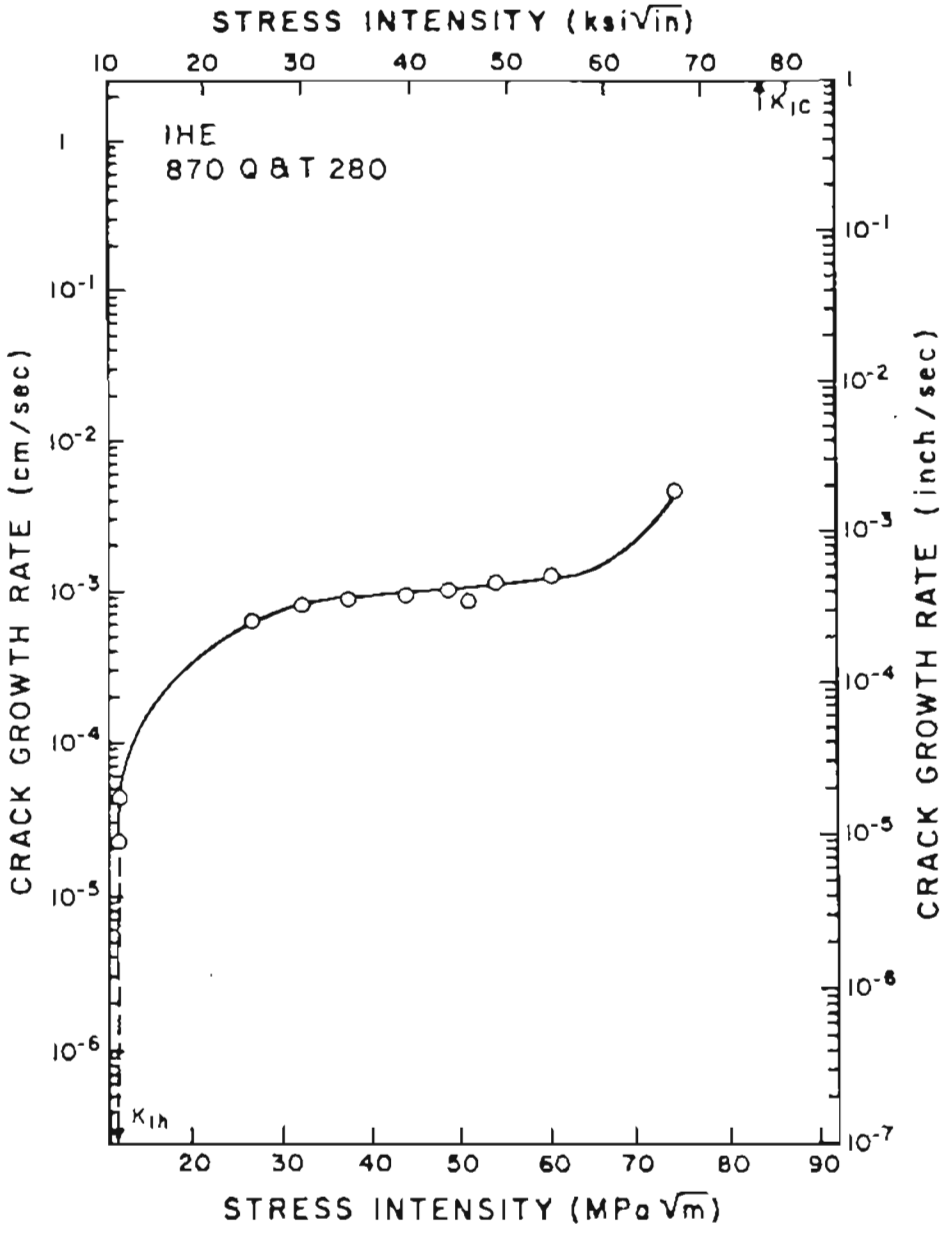

Figure 18. Crack growth rate as a function of stress intensity for 870/280 heat treatment for hydrogen charged specimens (IHE).

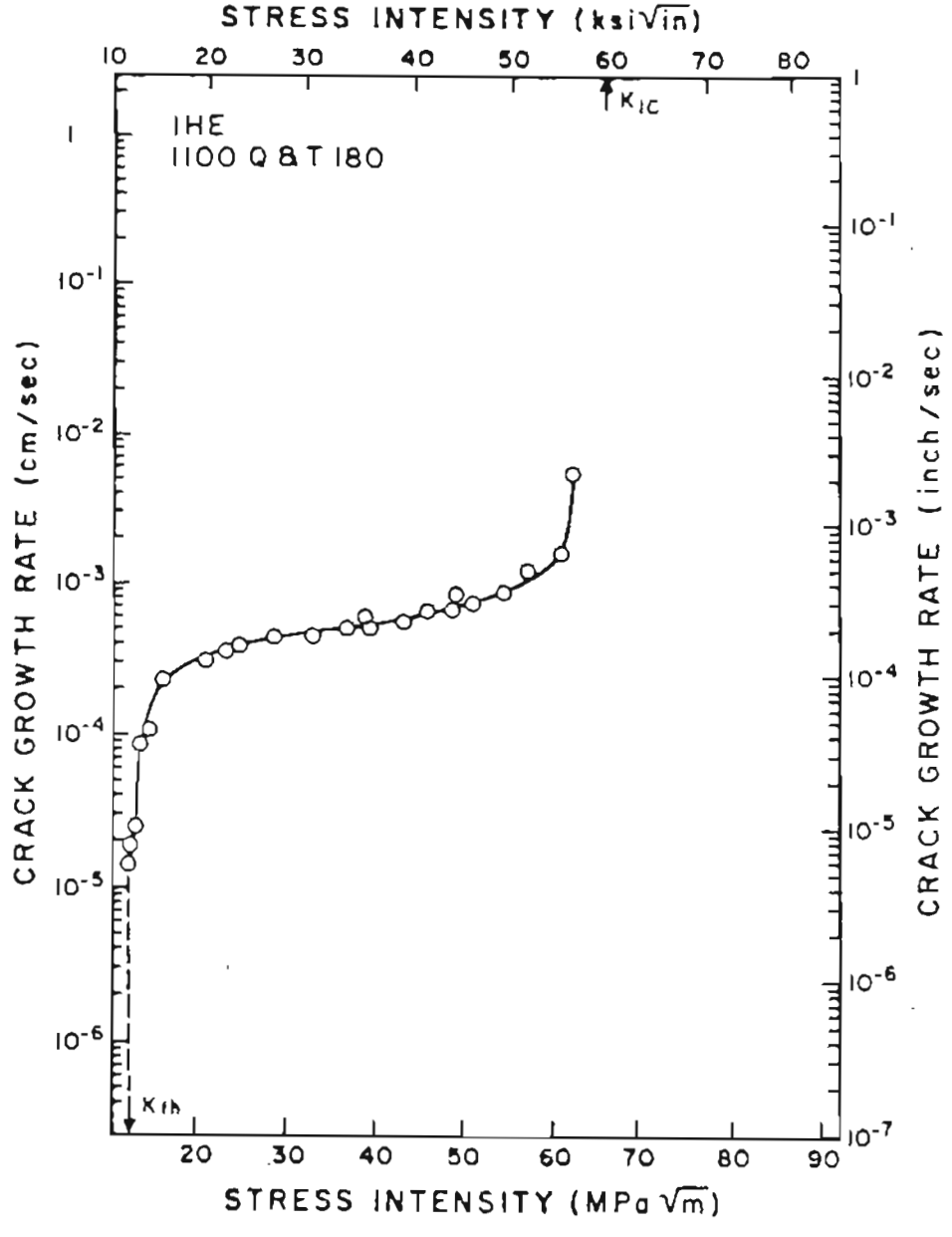

Figure 19. Crack growth rate as a function of stress intensity for 1100/180 heat treatment for hydrogen charged specimens (IHE).

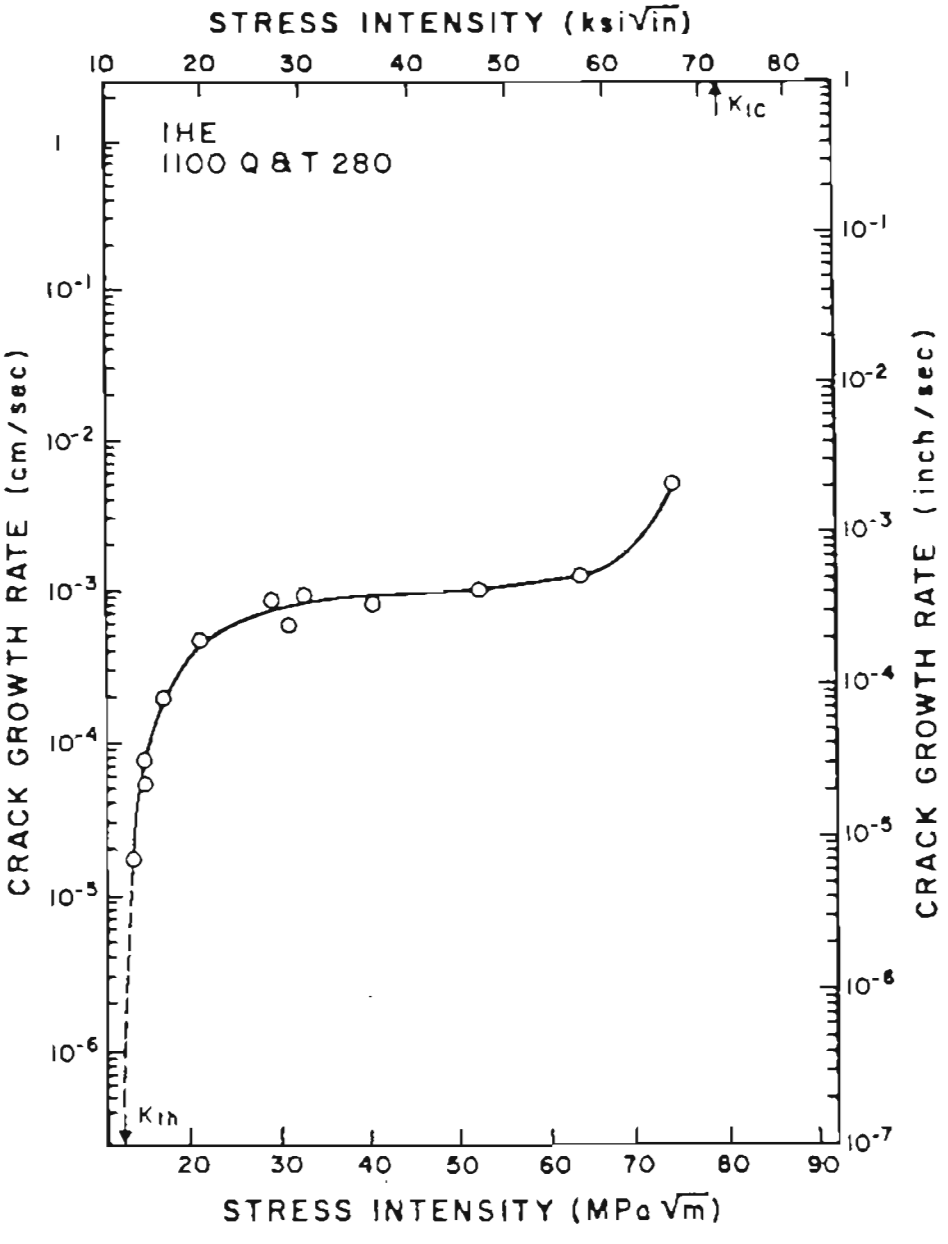

Figure 20. Crack growth rate as a function of stress intensity for 1100/280 heat treatment for hydrogen charged specimens (IHE).

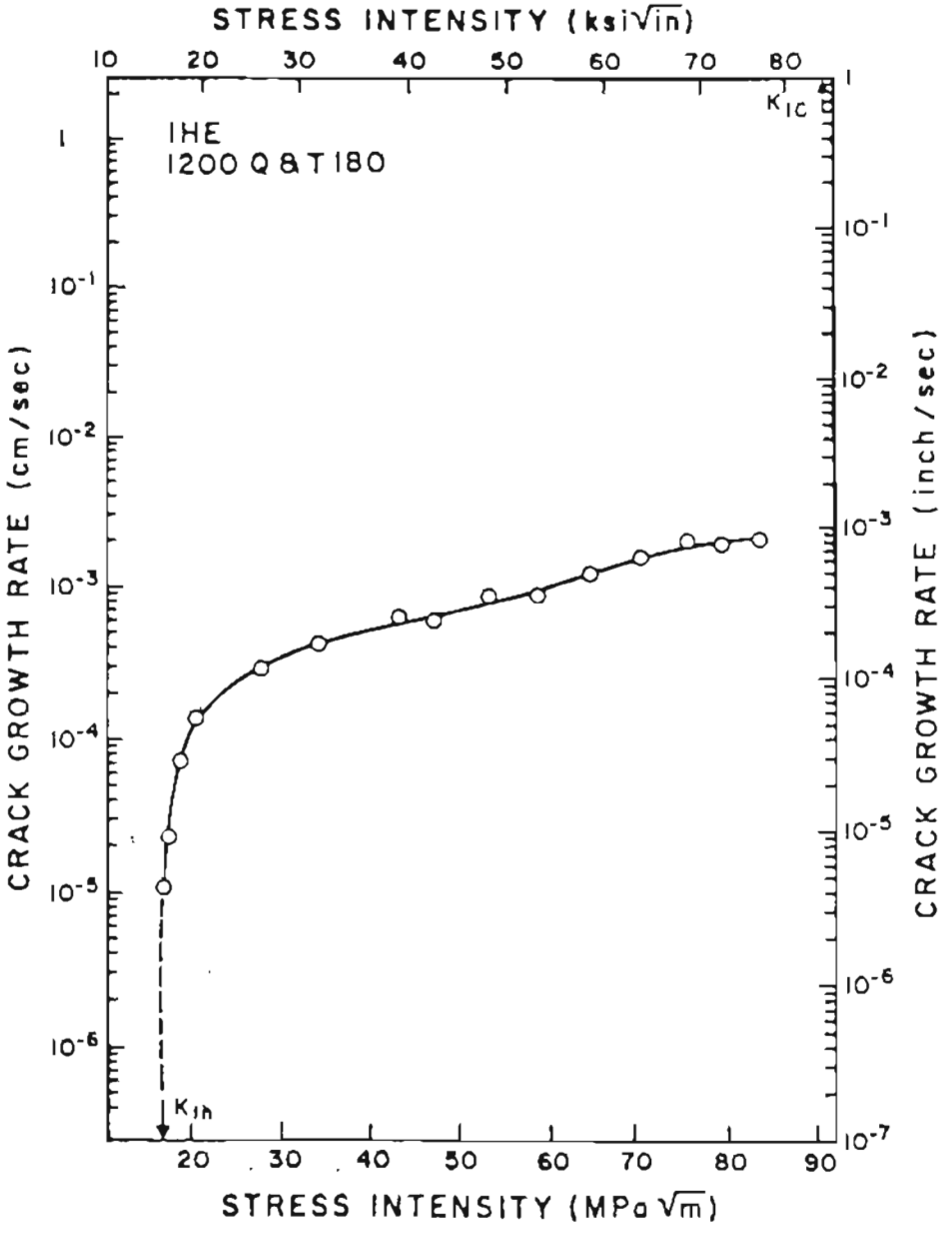

Figure 21. Crack growth rate as a function of stress intensity for 1200/180 heat treatment for hydrogen charged specimens (IHE).

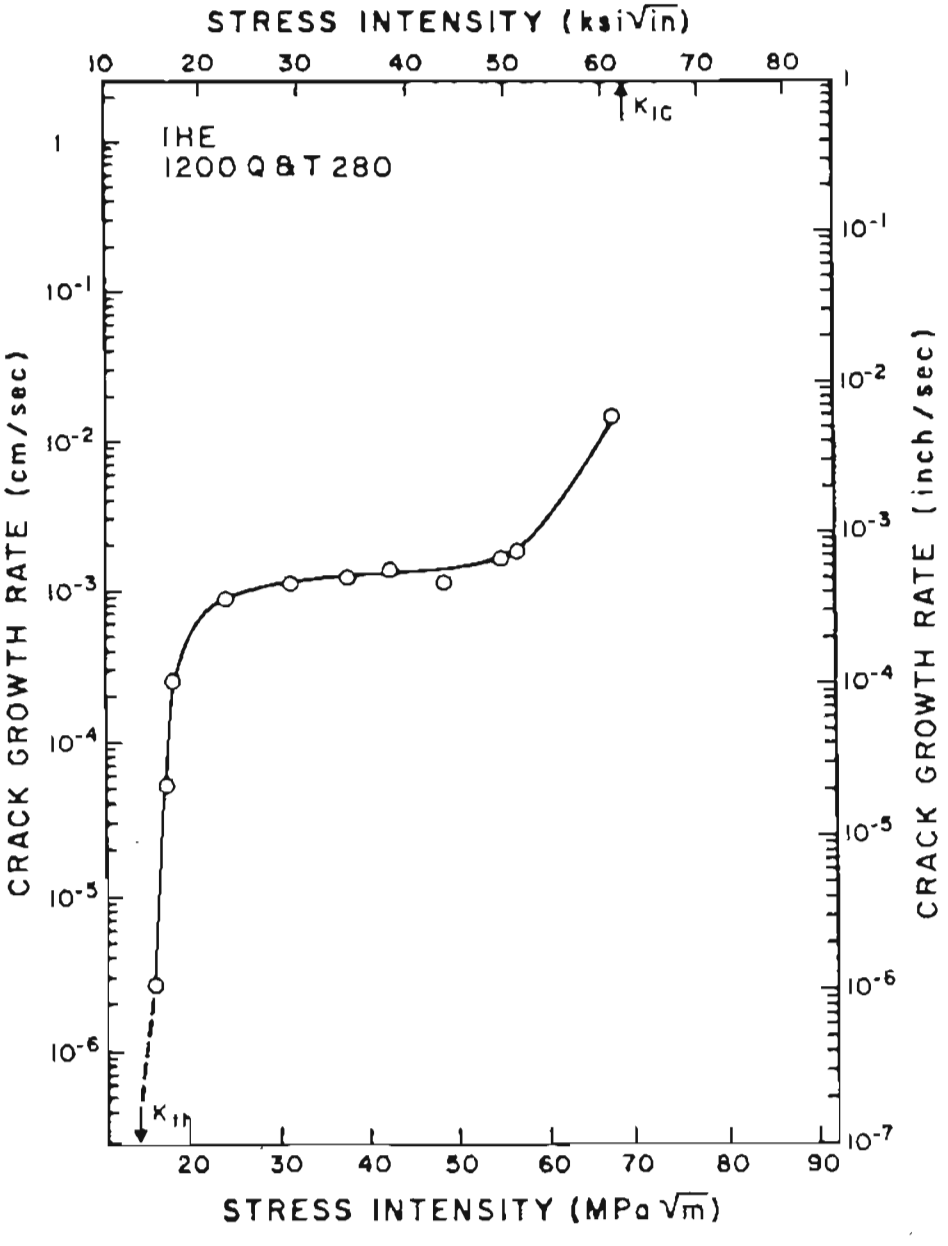

Figure 22. Crack growth rate as a function of stress intensity for 1200/280 heat treatment for hydrogen charged specimens (IHE).

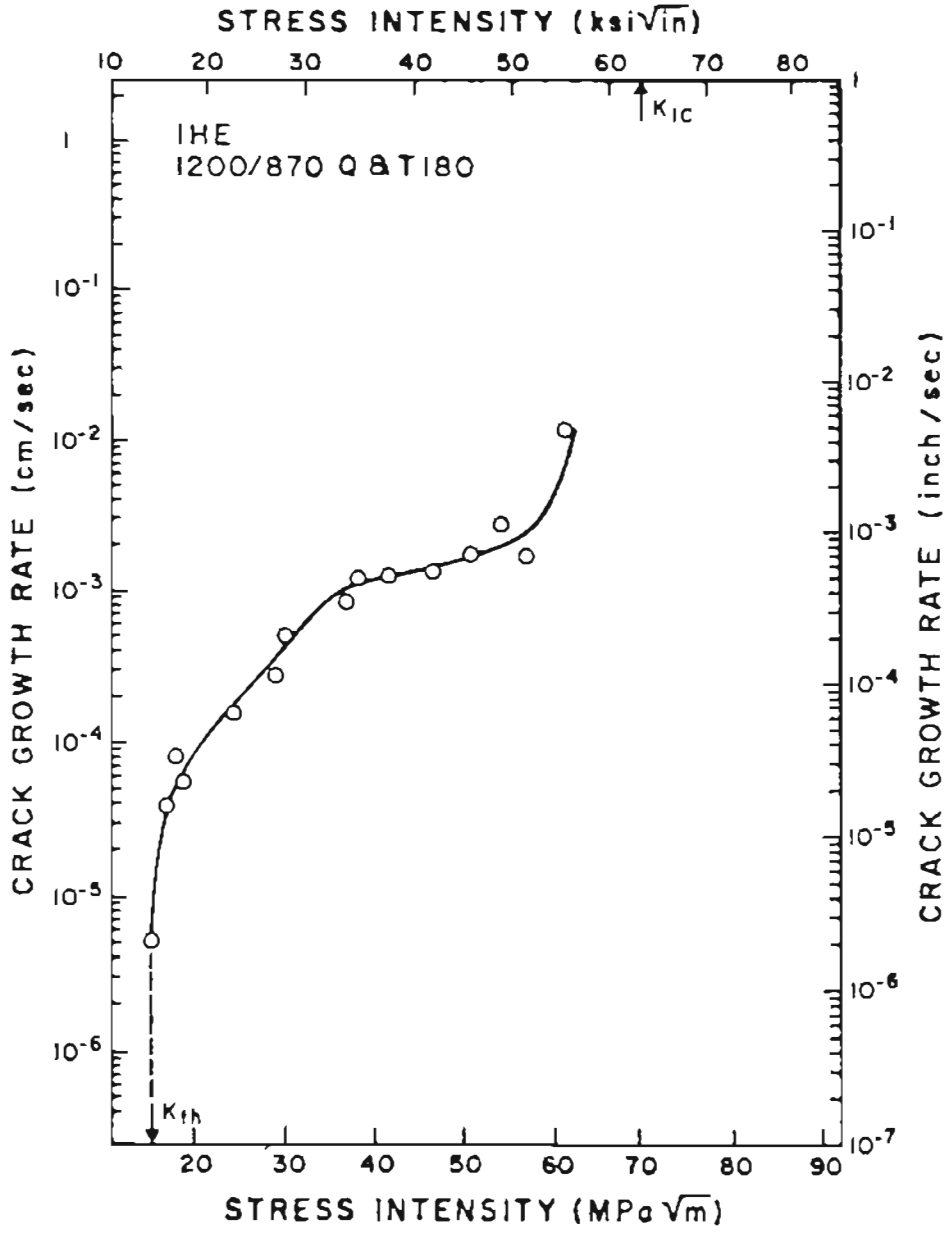

Figure 23. Crack growth rate as a function of stress intensity for 1200-870/180 heat treatment for hydrogen charged specimens (IHE).

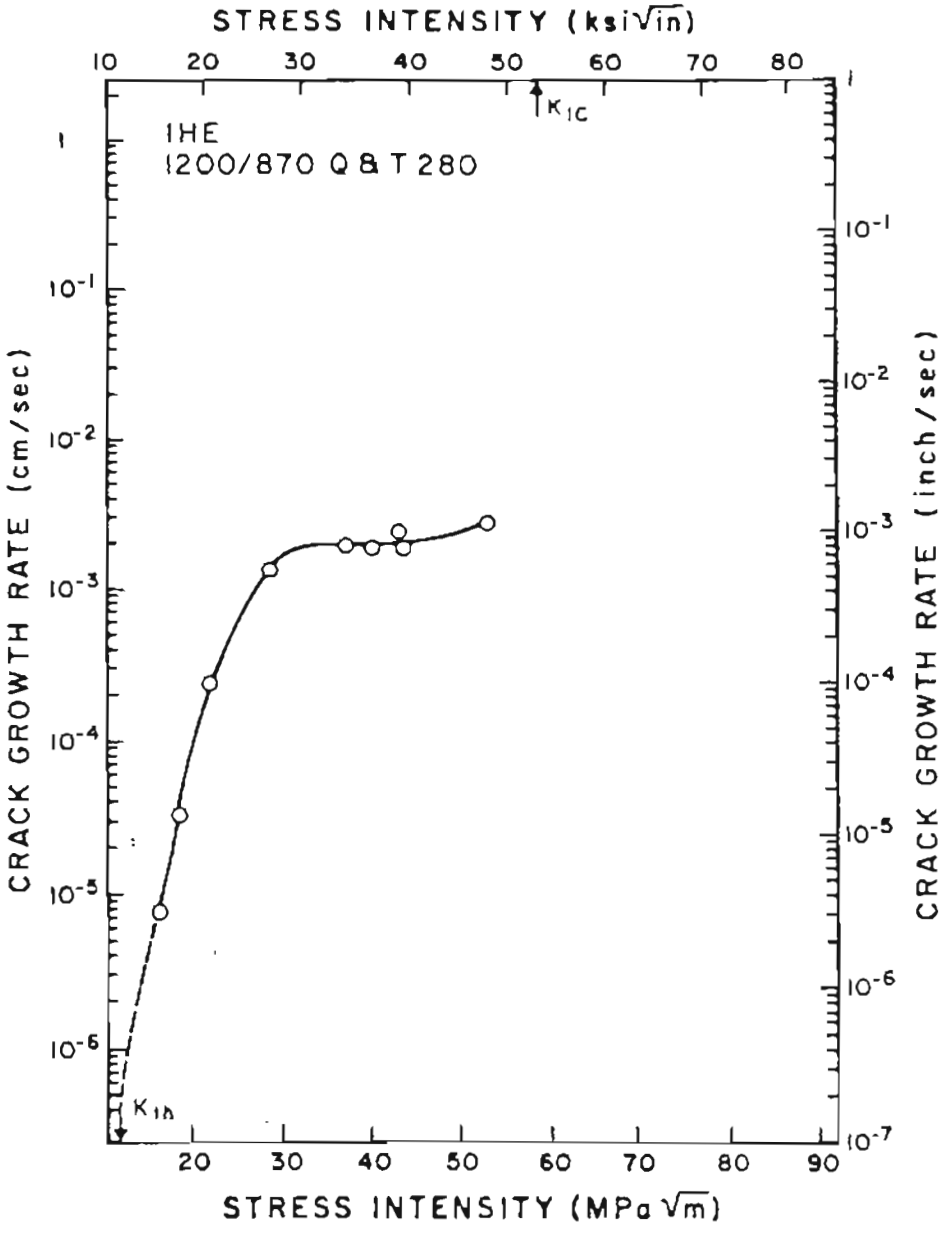

Figure 24. Crack growth rate as a function of stress intensity for 1200-870/280 heat treatment for hydrogen charged specimens (1HE).

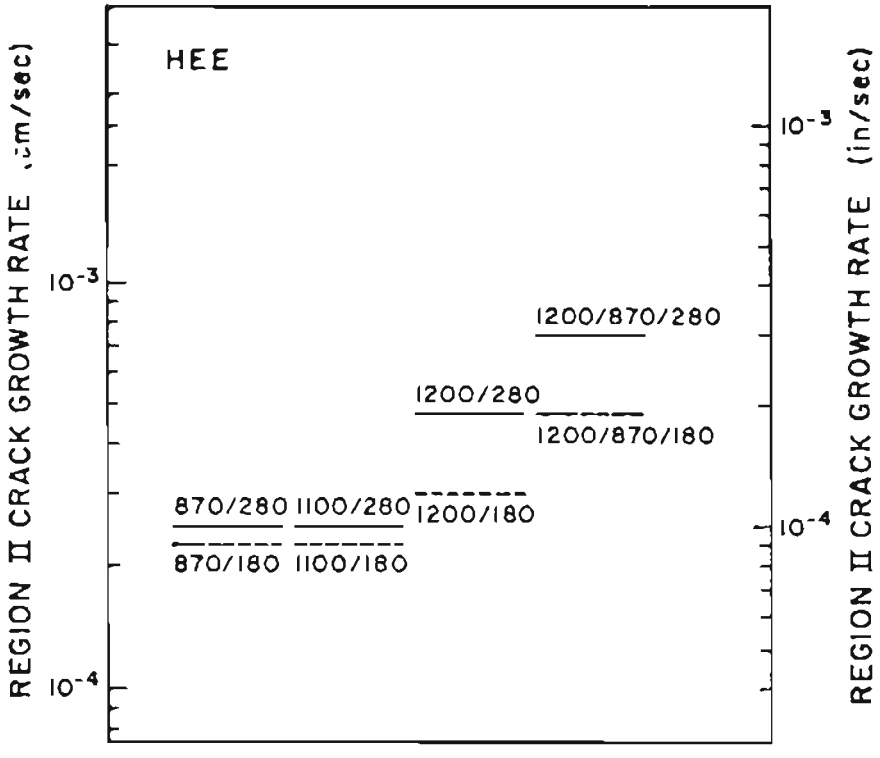

Figure 25. Region II crack growth rates for various heat treatments in the environment of 3.5% NaCl solution (HEE). The x-axis here has no significance.

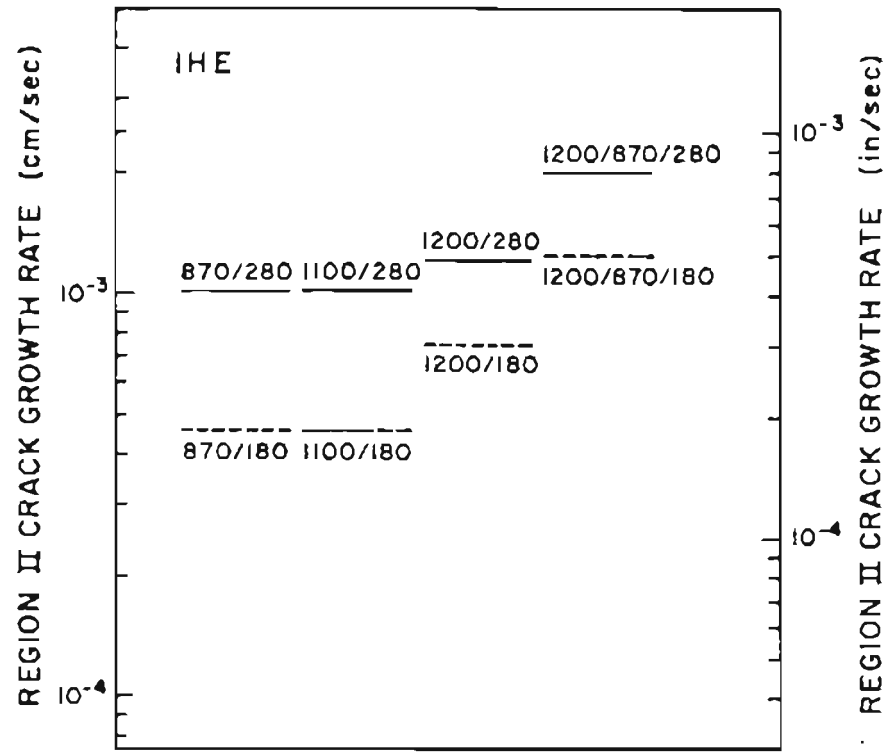

Figure 26. Region II crack growth rates for various heat treatments for hydrogen-charged specimens (IHE). The x-axis here has no significance.

Comparison of heat treatments 870/180 and 870/280 revealed that the region II crack growth rates increased slightly in the case of 280°C temper. This increase in crack growth rate is attributed to a change in carbide morphology from fine epsilon carbide to coarser cementite. A similar increase in crack growth rate from 1100/180 to 1100/280 was observed for the same reason. The increase in crack growth rates that occurred after tempering at 280° as opposed to 180°C in the case of 1200°C and 1200-870°C austenitizing treatments was greater than in the case of 870° and 1100°C austenitizing treatments. This was because in 1200°C and 1200-870°C austenitizing treatments, in addition to the change in carbide morphology, the decomposition of retained austenite because of 280°C temper also made the structure more susceptible to hydrogen assisted cracking and thus further increased the region II crack growth rates.

The only difference between the 870/180 and 1100/180 or between the 870/280 and 1100/280 heat treatments was that grain size which increased by about five times by 1100°C austenitization treatment. This did not have any effect on the region II crack growth rates. So, the grain size per se did not contribute to any change in region II crack growth rates.

The 1200/180 heat treatment exhibited a slightly higher region II crack growth rate as compared to 870/180 or 1100/180. In addition to larger grain size, which was shown not to have any effect on crack growth rate, the microstructure resulting from 1200/180 heat treatment contained about 5 percent retained austenite present as fine films on lath and grain boundaries. The presence of this mechanically unstable retained austenite thus slightly increased the stage II crack growth rate.

The 1200-870/280 heat treatment exhibited slightly higher region II crack growth rate than the 1200/280 heat treatment. The two microstructures are similar in all respects except that the former had more grain boundary segregation because of the step quenching to 870°C prior to oil quenching.

Summarizing the region II crack growth rate results as related to the microstructure, a change from epsilon carbide to cementite, the presence of mechanically unstable retained austenite and enhanced grain boundary segregation — all increased the region II crack growth rates. The grain size did not have any effect on region II crack growth rates.

4.4 FRACTOGRAPHY

Following crack growth rate testing, the fracture surface of each specimen was examined to determine the failure mode. The fractographs were obtained at various stress intensity levels, ranging from K_{th} to K_{Ic}, for each heat treatment. A typical set of fractographs showing fracture morphology as a function of stress intensity is shown in Figure 27. The failure mode was predominantly intergranular for all heat treatments. There was very little plasticity when the stress intensity was near K_{th} and the extent of plasticity increased with stress intensity. It was not possible to distinguish any sharp difference in fracture appearance for various regions of crack growth rates. These fractography results were similar for HEE and IHE.

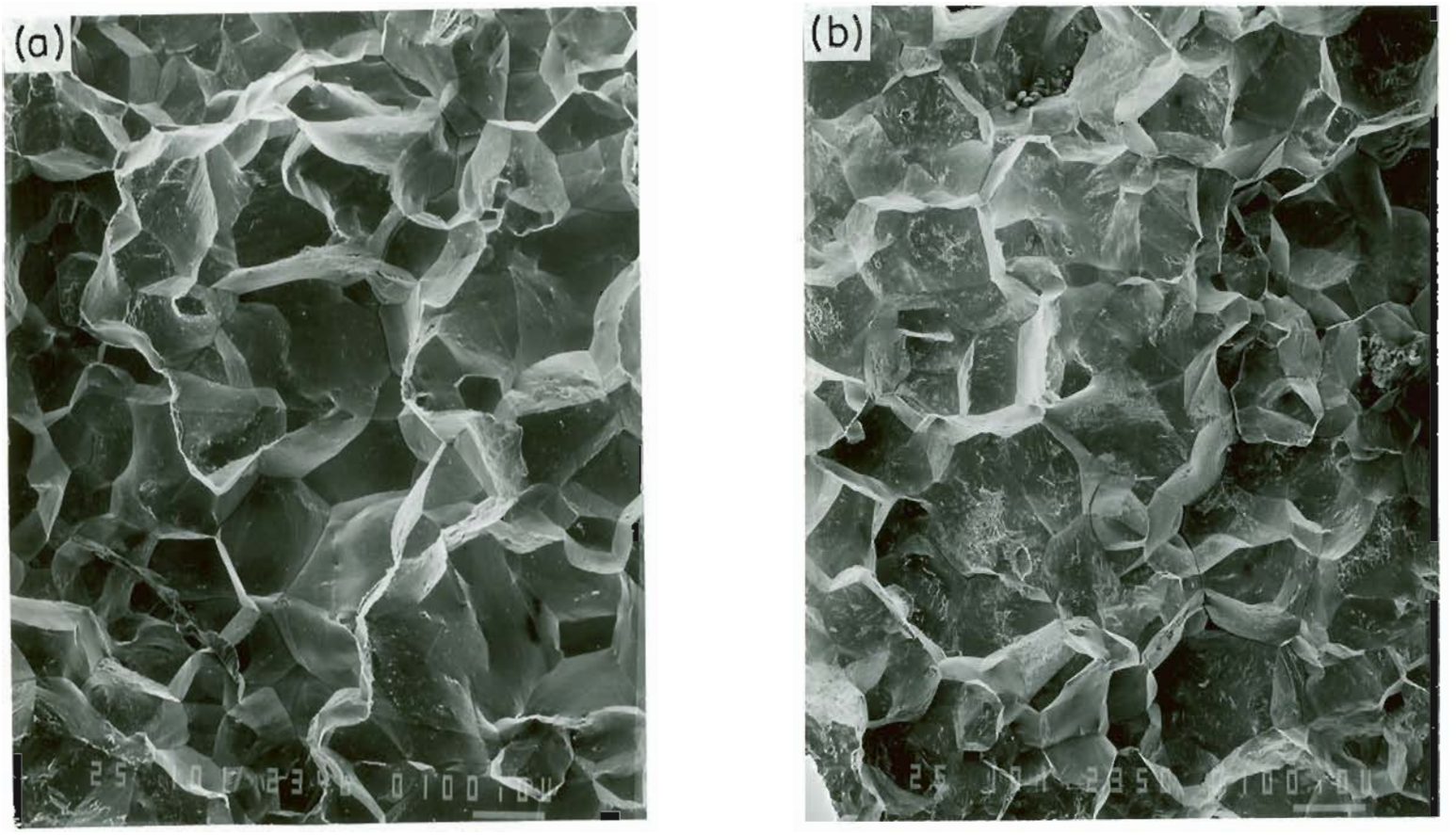

Figure 27. A typical set of fractographs showing predominantly intergranular nature of hydrogen-assisted fracture. At higher stress intensities, some plasticity is visible on fractured surfaces. (Heat treatment 1100/280).

Stress intensity-- (a) 19 ksi$\sqrt{in}$ (b) 47 ksi$\sqrt{in}$

Figure 27. A typical set of fractographs showing predominantly intergranular nature of hydrogen-assisted fracture. At higher stress intensities, some plasticity is visible on fractured surfaces. (Heat treatment 1100/280).

Stress intensity-- (c) 74 ksi$\sqrt{in}$

4.5 ACOUSTIC EMISSION RESULTS

During hydrogen assisted cracking of compact tension specimens, acoustic emission parameters were recorded as a function of crack length. Cumulative counts, cumulative events and amplitude distribution were the acoustic emission variables that were studied as a function of crack length, stress intensity and microstructure. Since there are no standard procedures available for analysis and interpretation of acoustic emission data, the following data reduction technique was used for analysis and interpretation of acoustic emission data. The background for using this methodology is described in the Appendix.

The initial results considered were cumulative events as a function of crack length for compact tension specimen under static load. Figure 28 shows two experimental curves of cumulative events as a function of crack length for two different loads. Considering one of the cumulative events – crack length curve (Figure 28), it is seen that the number of events for a given crack extension (i.e. the slope of the curve) increased with increasing crack length. For the compact tension geometry, the stress intensity increases with increasing crack length for a constant load. Hence the increase in the number of events for a given crack length increased at higher crack lengths solely because of increase in stress intensity accompanying increase in crack length. Now, comparing the two curves in Figure 28, the curve which was obtained from compact tension specimen at higher load (1800 lbs) is above the one with 1400 lbs. This was again due to the same reason – for a given crack length, the stress intensity was higher for higher load. The general

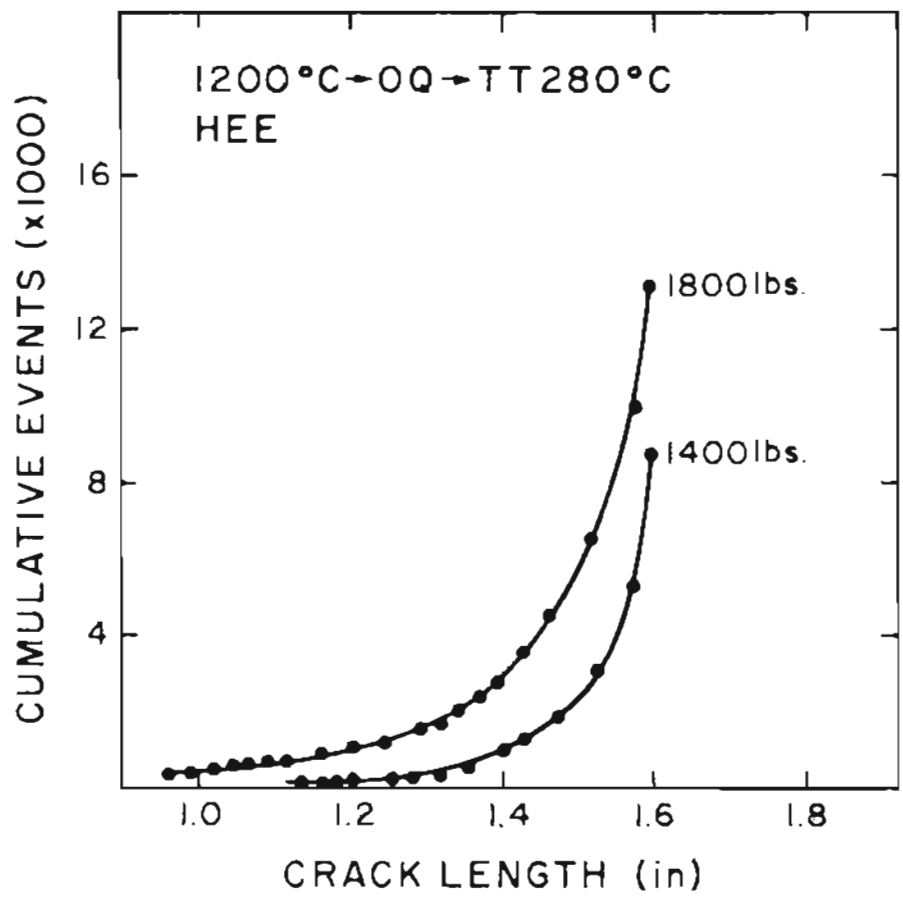

Figure 28. Cumulative acoustic emission events shown as a function of crack length and static load.

nature of the cumulative events versus crack length data was the same for all heat treatments — namely that the number of events for a given incremental crack length increased with increasing stress intensity.

For further analysis of these data, a cubic spline interpolation was used to smoothen the crack length — cumulative events curve. The resulting smoothened curve was differentiated once to obtain the dE/dA (number of events per unit extension in crack length) and this was plotted as a function of stress intensity. Such curves for various grain sizes were plotted on the same graph (Figure 29). This technique made it possible to present the interrelationship between four variables — crack length, cumulative events, stress intensity and grain size. Such dE/dA data as a function of stress intensity and grain size are presented for each tempering temperature and for HEE as well IHE (Figures 29-32). In each case, the general trend observed was that the dE/dA increased both with increasing stress intensity and with grain size.

The cumulative counts showed exactly the same trend as the cumulative events, that is, for a given heat treatment and hydrogen source, the cumulative counts were linearly related to the cumulative events. For this reason, the average counts per event, which remained constant for a given heat treatment and hydrogen source but varied from one heat treatment to another and also with hydrogen source, are reported separately (Table 6-9). In general, as shown in Table 6-9, the average counts per event increased with grain size. For a given heat treatment, the average counts per event were higher when the source of hydrogen was internal as compared to the external. The basis for using the counts per events analysis is discussed in the Appendix.

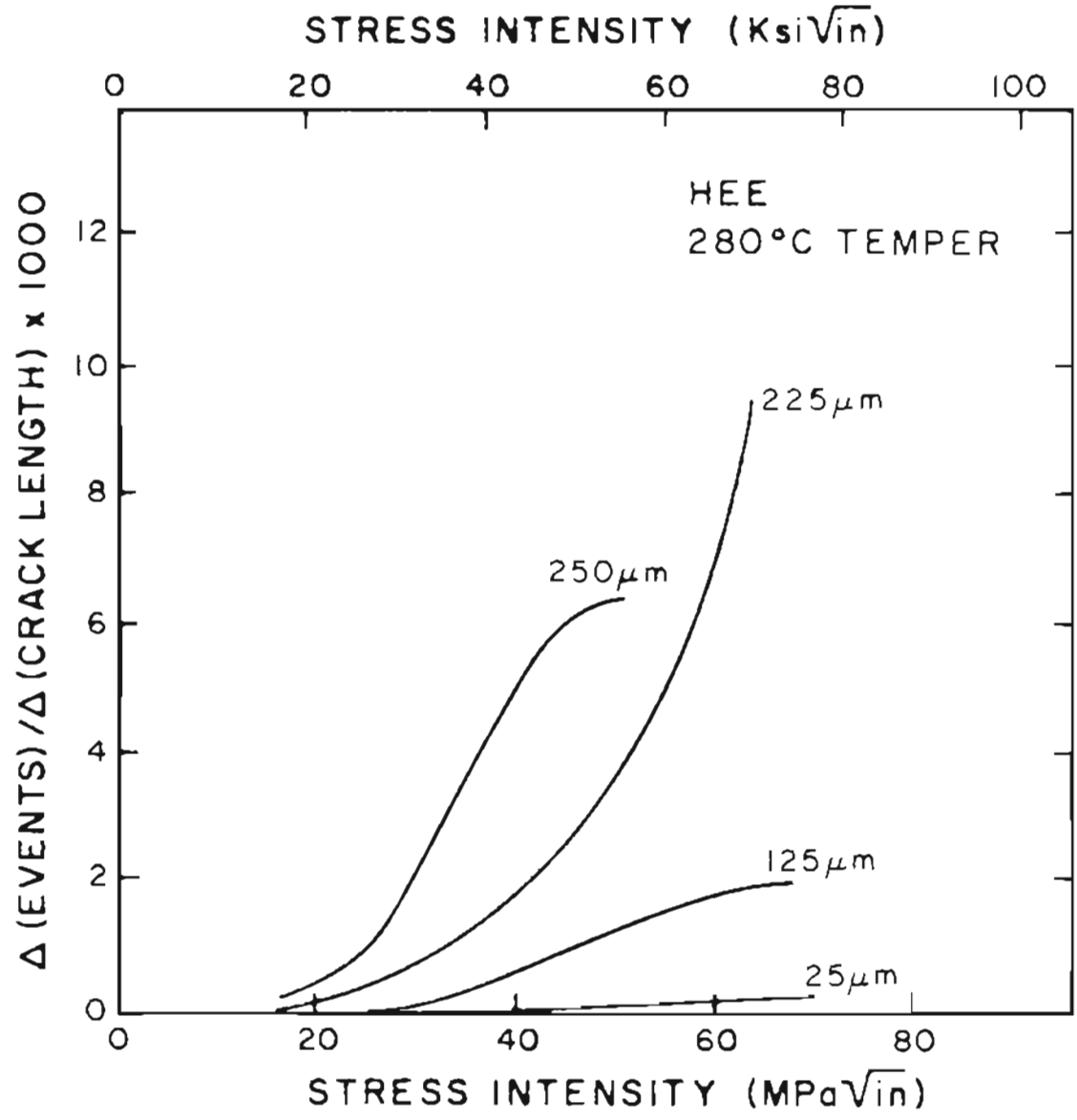

Figure 29. Acoustic emission events rate (dE/dA) as a function of stress intensity and grain size for HEE (tempering temperature 280°C).

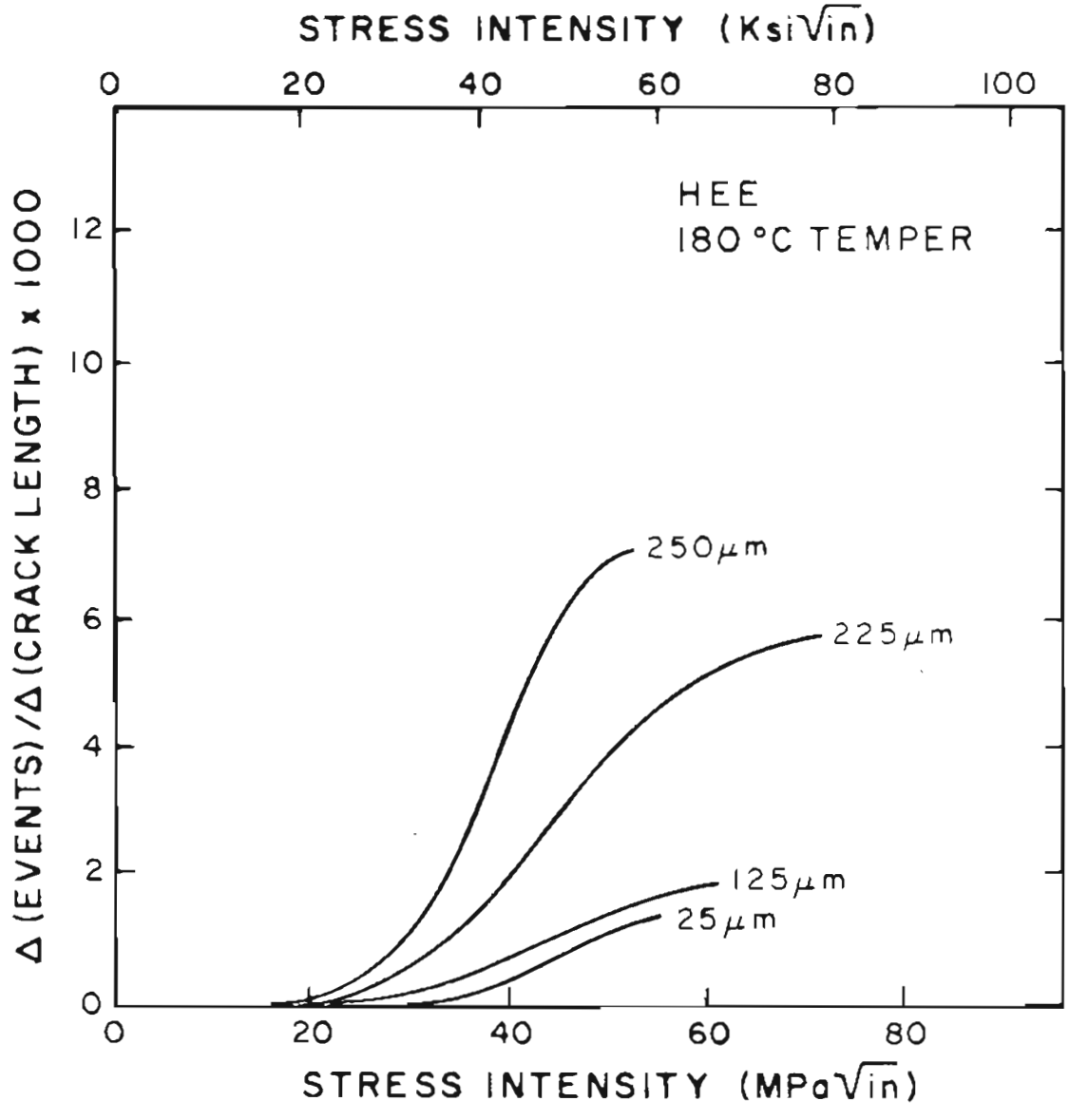

Figure 30. Acoustic emission events rate (dE/dA) as a function of stress intensity and grain size for HEE (tempering temperature 180°).

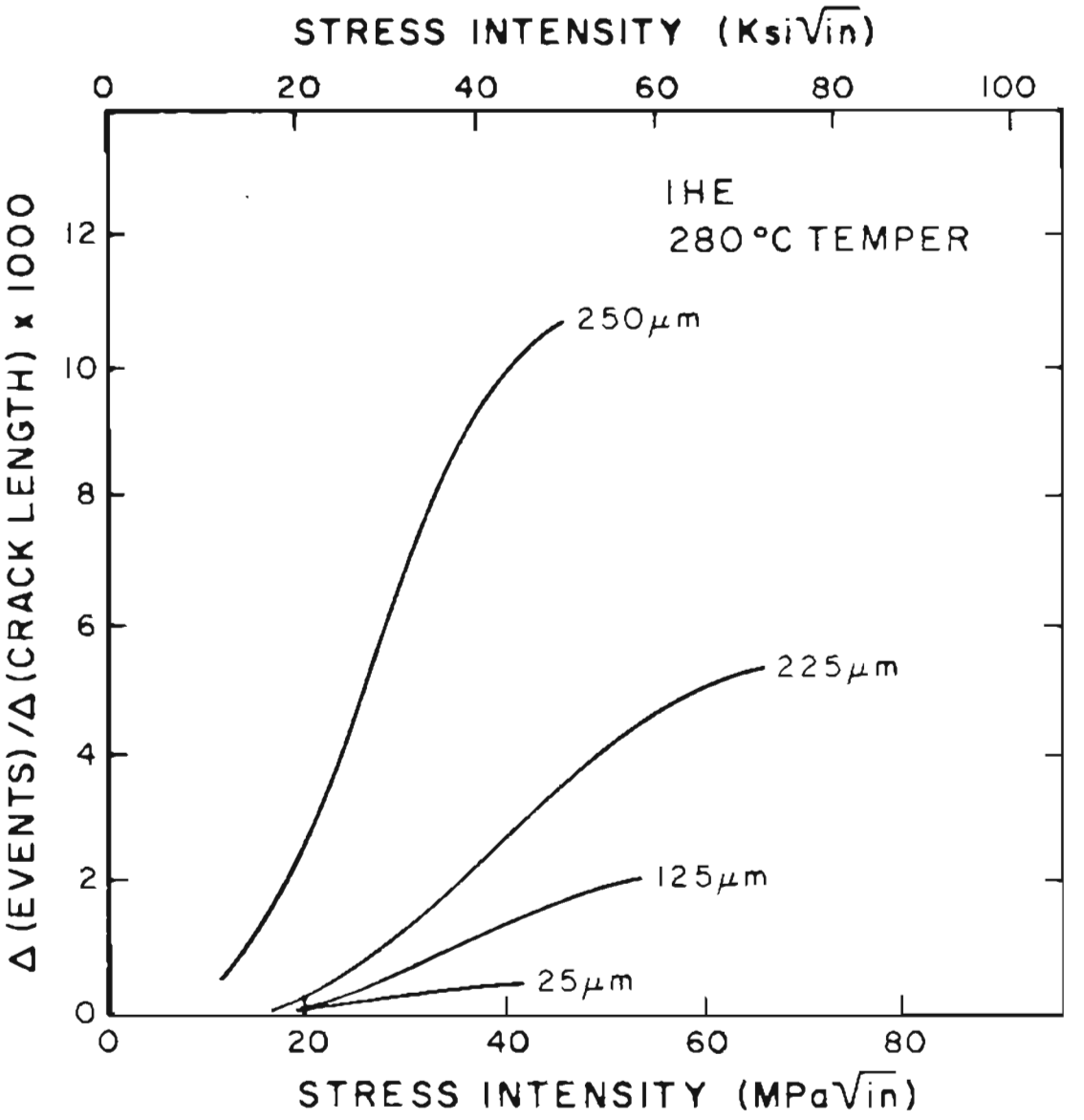

Figure 31. Acoustic emission events rate (dE/dA) as a function of stress intensity and grain size for IHE (tempering temperature 280°C).

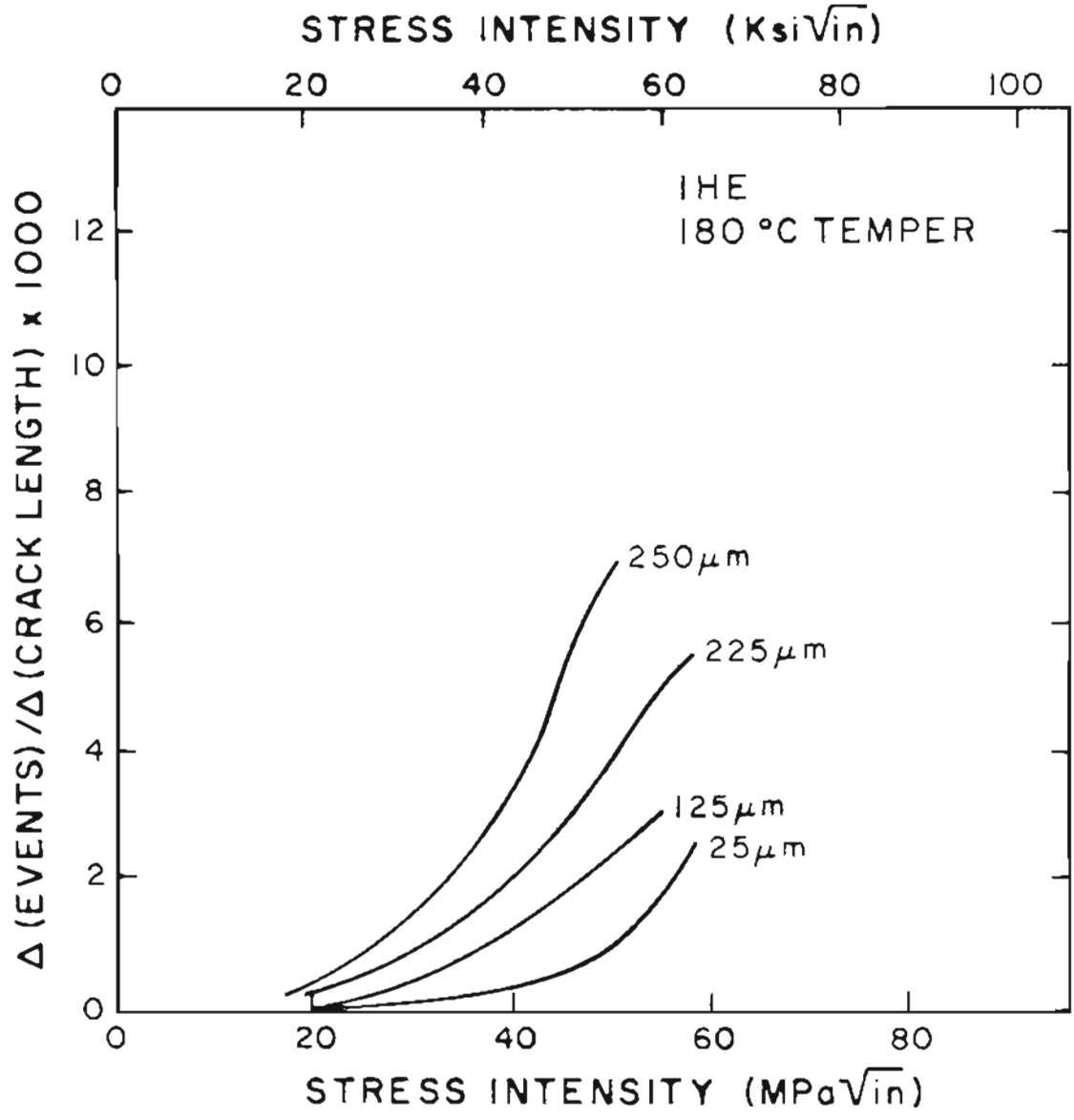

Figure 32. Acoustic emission events rate (dE/dA) as a function of stress intensity and grain size for IHE (tempering temperature 180°C).

The amplitude distribution histograms for each test were obtained as number of events versus amplitude (see Appendix). According to the generally accepted technique, amplitude distribution data were fitted to a model as proposed by Pollock. Based on this model, the slope of the cumulative events versus amplitude curve plotted on a log scale was evaluated for each test. This slope, designated as b, characterizes the amplitude distribution and is known as the amplitude distribution parameter. The values of 1/b (1/b characteristizes the average amplitude) for each heat treatment and hydrogen source are listed in Table 6-9. In general, the value of average amplitude increased with increasing grain size and for a given heat treatment, the value of the average amplitude was higher when the source of hydrogen was internal as compared to the external source.

An exception to the general observation that counts per event and average amplitude increased with grain size was noticed in the case of smallest grain size (25 μm). The specimens with this grain size always showed higher counts per event and higher average amplitude.

4.6 HYDROGEN ANALYSIS

The bulk hydrogen content was obtained by analyzing coupons cut from compact tension specimens that were either charged previously with hydrogen or exposed to hydrogen producing environment. The bulk hydrogen content for various heat treatments are listed as a function of region II crack growth rates (Table 10). In general, for identical charging conditions, the hydrogen content was higher for specimens that contained a significant amount of retained austenite. There was no correlation

between the hydrogen content and the region II crack growth rates for any given heat treatment. In fact, often ,two coupons cut from the same specimen showed widely varying hydrogen content, thus showing the non uniform distribution of hydrogen obtained by the charging procedures. This non uniform hydrogen distribution and varying hydrogen levels from one specimen to another for a given heat treatment did not have any effect on the region II crack growth rates.

The results of local hydrogen analysis of fractured specimens exposed to hydrogen producing environment are shown in Figure 33. In the area of the fatigue precrack, which was exposed for the longest time, the hydrogen concentration was the highest (3.5 ppm). The area corresponding to region II crack growth, the hydrogen concentration showed a considerable gradient. The baseline hydrogen content was obtained by analyzing a coupon cut away from the fractured surface, which gave the average hydrogen content as 2.4 ppm. The level of absorbed hydrogen during HEE has been shown to be related to the susceptibility of the steel to that particular environment[11]. Any inhibitor that decreases the susceptibility of the steel, would result in reduced hydrogen absorption on the fractured surface[11]. The hydrogen analysis of these specimens thus confirmed the role of hydrogen in stress corrosion cracking (HEE).

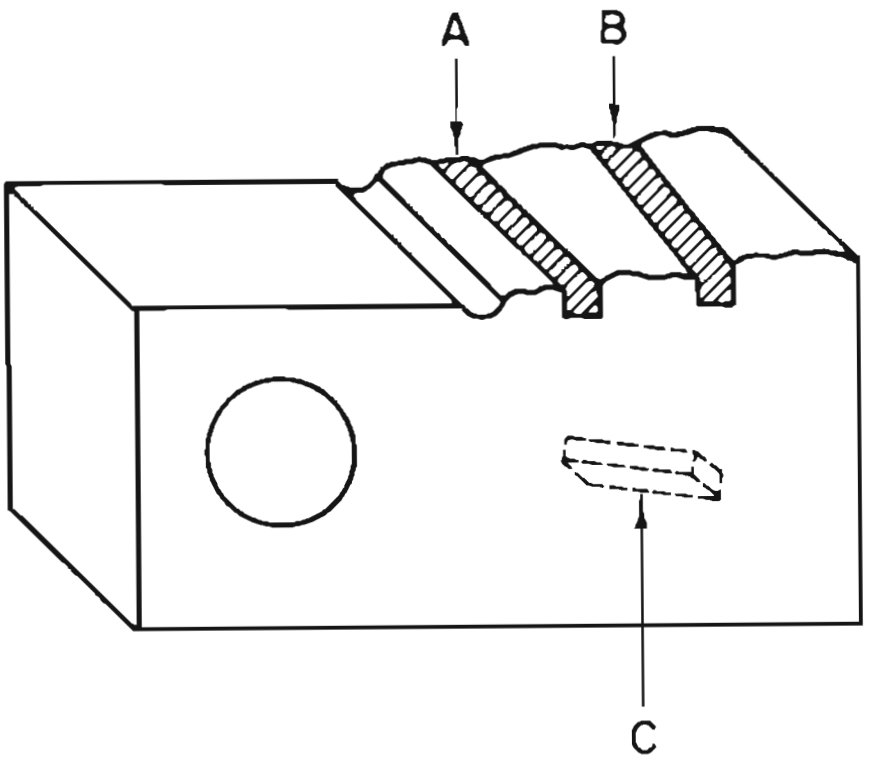

Figure 33. Hydrogen content at various locations on a fractured specimen tested in 3.5 percent sodium chloride solution; 3.5 ppm at A, 3.2 ppm at B and 2.4 ppm at C.

5. DISCUSSION

5.1 ACOUSTIC EMISSION ANALYSIS

Acoustic emission generated during fracture of materials contains potential information about the fracture mechanisms. In the discussion that follows, the interrelationship between acoustic emission parameters such as counts, events and amplitude distribution is derived and their dependence on material behavior during hydrogen assisted cracking is discussed. From linear elastic fracture mechanics[39], the energy released (E_R) when crack extends by ΔA, at stress intensity K, is given by

$$E_R = \frac{K^2}{E} \cdot B \cdot \Delta A \, (1-\upsilon^2) \qquad (1)$$

where B = thickness of the specimen

E = elastic modulus

υ = Poisson's ratio

In the above equation, B. ΔA is area of the new surface created as a result of crack extension.

$$E_R \propto K^2 \cdot \Delta \text{ (area)} \qquad (2)$$

Now considering the following points: (1) In high strength steels, the mechanism of stress corrosion crack extension involves hydrogen atoms[40] which are liberated by electrochemical reaction at the crack tip.
(2) The fracture surface is essentially intergranular and it is generally assumed that the crack nucleates at the grain boundary junctions ahead

of the crack tip[8] and then jumps back to the main crack. This explains the discontinuous nature of hydrogen assisted cracking.

Based on these two points, it is assumed that the step size of the discontinuous cracking is a function of grain size. For the purpose of this discussion, this step size is considered as the grain size itself.

When the crack advances by a grain of diameter d_i, the energy released, according to equation 2, will be

$$E_R \alpha K^2 \cdot \pi \left(\frac{d_i}{2}\right)^2$$

$$\text{or,} \qquad E_R \alpha K^2 \cdot d_i^2 \tag{3}$$

Now when the crack advances by this small step, the corresponding acoustic wave produced will be picked up by the monitoring system as an emission event of peak amplitude Vi. The energy of such an event from first approximation would then be Vi^2.

Comparing the energy released as given by equation 3 and the energy of the emission event,

$$Vi^2 \alpha K^2 \cdot d_i^2$$

$$Vi \alpha K \cdot d_i \tag{4}$$

According to the above equation, the peak amplitude of the emission event increases with stress intensity and grain size (or the step size).

The following discussion shows how this increase in the peak amplitude of an emission event with stress intensity and grain size can account for the increase in the number of events with stress intensity and grain size (Figures 29-32).

Consider a hypothetical case where a compact tension specimen is under constant load. The load is such that the stress intensity at the crack tip is greater than the threshold stress intensity, and the hydrogen assisted cracking is occurring grain by grain, as explained earlier.

It is known that,for a given austenitization temperature, the occurrence of grains of various sizes follow a lognormal distribution. For the hypothetical case under consideration, let the mean of the log-normal distribution be 100 μm and the variance 40 μm. According to equation 4, the amplitudes (V_i) of the emission events at a given stress intensity will follow the same distribution as the grain size (d_i) distribution. But the minimum amplitude that can be detected by the acoustic emission system is controlled by the electronic noise level of the amplifier. To obtain the emission data, a noise threshold is set just above the noise level,and the acoustic emission events whose amplitudes exceed this threshold will only be detected. This is explained graphically in Figure 34 for the hypothetical case.

The threshold is set at 6 volts. The cumulative grain size distribution is shown at the left. For instance, when the stress intensity is 40 Mpa $\sqrt{m}$, using equation 4, only the grains that are larger than 0.15 mm dia will generate emission that will exceed the noise threshold and

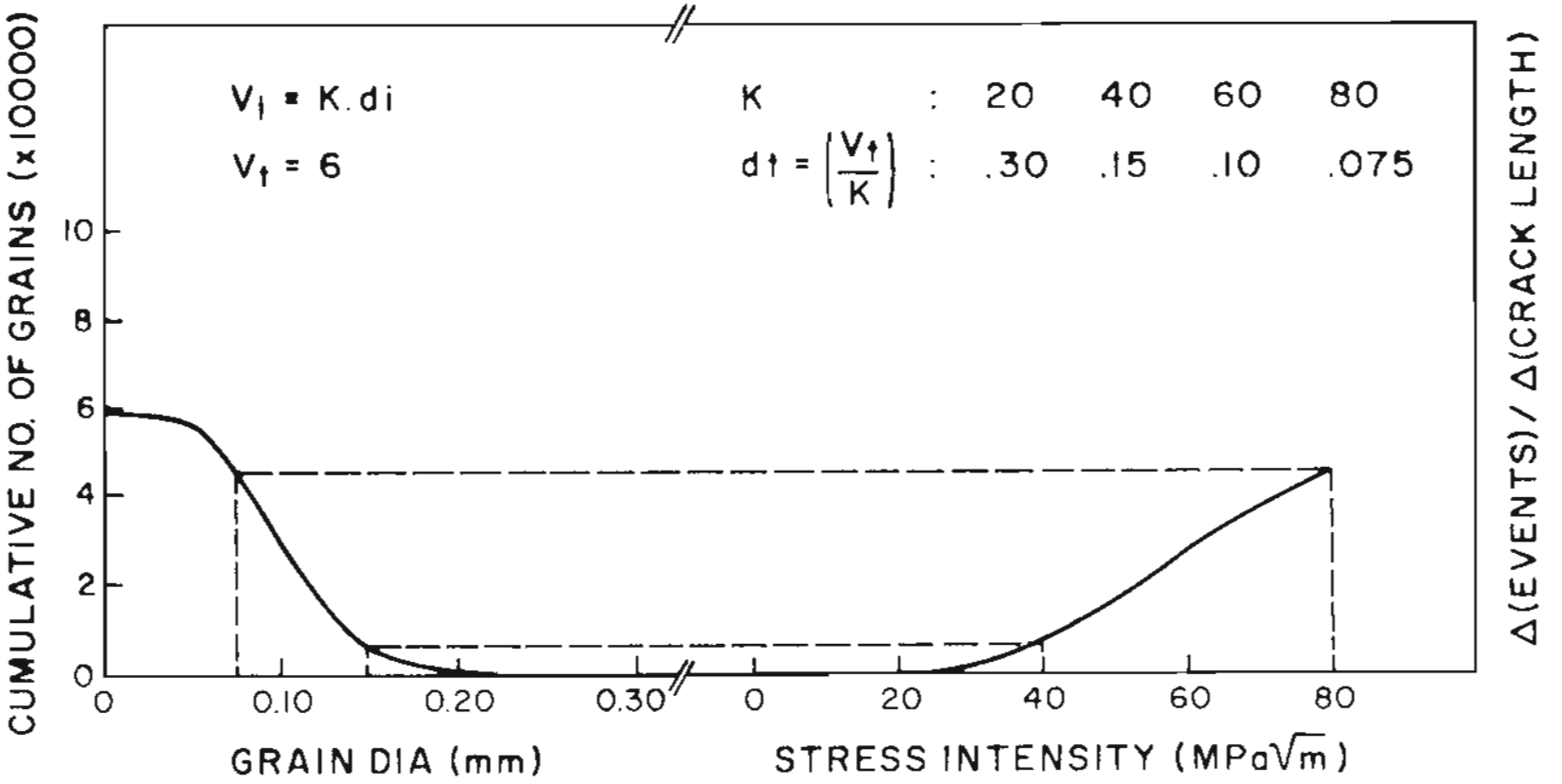

Figure 34. Graphical representation of the model to explain the acoustic emission response based on log-normal grain size distribution.

will be registered by the acoustic emission system. As the stress intensity increases, the minimum grain dia that can produce a detectable emission event will go on decreasing, and an increasing number of emission events (per unit extension in crack length) will be detected. The shape of the dE/dA versus stress intensity curve will thus depend on the shape of the inherent distribution of the steps by which the crack growth occurs.

The dE/dA data as shown in Figures 29-32 for various grain sizes can then be explained. (It is assumed that only the events from the tail end of the lognormal distribution are detected, even at the highest stress intensity). In the case of 25 μm grain size, only the grains in the tail end of the log normal distribution can generate emissions of detectable amplitudes even at high stress intensity. On the other hand, in the case of 250 μm grain size material, even though there are fewer number of grains per unit area, most of them are large enough to generate detectable emission and hence result in a higher dE/dA as compared to the 25 μm grain size. Similar results were obtained for each tempering temperature and hydrogen source.

Similar results have been obtained by other investigators[41-42] and often the variation in the emission as a function of stress intensity has been explained[37] by a K^m type relationship. The present investigation shows that such an approach does not explain the situation clearly, since it is based on the assumption that by monitoring the emission above the threshold, we are monitoring a fixed portion of the emission, which is shown in the preceding discussion not to be correct.

For a resonant frequency transducer, f does remain constant. But, when the pulse generated by any activity in the material lasts longer than the natural period of the transducer, there will be an apparent increase in τ. This will also happen when the events occur in rapid succession. In this case, the event counter may not be able to distinguish two events and the result would be more counts per event than that predicted by equation 5. Hence, an increase in average counts per event either is due to the increase in average amplitude (1/b) of the events, or an increase in apparent decay time of the event, τ.

The change in the average counts per event with grain size was generally consistent with change in average amplitude obtained from histograms. This was true when these results were compared for each hydrogen source. The average counts per events were considerably higher in the case of internal hydrogen embrittlement as compared to external hydrogen embrittlement, for corresponding heat treatments. This increase in average counts per event is not reflected in the average amplitude data obtained from the amplitude distribution data. This increase in average counts per event then indicates an increase in the apparent increase in the decay time of the burst envelope, τ. As explained earlier,τ will increase if the events occur in quick succession. In the case of specimens charged with hydrogen (internal hydrogen embrittlement), the hydrogen distribution may not be uniform on a microscopic scale and there would exist isolated locations where permanent damage could occur[43] because of hydrogen charging. When the advancing crack front reaches any such regions, the crack would jump over this area almost immediately. This would create acoustic emission

events in quick succession and these two events would be counted as one, but with longer decay time. This could explain the higher average counts per event observed in the case of internal hydrogen embrittlement.

The average counts per event and the average amplitude were much higher in the case of specimens with the smallest grain size (25μm). This apparent contradiction is explained by fractographic analysis. In a considerable region of the specimens, crack jumped by large steps in region B (Figure 35). This was clearly evident when fractographs were taken at higher magnifications (Figure 36) for the regions A and B. Predominantly transgranular fracture in region B as opposed to completely intergranular fracture in region A (at the same stress intensity) indicated that the hydrogen assisted cracking occurred in region A and the failure in region B was purely by mechanical overload resulting in large crack jumps. This resulted in a few emission events of very large amplitudes and this was reflected in higher average counts per event and higher average amplitude. The dependency of average amplitude and average counts per event based on average step size of crack extension is thus consistent.

5.2 EFFECT OF RETAINED AUSTENITE

It has been well established that AISI 4340 steel austenitized at higher[4,35,37] than conventional temperatures and quenched in oil, has a predominantly lath martensitic structure with about five percent retained austenite distributed along lath and grain boundaries in the form of 100-200Å thick films. The presence of this retained austenite does not affect the yield strength significantly. On the other hand, it has been shown that it improves the fracture toughness of the steel. The retained

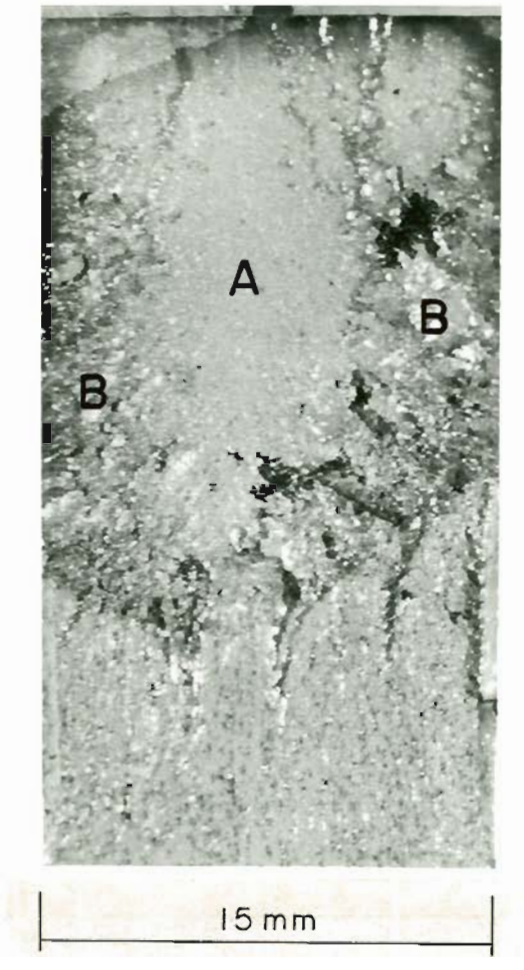

Figure 35. Fracture surface of a Compact Tension specimen austenitised at 870°C to obtain grain size of 0.025mm.

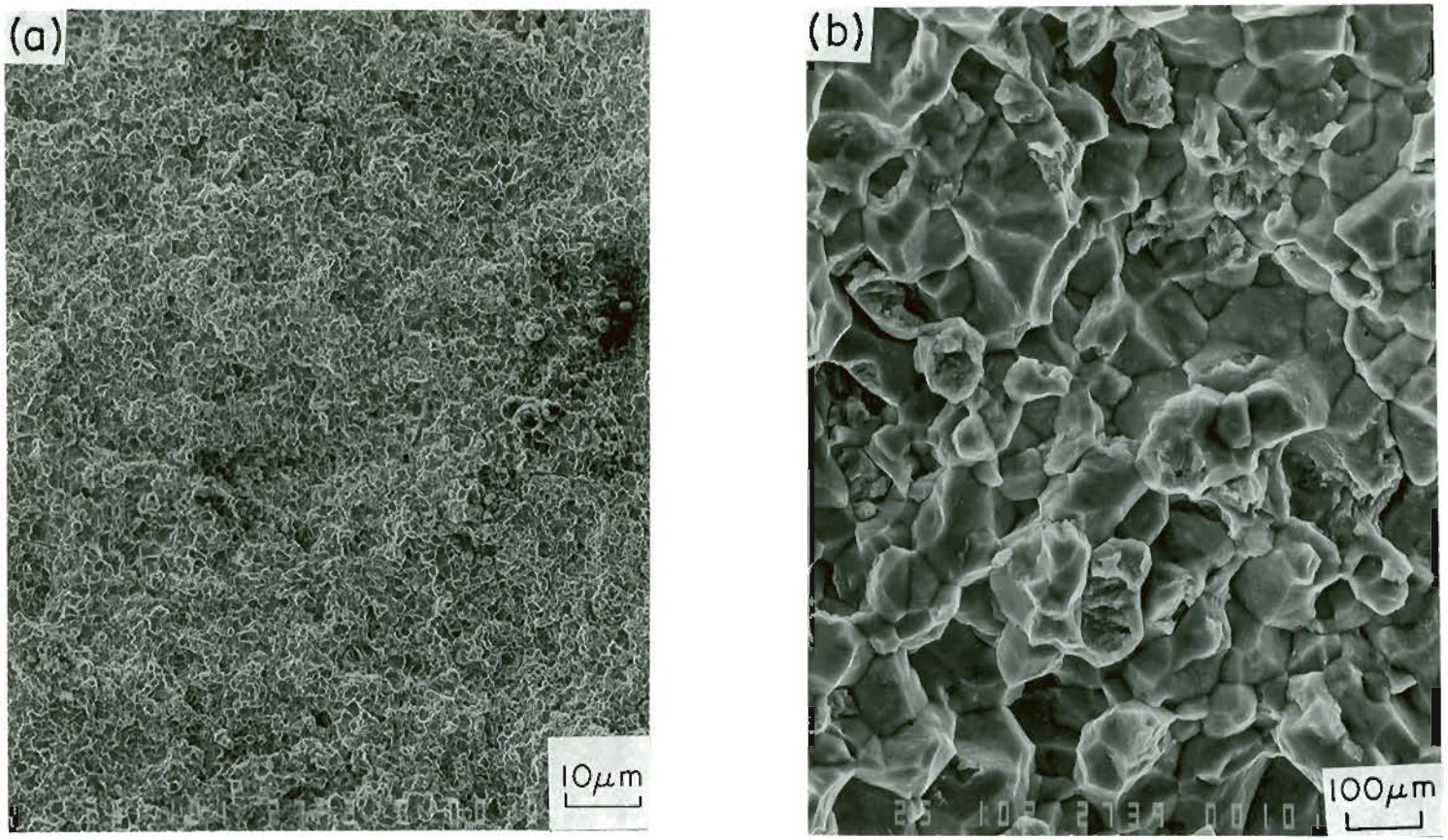

Figure 36. High magnification fractographs showing predominantly intergranular fracture in region A.

(a) 100 X
(b) 1000 X

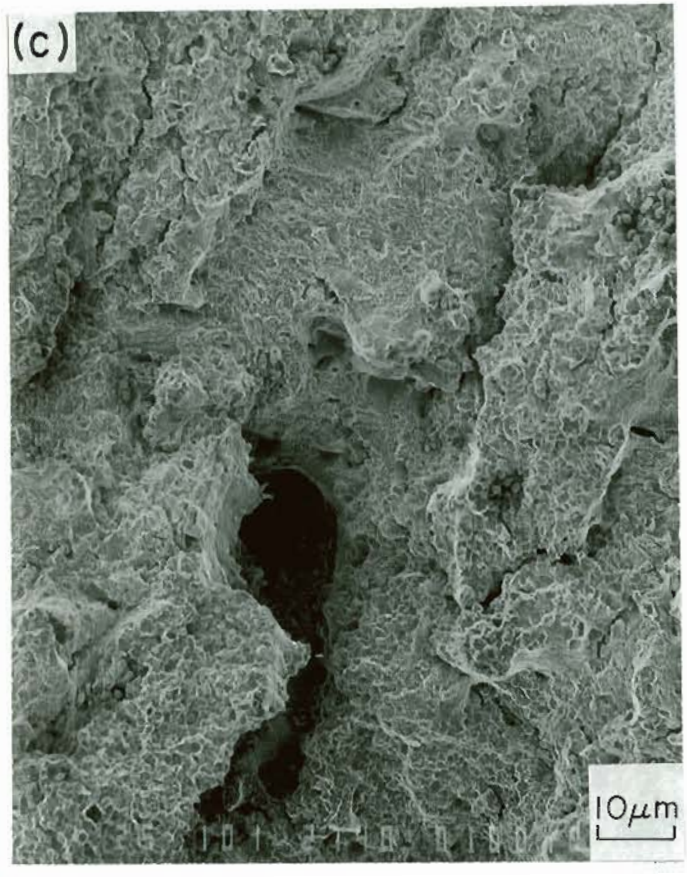

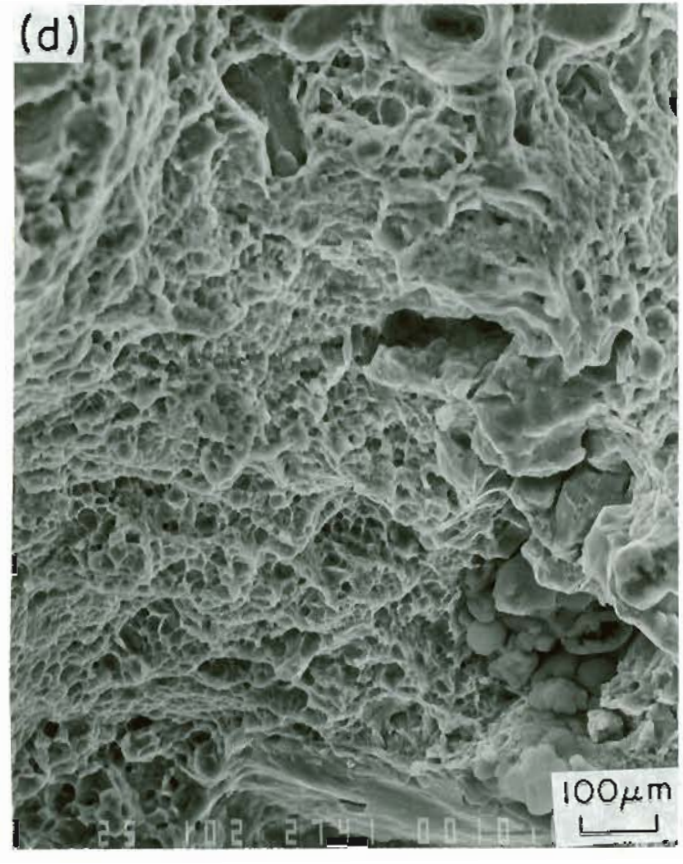

Figure 36. High magnification fractographs showing complete transgranular fracture in region B.

(c) 100 X
(d) 1000 X

austenite has a higher solubility for hydrogen and the diffusivity of hydrogen in austenite is much lower than in martensite. Because of these two reasons, the presence of finely dispersed retained austenite should act as an ideal trap for hydrogen as well as a barrier for hydrogen diffusion. This, in principle, should improve the susceptibility of the steel to hydrogen assisted cracking. Contrary to expectations, the present investigation showed that there was no noticeable improvement in threshold stress intensity due to the presence of retained austenite. In fact, the crack growth rates actually increased slightly when retained austenite was present. This was observed whether the source of hydrogen was internal or external.

These results could be explained when we consider the mechanical stability of the retained austenite. Ritchie and Horn[44] did magnetic saturation induction measurements during monotonic plane stress tensile test specimens to assess the extent of any stress induced austenite to martensite transformation. They found that most of the retained austenite was transformed to martensite at stress corresponding to 0.2 percent strain. In a recent TEM investigation[36] of thin foils taken from the plastic zone in front of the crack tip directly confirmed the earlier observations that the retained austenite is mechanically unstable. The retained austenite was found transformed to martensite in plane strain as well as plane stress plastic zone region.

Consider the case when the source of hydrogen is internal, that is, a specimen has some amount of hydrogen which is sufficient to cause delayed failure. The hydrogen is assumed to be uniformly distributed. In the case when retained austenite is present, because of the

higher solubility of hydrogen in fcc structure, the retained austenite will have a much higher concentration of hydrogen than the bulk concentration. Now consider that the specimen has a sharp crack and a load is applied to raise the stress intensity higher than the threshold stress intensity for cracking. Immediately upon loading, the plastic zone will be formed in front of the crack tip. The size of the plastic zone would depend on the stress intensity at the crack tip. In the case of plane strain conditions, in the region surrounding the plastic zone and extending up to twice its dimensions, the stress would still be greater than the uniaxial yield strength of the material (Figure 37). According to earlier observations, the retained austenite present in the plastic zone and the surrounding region would be thus transformed to untempered martensite. The solubility of hydrogen which was much higher in retained austenite would suddenly decrease in the transformed martensite. This supersaturated martensite would now release the hydrogen which in turn would redistribute in the stressed region according to the stress gradient. In ultra high strength commercial steels, like the one used in this investigation, considerable amount of trace impurities are present which are segregated at the grain boundaries and weaken them. Only a small amount of hydrogen is probably required to cause grain boundary fracture, and a considerable part of this amount could be provided by the above mechanism, i.e, the hydrogen released by the stress assisted austenite to martensite transformation in the region of the crack tip. Thus the presence of the mechanically unstable retained austenite can in fact increase the region II crack growth rates. It could have a beneficial effect near

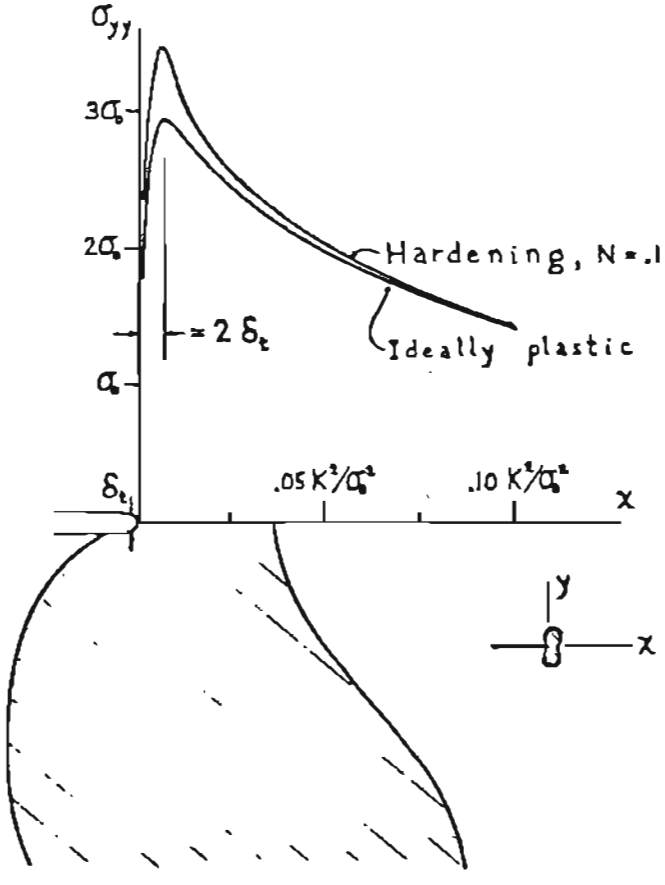

Figure 37. A schematic representation of the stress distribution ahead of a sharp crack under load. Cross-hatched area is the plastic zone.

threshold stress intensity where the stressed region in front of the crack tip would be relatively small and the retained austenite can act as a trap for hydrogen.

The presence of retained austenite can possibly have a beneficial effect on the region II crack growth rates if the trace impurity content of the steel is drastically reduced, in which case, much more hydrogen would be required to cause cracking. This may create a situation where the hydrogen released in the stressed zone because of austenite to martensite transformation may not be enough to cause cracking and it may be necessary to draw hydrogen from the regions further away from the crack tip where retained austenite is not transformed. This would require long range diffusion of hydrogen and the presence of retained austenite will be beneficial as a trap as well as a barrier to diffusion of hydrogen. This in turn would reduce the region II crack growth rate, which is diffusion controlled.

The results obtained in the present study on internal and external hydrogen embrittlement can thus be explained by the above discussion.

In their investigation of internal hydrogen embrittlement of AISI 4340 steel, Lessar and Gerberich[25] concluded that increase in grain size decreased the crack growth rates and attributed this improvement with grain size partly to the retained austenite which was present in the specimens with larger grain size. There are two points to be noted about their study. First, their heat treatment involved a 300°C temperature and it is now well established that the retained austenite is not stable at this temperature and hence cannot have any beneficial effect. Second,

the method they used to report the crack growth as function of grain size was questionable. The crack growth rates were taken at one particular stress intensity chosen arbitrarily at 30 ksi in for all the heat treatments. Now, all these heat treatments had widely varying threshold stress intensity and fracture toughness values. On crack growth rate versus stress intensity curves,at 30 ksi in, it was stage I for some heat treatment, stage II for other and probably stage III for the third one. In fact, for specimen with 140 μm grain size, the crack growth rate could not be reported as a function of grain size because the threshold stress intensity was higher than 30 ksi in. If their stage II crack growth rates for each heat treatment were to be taken in between K_{Ic} and K_{th} as was done in the present investigation,then,only a slight improvement would be observed with increase in grain size. This improvement in crack growth rates with grain size is probably due to decrease in the yield strength with increase in grain size.

In a recent study on environmental hydrogen embrittlement of AISI 4340 and 300M steel, Ritchie[27] concluded that the presence of retained austenite decreased the stage II crack growth rates. This conclusion was based on the fact that the 300M steel given isothermal heat treatment before oil quenching and tempered at 300°C showed considerably lower stage II crack growth rates than the same steel austenitized at 870°C oil quenched and tempered at 470°C. The former heat treatment produced about 10-12 percent retained austenite whereas the latter had very little retained austenite. The yield strengths obtained by both the heat treatments were comparable.

Besides the amount of retained austenite, there was one more difference in microstructure obtained by the above two heat treatments. The 300M steel given isothermal treatment was tempered at 300°C and contained epsilon carbide, whereas the steel which was directly quenched from 870°C was tempered at 470°C and hence contained cementite. The change in carbide type, as will be shown in the later section, increases the susceptibility of the steel to hydrogen assisted cracking. This probably is the reason for the higher crack growth rates observed for 870/470 treatment as compared to isothermal treatment which involved a 300°C tempering treatment.

Hence from the present study and from the data reported in literature there is sufficient evidence to believe that mechanically unstable retained austenite cannot have a beneficial effect on region two crack growth rates. In the case of internal hydrogen embrittlement, the presence of mechanically unstable retained austenite could increase the crack growth rates if long range transport of hydrogen is required in a steel where impurity levels are low and may require higher amount of hydrogen for cracking. The presence of retained austenite could improve the threshold stress intensity, where the stressed zone in front of the crack tip is relatively small.

5.3 EFFECT OF IMPURITY SEGREGATION

It is well known that segregation of metalloid impurities like P,S, Sb, et., to grain boundaries of iron base alloys leads to a reduction in the energy absorbed in the fracture of notched specimens. The embrittlement is also accompanied by a tendency for intergranular fracture.

It is generally concluded that[45-55] the impurity segregation leads to a reduction in the cohesion of the grain boundaries. Consider a situation where hydrogen has entered the steel in some way. When a stress is applied to the steel, the hydrogen begins to diffuse to the region of maximum triaxiality and to the stressed region in front of it. Because of the high mobility of hydrogen in bcc iron, it will be distributed uniformly over the grain boundaries and the matrix. Assuming that the hydrogen lowers cohesion everywhere uniformly, the critical concentration needed to form a crack will be reached first along the weakest interface, because this interface energy has already been reduced by segregation of metalloids and will need a minimum amount of hydrogen. Thus segregated impurities can have an additive effect on the ability of hydrogen to reduce the cohesive strength of the steel.

There is another possible mechanism by which the segregated impurities can have a synergistic effect. If the hydrogen that resides at the grain boundaries at any instant of time can be trapped there in some way, for example, by interacting with impurity atoms which are already segregated to the grain boundaries, then the hydrogen will be prevented from diffusing into the bulk. In this case, the hydrogen concentration could build up preferentially at the boundaries to cause intergranular fracture, even though the cleavage planes may initially have a lower fracture energy.

The effect of segregated impurities on hydrogen assisted cracking of a high strength steel were first studied by Cabral et al[47]. They found that the threshold stress for cracking of smooth specimens of a

Ni-Cr steel in H_2SO_4 solution decreased significantly when the steel was tempered at 500°C, i.e., in temper embrittlement range. The fracture mode changed from transgranular to intergranular as a result of the tempering treatment.

Yoshino and McMahon[48] performed a similar study on HY 130 steel using precracked specimens in a similar H_2SO_4 environment. They compared unembrittled (in which the impurities are held in the matrix) and the step cooled (in which a large amount of grain boundary segregation occurs) conditions. In both cases, hydrogen caused delayed failure, but the time to failure for a given stress intensity was much shorter in the case of step cooled specimens. Also, there was a difference in the fracture modes, the unembrittled specimens failing by cleavage whereas the step cooled specimens failing by intergranular mode. The Auger analysis of the grain boundaries of the step cooled specimens revealed them to be rich in silicon, phosphorous and nitrogen.

Briant et al.[28] in their study on HY180 steel investigated crack growth rates in gaseous hydrogen as a function of grain boundary impurity concentration. They found that as the aging time increased, which caused increased grain boundary segregation, the threshold stress intensity decreased and the crack growth rate increased. In this case also, the unembrittled specimens failed by cleavage and the amount of intergranular fracture increased as the amount of grain boundary segregation increased. Their results are in agreement with the present study of AISI 4340 steel.

In steels with yield strength greater than 200 ksi, only a very small amount of grain boundary impurity segregation is needed to embrittle

the steels. Banerji et al.[30] studied the behavior of AISI 4340 type steel in a gaseous hydrogen environment. They have shown that all commercial varieties of this steel are highly susceptible to hydrogen assisted cracking and the hydrogen assisted fracture was always predominantly intergranular. The observed intergranular fracture implied that the impurity segregation was also demonstrated when the pure steel showed a five fold increase in the threshold stress intensity for hydrogen assisted cracking, as compared to the commercial steel. Also, in the pure steel, the fracture mode was no longer intergranular. These results support the hypothesis that the hydrogen assisted cracking in steels is intergranular only when the grain boundaries are already weakened due to the segregated impurities.

It can also be argued that the segregated impurities which are also known to be recombination poisons[49-50] for atomic hydrogen, can increase the local hydrogen concentration at the grain boundaries and thus produce the same results. At the present time, the exact mechanism is not known, but the major effect that segregation of these elements has no hydrogen cracking has been clearly demonstrated.

5.4. EFFECT OF CARBIDE MORPHOLOGY

Carbon steels containing more than 0.2 percent carbon will precipitate epsilon-carbide when tempered at 100-200°C. This precipitate has been proposed to be coherent with the matrix[51]. Tempering at temperatures above 250°C result in the formation of cementite and dissolution of carbide. This cementite is coarser than epsilon-carbide and unlike

epsilon-carbide, it is incoherent with the matrix. The change in carbide morphology from ε-carbide to cementite can affect the susceptibility of the steel to hydrogen assisted cracking by changing the trapping ability of the steel. Also the coarse cementite particles present at the grain boundaries may act as nucleation sites for cracking.

From strain energy calculations, Craig[52] has showed that fully coherent precipitates such as epsilon carbide would be very effective trapping sites for hydrogen by disregistry. If the steel contains some silicon, then it would be present in ε-carbide and because of the low diffusivity of hydrogen in the presence of silicon, the ε-carbide would be a much more effective trap. When the tempering temperature used is greater than 250°C, the cementite formed is incoherent with the matrix and the trapping ability would be drastically reduced because of the minimization of strain energy and also because of the larger interparticle spacing which reduces the effective capture distance of a particle.

In stress corrosion study of AISI 4340 steel, Davis et al.[26] found the specimens tempered at 260°C to be most susceptible. This was associated with the presence of grain boundary platelet carbides. When 1.5 percent silicon was added to this steel, the most susceptible condition was shifted to tempering temperature range of 375-420°C. It is well known that silicon shifts the tempering reactions upwards by about 100°C and this suggests that cementite promotes hydrogen assisted cracking, particularly when present at the grain boundaries.

Tiner and Gilpin[53] evaluated the failure times for smooth specimens of AISI 4340 steel in sodium chloride solution. They found an increase in failure times for specimens with cementite than with ε-carbide. But this increase in failure times could have come from an increase in fracture toughness of the specimens with cementite.

Ritchie et al.[27] and Carter[54] in their study on hydrogen assisted cracking of AISI 4340 and 300M steels in 3.5 percent sodium chloride solution reported that for either 4340 or 300M in quenched and tempered conditions, structures hardened by epsilon carbide showed lower crack rates than the structures hardened by cementite. They did not observe any change in threshold stress intensity due to the change in carbide morphology from epsilon-carbide to cementite.

Tempering at 280° can also cause tempered martensite embrittlement in the steel when retained austenite is present,[44] as is the case with 1200°C austenitization treatment. This high carbon austenite on lath and grain boundaries can act as a primary source for the precipitation and growth of embrittling carbide films, thus weakening the interfaces. This effect is in addition to the precipitation of coarse cementite on grain boundaries acting as crack nucleation sites. Thus the change in tempering temperature from 180°C to 280°C has an additional effect on increasing the susceptibility of the steel to hydrogen assisted cracking in the case of coarse grain structures resulting from 1200°C austenitization treatment.

5.5 EFFECT OF GRAIN SIZE

In high strength steels, hydrogen assisted cracking is often along prior austenite grain boundaries and therefore, the effect of grain size is of obvious importance. The grain boundaries are already weakened because of the segregated impurities and it is along the grain boundaries that the hydrogen concentration first exceeds the critical level to cause fracture. The hydrogen induced cracking initiates at a point ahead of the main crack and the grain boundary triple point provides such a crack nucleation site.

First consider the various proposed mechanisms for hydrogen assisted cracking. Crack propagation has been observed in high strength steels exposed to molecular hydrogen gas at pressures down to 10 torr[55]. In such cases, no equilibrium hydrogen activity exists between the gas phase and the metal lattice, such that internal hydrogen pressures, sufficient for lattice bond decohesion, can exist within the steel. Therefore, the validity of the pressure theory is questioned.

Oriani's model is based on the postulate that dissolved hydrogen in iron at sufficiently high concentration decreases the maximum cohesive force between the iron atoms at the crack tip, and thus predicts, atom by atom crack advance. This is certainly at odds with the jerky and discontinuous crack propagation observed in high strength steels[25,30].

A model is developed in the following discussion which combines the Troiano's theory that a microcrack develops in the stressed region in front of the crack tip and the Petch and Stables criterion that the

surface energy of the lattice is lowered by the adsorption of hydrogen upon the surfaces of the crack.

Consider a steel specimen with a sharp crack under load such that plane strain conditions exist. The stress distribution predicted on the plane immediately ahead of the crack, for an ideally plastic material is shown in Figure 38. According to this model, the peak stress is very near the crack tip. This occurs at a distance of approximately $2\delta_t$ ahead of the tip, where δ_t is the amount by which the crack has been opened at its tip by plastic deformation[56]. In a steel with yield strength 200 ksi and at stress intensity 50 ksi in, the location of maximum triaxiality is about 10 microns away from the crack tip. This is smaller than the smallest grain size investigated in the present investigation. Hence this rules out the necessity for coinciding the grain boundary junction with maximum triaxiality as a precondition for hydrogen assisted cracking. But, beyond this region of maximum stress in front of the crack tip, there is a large region over which a stress gradient exists. This stress gradient will draw hydrogen in front of the crack tip. The hydrogen concentration will vary with position ahead of the crack, partly because of diffusion and partly because of the effect on solubility. This hydrogen accumulation in the stressed region would lower the surface energy of the steel lattice, particularly of the grain boundaries because of the presence of impurities and because of the possible impurity hydrogen interactions at the grain boundaries (as discussed in the section on effect of segregation). Since grain boundary junctions or grain boundary triple points are the weakest points in the lattice, the surface energy of the grain boundary at and near the triple point will be

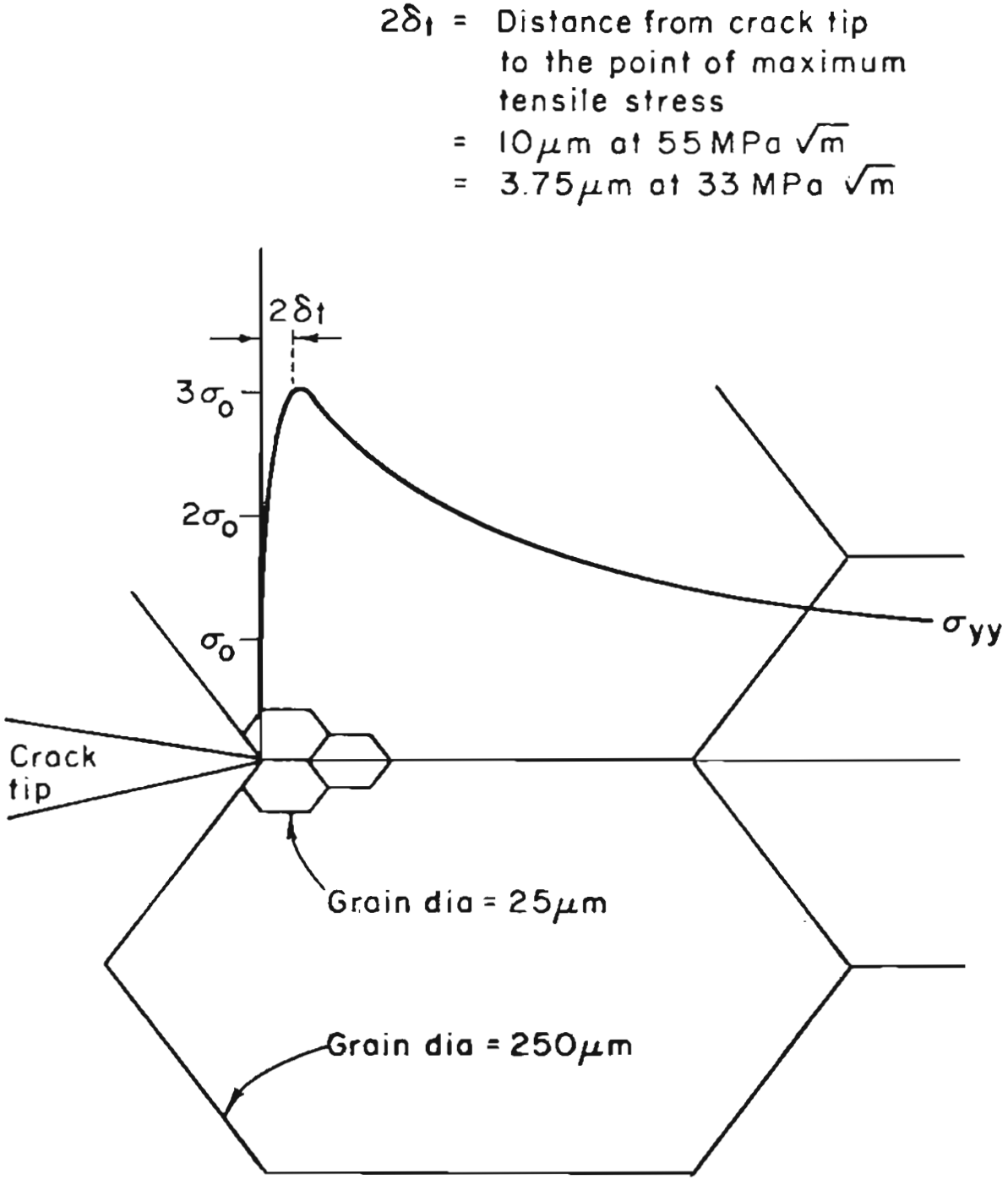

Figure 38. Stress distribution ahead of a sharp crack under load at a stress intensity of 55 MPa m shown in relation to mean grain sizes of 25 μm and 250 μm.

reduced more rapidly than the rest of the grain boundary area. According to Troiano's model, this can be visualized as a microcrack at the grain boundary junction. But this is not sufficient condition for the crack to extend up to this point from its original location. The rest of the grain boundary area must have enough hydrogen so that the Griffith criterion for lowering of surface energy over that area is satisfied. This is the same as Petch and Stables condition. The lowering of the total surface energy over the whole grain boundary could certainly get sizeable contribution from the microcrack at the grain boundary. Combining these two conditions, it is suggested that both of the above criteria are necessary for crack extension, i.e., the lowering of surface energy over the intergranular surface (or any interface) is necessary and is aided by the weak grain boundary junction.

With reference to crack growth rate studies, it was confirmed by acoustic emission analysis that the crack advances one grain at a time, independent of the grain size. Then, according to the above proposed mechanism, crack growth rate would not be affected by grain size, as was observed in the present investigation. In the case of small grain size, the Petch-Stables condition will be satisfied sooner for an average jump as compared to large grain size. But the actual crack advance will be much smaller in the case of small grain size. So, overall there would not be any significant effect of grain size on crack growth rate.

The increase in K_{th} with grain size can also be explained on the basis of the proposed mechanism. The formation of a microcrack at the

grain boundary junction requires that, for a given hydrogen activity, a critical stress be present at the grain boundary junction. As the stress intensity is decreased, the stress at the grain boundary junction or any crack nucleation site would decrease and at some given stress intensity, the critical stress to form a microcrack will not be attainable. With decreasing stress intensity, this will happen first in the specimen with the largest grain size. Because of this, a specimen with a larger grain size is expected to have a higher threshold stress intensity than the one with the smaller grain size. This was observed in the present study and is supported by the acoustic emission results that even near threshold stress intensity, the crack jumps are controlled by the grain size.

Summarizing, it is suggested that the criteria for hydrogen assisted crack extension is the overall lowering of surface energy over the crack interfaces and aided by microcrack formation at grain boundary junction. This hypothesis is supported by the acoustic emission results which show grain-by-grain advance of the hydrogen assisted cracking. It explains the increase in the threshold stress intensity with grain size and also explains the independence of crack growth rate of grain size.

6. CONCLUSIONS

Following significant conclusions were drawn from the study of internal hydrogen embrittlement (IHE) and hydrogen environment embrittlement (HEE) of AISI 4340 steel heat treated to yield strength of above 200 ksi.

(1) The effect of microstructure on hydrogen assisted cracking was similar irrespective of the source of hydrogen-internal or external.

(2) An increase in grain size slightly increased the threshold stress intensity for hydrogen assisted cracking but did not have any effect on region II crack growth rates.

(3) The change from epsilon carbide to cementite increased the region II crack growth rates.

(4) The presence of retained austenite on prior austenite grain boundaries improved the threshold stress intensity but its mechanical and thermal instability increased the susceptibility of the steel to hydrogen assisted cracking.

(5) Acoustic emission analysis confirmed the discontinuous nature of hydrogen assisted cracking. These discontinuous steps were highly grain size dependent.

(6) From the acoustic emission analysis and based on the fact that the region II crack growth rate was independent of grain size, it was possible to propose a mechanism of hydrogen assisted cracking which combines the mechanisms proposed by Troiano and Petch and Stables.

(7) Finally, the high temperature austenitizing treatment (1200°C) which increased the fracture toughness considerably, and also the threshold stress intensity but only slightly increased the region II crack growth rates. could be used in practice even where hydrogen assisted cracking is expected. The higher fracture toughness resulting from 1200/180 treatment would extend the second stage of crack growth rate to higher stress intensities and would give longer time for crack detection.

TABLE 1

Chemical Composition of AISI 4340 Steel (Wt.%)

C	Mn	Cr	Ni	Mo	Si	Cu	S	P
.38	.69	.78	1.8	.23	.37	.17	.013	.008

TABLE 2

Heat Treatment Identification

ID	Austenitizing Treatment	Tempering Treatment
870/180	870°C/1 hour	180°C/1 hour
870/280	870°C/1 hour	280°C/1 hour
1100/180	1100°C/1 hour	180°C/1 hour
1100/280	1100°C/1 hour	280°C/1 hour
1200/180	1200°C/1 hour	180°C/1 hour
1200/280	1200°C/1 hour	280°C/1 hour
1200/870/180 or 1200-870/180	1200°C/1 hr — 870°C/.5 hr	180°C/1 hour
1200/870/280 or 1200-870/280	1200°C/1 hr — 870°C/.5 hr	280°C/1 hour

TABLE 3

Mechanical Properties of AISI 4340 Steel
as a Function of Heat Treatment

Heat Treatment	Yield Strength ksi	Yield Strength MPa	Tensile Strength ksi	Tensile Strength MPa	% Elongation	Fracture Toughness (K_{Ic}) ksi $\sqrt{in}$	Fracture Toughness (K_{Ic}) MPa $\sqrt{m}$
870/180	225	1550	280	1929	13.6	55	60
870/280	220	1515	240	1654	13.7	76	83
1100/180	220	1515	242	1667	9.0	59	64
1100/280	220	1378	228	1571	9.1	71	77
1200/180	220	1515	268	1847	8.6	86	94
1200/280	200	1378	227	1564	1.2	61	67
1200/870/180	220	1515	260	1791	7.1	62	68
1200/870/280	200	1378	240	1654	7.3	52	57

TABLE 4

Microstructural Features as a Function of Heat Treatment

Heat Treatment	Mean Grain Diameter (μm)	Amount of Retained Austenite (%)	Carbide Type	Other Factors
870/180	25	<2	ε-carbide	
870/280	25	<2	cementite	
1100/180	125	<2	ε-carbide	
1100/280	125	<2	cementite	
1200/180	225	~5	ε-carbide	
1200/280	225	<2	cementite	
1200/870/180	250	~5	ε-carbide	Extensive grain boundary segregation
1200/870/280	250	<2	cementite	

TABLE 5

Threshold Stress Intensity for Hydrogen Environmental Embrittlement (HEE) and Internal Hydrogen Embrittlement (IHE) as a Function of Heat Treatment

Heat Treatment	K_{th} (HEE) ksi $\sqrt{in}$	K_{th} (IHE) ksi $\sqrt{in}$
870/180	11.0	10.0
870/280	11.0	10.0
1100/180	12.5	11.5
1100/280	12.5	11.5
1200/180	16.0	16.0
1200/280	14.0	13.0
1200/870/180	14.0	14.0
1200/870/280	13.0	11.0

TABLE 6

Average Counts Per Event and Average Amplitude as a Function of Grain Size for HEE(Tempering Temperature 280°C)

Mean Grain Diameter (μm)	Average Counts Per Event	Average Amplitude (1/b)
25	32	1.33
125	10	.56
225	19	0.87
250	58	0.99

TABLE 7

Average Counts Per Event and Average Amplitude as a Function of Grain Size for HEF (Tempering Temperature 180°C)

Mean Grain Diameter (μm)	Average Counts Per Events	Average Amplitude (1/b)
25	29	1.21
125	11	0.60
225	20	0.80
250	22	0.88

TABLE 8

Average Counts Per Event and Average Amplitude as a Function of Grain Size for IHE. (Tempering Temperature 280°C.)

Mean Grain Diameter (μm)	Average Counts Per Events	Average Amplitude (1/b)
25	186	1.40
125	49	0.72
225	97	0.95
250	107	1.05

TABLE 9

Average Counts Per Event and Average Amplitude as a Function of Grain Size for IHE (Tempering Temperature 180°C.)

Mean Grain Diameter (μm)	Average Counts Per Events	Average Amplitude (1/b)
25	50	1.11
125	43	0.70
225	60	0.90
250	83	1.00

TABLE 10

Hydrogen Analysis Results

Heat Treatment	Region II Crack Growth Rate (in/sec) $x10^{-4}$	Hydrogen Content in ppm by Weight I*	II*
870/180	1.8	6.3	
	1.8	2.3	1.9
870/280	2.5	1.3	1.7
	2.5	3.7	
1100/180	1.9	2.7	
	1.9	2.5	
1100/280	2.5	5.4	
1200/180	3.0	4.5	6.4
1200/280	4.9	5.0	4.2
1200-870/180	5.0	5.0	6.5
1200-870/280	8.0	4.5	6.1

*I or II indicate the number of coupons analyzed from the same compact tension specimen.

REFERENCES

1. W.E. Wood: "Effect of heat treatment on the fracture toughness of low alloy steels," EFM, Vol. 7, 1975, p.219.

2. R.O. Ritchie, B. Francis and W.L. Server: "Evaluation of toughness in AISI 4340 alloy steel austenitized at low and high temperatures," MT, Vol. 9A, June 1976, p.831.

3. C.L. Briant and S.K. Banerji: "Tempered martensite embrittlement in phosphorus steels," MT, Vol. 10A, Nov. 1979, p.1729.

4. G.Y. Lai, W.E. Wood, R.A. Clark, V.F. Zackay and E.R. Parker: "The effect of austenitizing temperature on the microstructure and mechanical properties of as quenched 4340 steel", MT, Vol 5, July 1974, p.1663.

5. W.W. Gerberich and Y.T. Chen: "Hydrogen controlled cracking — an approach to threshold stress intensity," MT, Feb 1975, p.271.

6. H.H. Johnson, J.G. Morlet and A.R. Troiano: "Hydrogen crack initiation and delayed failure in steel," Trans. Met. Soc. AIME, Aug 1958, p.528.

7. M.F. McGuire, A.R. Troiano and R.F. Hehemann: "Stress corrosion of ferritic and martensitic stainless steels in saline solutions," Corrosion, Vol. 29, 1979, p.279.

8. A.R. Troiano: "The role of hydrogen and other interstitials in the mechanical behavior of metals," Trans ASM, Vol. 52, 1960.

9. C.D. Beachem: "A new model for hydrogen assisted cracking (hydrogen embrittlement)", MT, Vol. 3, Feb. 1972, p.437.

10. C.S. Kortovich and E.A. Steigerwald: "A comparison of hydrogen embrittlement and stress corrosion cracking in high strength steels," EFM, Vol. 4, 1972, p.637.

11. P.A. Parish, K.B. Das, C.M. Chen and E.D. Verniki, "Inhibition of hydrogen embrittlement of D6aC steel in aqueous oxidizing media", Effect of hydrogen on behavior of materials, Ed. A.W. Thompson and I.M. Bernstein, 1975.

12. E.A. Steigerwald, E.W. Schaller and A.R. Troiano: "The role of stress in hydrogen induced delayed failure," Trans. Met. Soc. AIME, Vol. 218, Oct. 1960, p.832.

13. G. Sandoz: "The effect of alloying elements on the susceptibility of stress corrosion cracking of martensitic steels in sea water", MT, Vol. 2, April 1971, p.1169.

14. G. Sandoz: A unified theory of hydrogen source, alloying elements and potential on crack growth in martensitic AISI 4340 steel," MT, Vol. 3, May 1972, p

15. C.A. Zapffe and C.E. Sims: "Hydrogen embrittlement, internal stress and defects in steel", Trans. AIME, Vol. 145, 1941.

16. F. deKazinczy: "A theory of hydrogen embrittlement", JISI, Vol.177, May 1954.

17. A.S. Tetelman: "The mechanism of hydrogen embrittlement in steel," in Fundamental Aspects of Stress Corrosion Cracking, Pub. NACE, 1967, p.446.

18. N.J. Petch and P. Stables: "Delayed fracture of steel under static load", Nature, Vol. 169, May 1954.

19. N. J. Petch: "The lowering of fracture stress due to surface adsorption", Phil. Mag., Series 8, 1956, p.331.

20. R. A. Oriani and P.H. Josephic: "Equilibrium aspects of hydrogen induced cracking of steels", Acta Metallurgica, Vol. 22, Sept. 1974, p. 1065.

21. R.A. Oriani and P.H. Josephic: "Equilibrium and kinetic studies of the hydrogen assisted cracking of steel", Acta Metallurgica, Vol. 25, 1977, p.979.

22. R.A. Oriani: "A mechanistic theory of hydrogen embrittlement of steels", Ber. Bunsen. Ges. Physik. Chem., Vol. 76, 1972, p.848.

23. R. A. Oriani: "A decohesion theory of hydrogen induced crack propagation", in Stress corrosion cracking and hydrogen embrittlement of iron base alloys, Pub. NACE, 1973.

24. R.P.M. Proctor and H.W. Paxton: "The effect of prior austenite grain size on stress corrosion cracking susceptibility of AISI 4340 steel", Trans. ASM, Vol. 62, 1969, p.989.

25. J.F. Lessar and W.W. Gerberich: "Grain size effects in hydrogen assisted cracking", MT, Vol. 7A, July 1976, p.953.

26. R. A. Davis et al: Corrosion, Vol. 20, 1964, p.93.

27. R.O. Ritchie, M.H. Castro Cedeno, V.F. Zackay and E.R. Parker: "Effect of silicon additions and retained austenite on stress corrosion cracking of high strength steels", MT, Vol. 9A, p.35.

28. C.L. Briant, H.C. Feng and C.J. McMahon: "Embrittlement of a 5 percent Hi high strength steel by impurities and their effect on hydrogen induced cracking", MT, Vol. 9A, May 1978, p.625.

29. J. R. Low: in Fracture of Engineering Materials, Pub. ASM, 1964.

30. S.K. Banerji, C.J. McMahon and H.C. Feng: "Intergranular fracture in 4340 type steels: Effect of impurities and hydrogen", MT, Vol. 9A, Feb 1978, p.237.

31. A.W. Porter, M.L. El Osta and D.J. Kusec: "Prediction of failure of finger joints using acoustic emission", Forest Products Journal Vol. 22, Sept. 1972, p.74.

32. L.J. Graham and G.A. Alers: "Investigation of acoustic emission from ceramic materials", NTIS Report AD-45-000, May 1972.

33. D.O. Harris, A.S. Tetelman and F.A.I. Darwish: "Detection of fiber cracking by acoustic emission", in Acoustic Emission, ASTM STP 505, Pub. ASTM, 1972, p.238.

34. K.B. Das: "An ultrasensitive hydrogen detector", in Hydrogen Embrittlement Testing, ASTM STP 543, Pub. ASTM, 1974, p.106.

35. K.H. Khan and W.E. Wood: "The effect of step quenching on the microstructure and fracture toughness of AISI 4340 steel", MT, Vol. 9A, July 1978, p.899.

36. C. N. Sastry, K. H. Khan and W.E. Wood: "The mechanical stability of retained austenite in quenched and tempered AISI 4340 steel," to be presented at AIME Annual Meeting, Feb. 1980.

37. C.N. Sastry and W.E. Wood: "The presence of retained austenite at prior austenite grain boundaries" Submitted for publication.

38. C.S. Carter: Corrosion, Vol. 27, 1971, p.471.

39. J. F. Knott, Fundamentals of Fracture Mechanics, Pub. Wiley, 1973.

40. J. A. Smith, M. H. Peterson and B. F. Brown: "Electrochemical conditions at the tip of an advancing stress corrosion crack in 4340 steel", Corrosion, Vol. 26, Dec 1970, p.539.

41. H.L. Dunegan: "Using acoustic emission technology to predict structural failure", Metals Engg Quarterly, Feb. 1975, p.8.

42. P. McIntyre and G. Green: "Acoustic emission during stress corrosion cracking in high strength steels", British J NDT, May 1978, p.135.

43. A.S. Tetelman and W.D. Robertson: "The mechanism of hydrogen embrittlement observed in iron-silicon single crystals", Trans. Met. Soc. AIME, Vol. 224, Aug 1962.

44. R. M. Horn and R.O. Ritchie: "Mechanism of tempered martensite embrittlement in low alloy steels", MT, Vol. 9A, Aug 1978, p.1039.

45. C. J. McMahon and V. Vitek: "The effect of segregated impurities on intergranular fracture energy", Acta Metallurgica, Vol. 27, 1979, p.507.

46. C. J. McMahon, K. Yoshino and H. C. Feng: "Hydrogen embrittlement in impure steels", in Stress corrosion cracking and hydrogen embrittlement of iron base alloys, Pub. NACE, 1973.

47. U. Q. Cabral: C.R. hebd. Seances Acad. Sci., 1965, p.6887.

48. K. Yoshino and C.J. McMahon: "The cooperative relationship between temper embrittlement and hydrogen embrittlement in high trength steels", MT, Vol. 5, Feb 1974.

49. B.J. Berkowitz et al. Scr. Metall., Vol. 10, 1976, p.871.

50. R. D. McCright and R.W. Staehle: J. Electrochem. Soc., Vol.121, 1974, p.609.

51. R.W.K. Honeycombe: ISI Special Report 86, 1964.

52. B. D. Craig: "On the elastic interaction of hydrogen with precipitates in lath martensite", Acta Metallurgica, Vol. 25, p.1027.

53. H. A. Tiner and C.. Gilpin: "Microprocesses in stress corrosion of martensitic steels", Corrosion, Vol. 22, Oct. 1966, p.271.

54. C. S. Carter: "The effect of silicon on stress corrosion resistance of low alloy high strength steels", Corrosion, Vol.25, No. 10, 1969, p.423.

55. G. E. Kerns, M.T. Wang and R. W. Staehle: "Stress corrosion cracking and hydrogen embrittlement in high strength steels", in stress corrosion cracking and hydrogen embrittlement of iron base alloys, Pub. NACE, 1973.

56. J. R. Rice: "Mechanics aspects of stress corrosion cracking and hydrogen embrittlement", in stress corrosion cracking and hydrogen embrittlement of iron base alloys, Pub. NACE, 1973.

APPENDIX

When a pzt transducer is excited by an impulse, it reaches a peak and then rings down according to its natural frequency. For the analysis of acoustic emission burst signals, the most often used model for burst emission is the decaying sinusoid type given by (Figure A1),

$$V = V_i \sin (2\pi ft) \cdot e^{-t/\tau} \qquad (A1)$$

where V = amplitude of the decaying sinusoid at time t

V_i = peak amplitude of the emission event

f = resonant frequency of the transducer

τ = decay time of the burst envelope

The burst shown in Figure A1 is defined as one emission event of peak amplitude V_i. The threshold counts (N) are obtained by counting the number of times the signal exceeds a predetermined threshold level (V_t). The threshold counts obtained from this event are 6 (Figure A1). The number of counts obtained from an event is a function of V_i, V_t, f and τ and given analytically by

$$\text{Threshold counts, } N = f\tau \cdot \ln \left(\frac{V_i}{V_t}\right) \qquad (A2)$$

From equation A2, it is clear that the counts being a logarithmic function of V_i, give relatively less importance to events of higher amplitude.

When a large number of events are considered, the peak amplitudes of these events are distributed in a pattern depending on the source mechanism. Most often, this distribution of peak amplitudes can be described (A1) by a power law distribution,

$$n(V_i) = K \cdot V_i^{-b} \tag{A3}$$

where $n(V_i)$ = number of events of amplitude exceeding V_i

K = a constant

b = amplitude distribution parameter

according to equation A3, the probability of occurrence of events of higher amplitudes decreases as V_i^{-b}. How rapidly this probability decreases depends on the value of b, which varies around 1 in most cases. This distribution was first proposed by Pollock[A1] and it was explained that an activity like brittle crack extension which results in emissions of higher amplitudes will give a lower value of b, in contrast to an activity like plastic deformation which progresses by relatively smaller steps and will result in a higher value of b. It has also been shown[A2] that 1/b is approximately the mean (average amplitude) of the distribution.

Now, differentiating equation A3, a mathematically more conventional probability distribution function can be derived as

$$m(V_i) = \frac{dn(V_i)}{dV_i} = bKV_i^{-b-1} \tag{A4}$$

where $m(V_i)$ = probability of occurrence of an event with amplitude V_i.

Consider that in the course of an activity which generates acoustic emission, a total number of P emission events were produced above a level V_o. Then, from equations A3 and A4, we get

$$K = PV_o^b$$

and $$m(V_i) = b \cdot PV_o^b \cdot V_i^{-b-1}$$

Now, the number of threshold counts (N) can be obtained as

$$N = \int_{V_t}^{\infty} m(V_i) \cdot f\tau \ln \frac{V_i}{V_t} \cdot dV_i$$

$$= \frac{Pf\tau}{b} \cdot \left(\frac{V_o}{V_t}\right)^b \qquad \text{(A5)}$$

Equation A5 suggests that when the emission data are not extrapolated below the level V_t, V_o can be set equal to V_t. In that case, the equation A5 is reduced to

$$\frac{N}{P} = \frac{f\tau}{b} \qquad \text{(A6)}$$

The factor $f\tau$ can be considered as a constant and that suggests that the average counts per event are directly related to 1/b, the average amplitube. Whenever $f\tau$ remains a constant, the average counts per event is a good measure of the average amplitude of the emission events.

A direct method of characterizing the amplitude distribution is to fit the amplitude distribution data to equation A3. Figure A2 is a

typical histogram of emission events sorted according to their amplitudes. According to equation A3, b is the slope of cumulative events versus amplitude curve plotted on a log curve. The data of Figure A2 are thus converted (points in Figure A3) and the slope of least square fitted line gives b. 1/b would then be approximately the mean of the distribution (average amplitude).

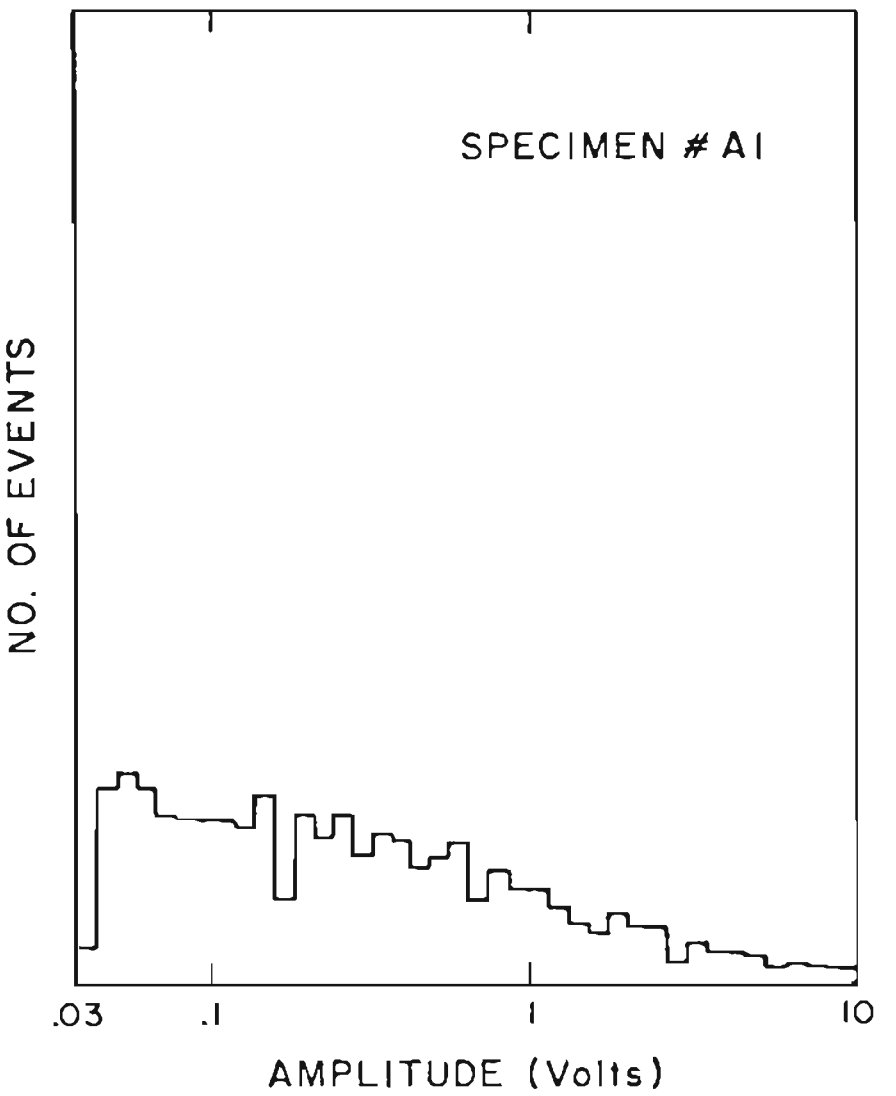

Figure A1. A schematic of the decaying sinusoid model for burst acoustic emission.

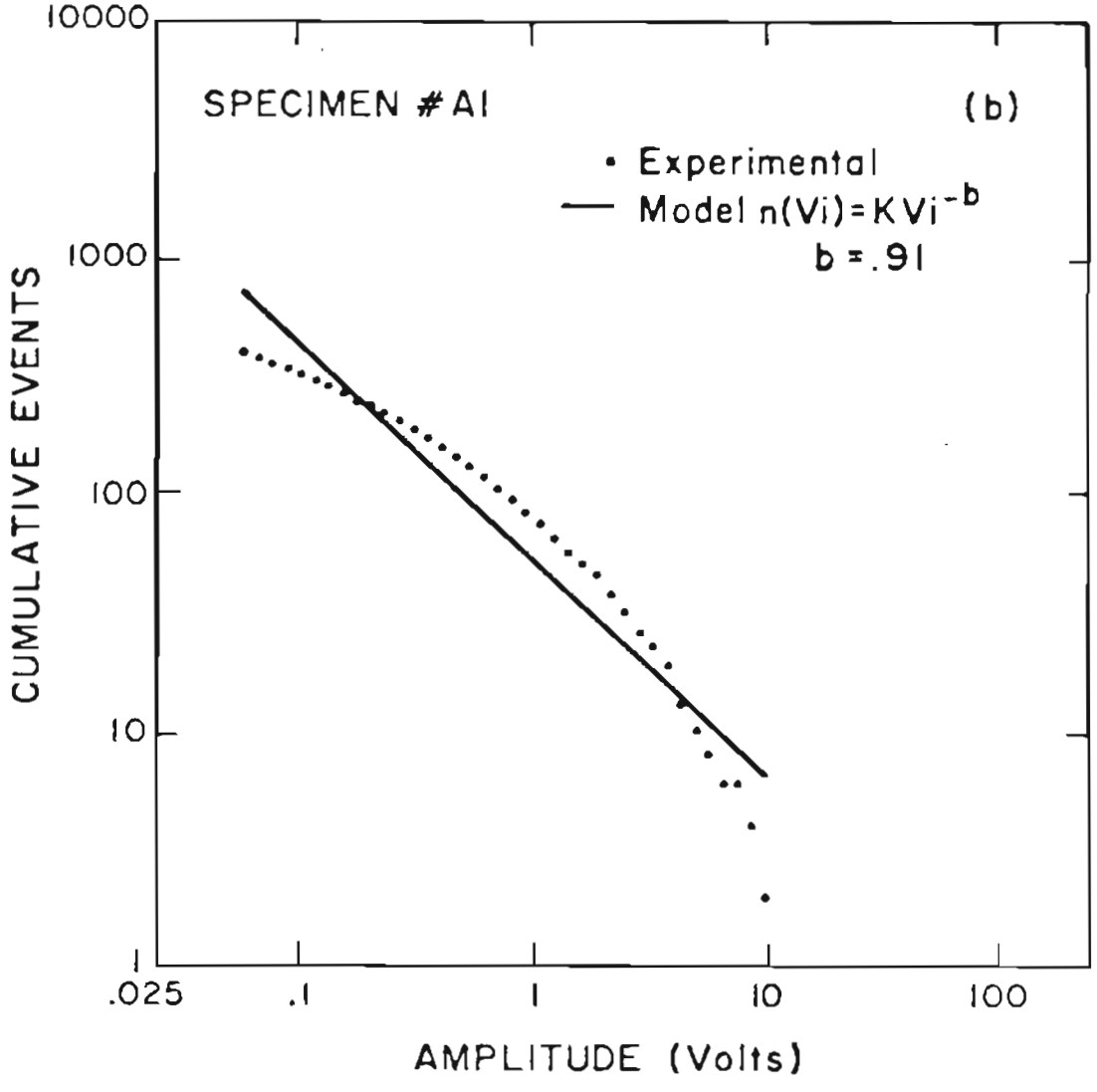

Figure A2. An experimental amplitude distribution histogram.

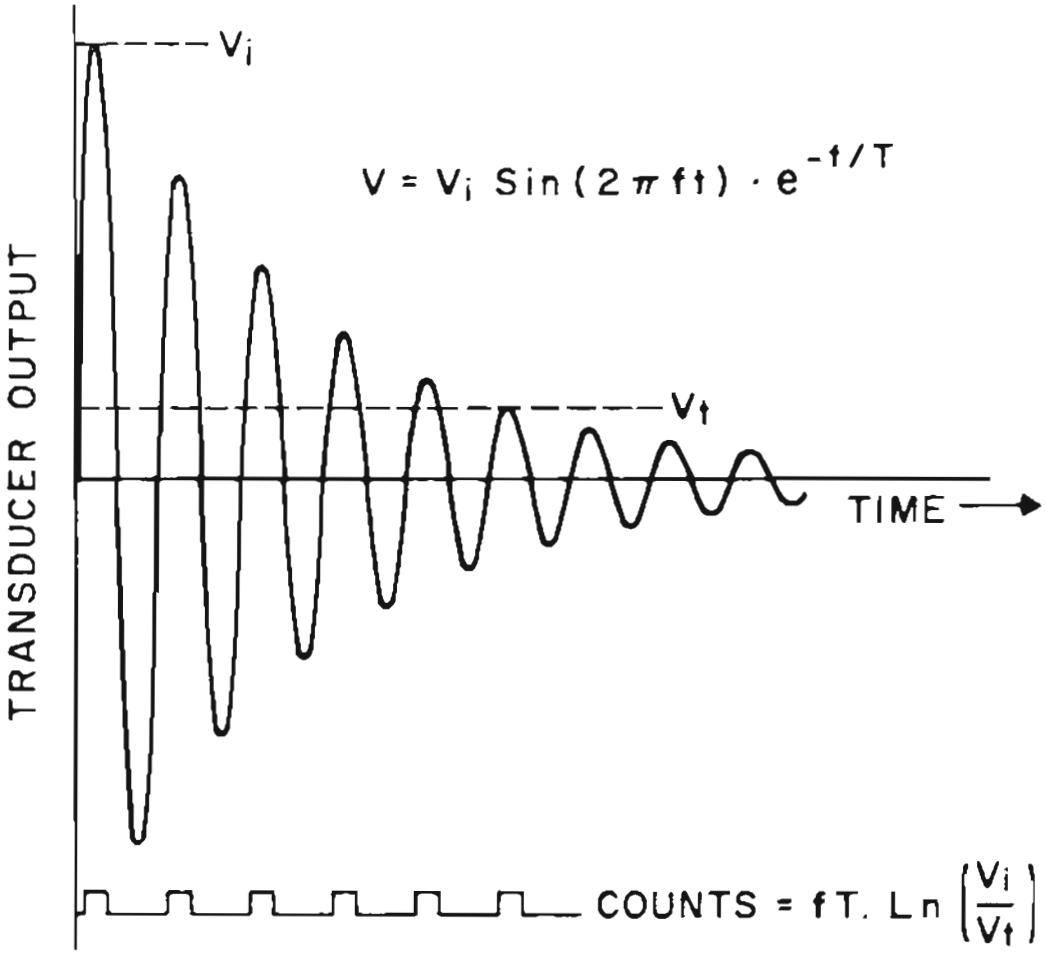

Figure A3. The experimental amplitude distribution data of Figure A2 as fitted to the power-law model.

REFERENCES

A1. A. A. Pollock: "Acoustic Emission", Acoustics and Vibrations progress, Vol. 1, Chapman and Hall, London, 1973.

A2. D. Dilipkumar, V.S.R. Gudimetla and W.E. Wood: "Amplitude distribution analysis of acoustic emission", Experimental Mechanics, Dec. 1979, p.438.

BIOGRAPHICAL NOTE

Dilipkumar Dedhia was born in Beraja, India on October 13, 1951. He received his Bachelor of Science degree in Chemistry from Madras University in 1972 and Bachelor of Engineering degree in Metallurgy from Indian Institute of Science in 1976.

He joined the Oregon Graduate Center in September 1976 as a graduate student.

In January 1980, he joined Science Applications, Inc., Palo Alto, California, as a Materials Scientist and is currently involved in fracture mechanics analysis of piping integrity of nuclear reactors, and applications of acoustic emission to on-line monitoring of integrity of power plant components.